Western Michigan University
ScholarWorks at WMU

Dissertations | Graduate College

8-1999

Active Local Volume Displacement Cancellation of a Vibrating Baffled Beam

Marcellin Zahui
Western Michigan University

Follow this and additional works at: https://scholarworks.wmich.edu/dissertations

 Part of the Aerospace Engineering Commons, and the Mechanical Engineering Commons

Recommended Citation

Zahui, Marcellin, "Active Local Volume Displacement Cancellation of a Vibrating Baffled Beam" (1999). *Dissertations*. 1540.
https://scholarworks.wmich.edu/dissertations/1540

This Dissertation-Open Access is brought to you for free and open access by the Graduate College at ScholarWorks at WMU. It has been accepted for inclusion in Dissertations by an authorized administrator of ScholarWorks at WMU. For more information, please contact wmu-scholarworks@wmich.edu.

ACTIVE LOCAL VOLUME DISPLACEMENT CANCELLATION OF A VIBRATING BAFFLED BEAM

by

Marcellin Zahui

A Dissertation
Submitted to the
Faculty of The Graduate College
in partial fulfillment of the
requirements for the
Degree of Doctor of Philosophy
Department of Mechanical and Aeronautical Engineering

Western Michigan University
Kalamazoo, Michigan
August 1999

Reproduced with permission of the copyright owner. Further reproduction prohibited without permission.

ACTIVE LOCAL VOLUME DISPLACEMENT CANCELLATION OF A VIBRATING BAFFLED BEAM

Marcellin Zahui, Ph.D.

Western Michigan University, 1999

An active noise control apparatus is developed. The device reduces the sound radiated from a vibrating clamped beam. The attenuation of the sound field is obtained through minimization of local volume displacements of the vibrating beam. Two single-input/single-output cancellation devices are used. Each device employs a motion sensor and an acoustic actuator. The actuator is a loudspeaker equipped with a pressure sensor to detect its volume displacement. The motion sensor signal is related to the local volume displacement of the structure which is then reduced by a loudspeaker driven with an equal but opposing volume displacement. The volume displacement sensors are developed and fabricated using Polyvinylidene Fluoride (PVDF). They measure the local volume displacements of the vibrating beam. The pressure sensor is mounted in the loudspeaker enclosure. It provides the feedback signal for the loudspeaker volume displacement control.

Previous work showed the successful implementation of this technique for uniformly vibrating radiators. This thesis presents the development of this technique for the reduction of sound radiated from a vibrating beam. First, a numerical local volume displacement cancellation experiment is performed using several loudspeakers, each canceling the volume displacement of a section of the beam. The

Reproduced with permission of the copyright owner. Further reproduction prohibited without permission.

finite element method is used to calculate the velocity distribution of the vibrating beam. A discretized form of the Rayleigh integral is then used to find the sound pressure and the sound power radiated before and after cancellation.

Second, the numerical results are verified by laboratory experiments using a beam divided into two sections. Two motion sensors for the beam and one pressure sensor for each loudspeaker are fabricated and thoroughly checked. The cancellation experiment is then performed on a broadband random noise using two independent Proportional-Derivative (PD) controllers.

Reproduced with permission of the copyright owner. Further reproduction prohibited without permission.

INFORMATION TO USERS

This manuscript has been reproduced from the microfilm master. UMI films the text directly from the original or copy submitted. Thus, some thesis and dissertation copies are in typewriter face, while others may be from any type of computer printer.

The quality of this reproduction is dependent upon the quality of the copy submitted. Broken or indistinct print, colored or poor quality illustrations and photographs, print bleedthrough, substandard margins, and improper alignment can adversely affect reproduction.

In the unlikely event that the author did not send UMI a complete manuscript and there are missing pages, these will be noted. Also, if unauthorized copyright material had to be removed, a note will indicate the deletion.

Oversize materials (e.g., maps, drawings, charts) are reproduced by sectioning the original, beginning at the upper left-hand corner and continuing from left to right in equal sections with small overlaps. Each original is also photographed in one exposure and is included in reduced form at the back of the book.

Photographs included in the original manuscript have been reproduced xerographically in this copy. Higher quality 6" x 9" black and white photographic prints are available for any photographs or illustrations appearing in this copy for an additional charge. Contact UMI directly to order.

UMI®

Bell & Howell Information and Learning
300 North Zeeb Road, Ann Arbor, MI 48106-1346 USA
800-521-0600

Reproduced with permission of the copyright owner. Further reproduction prohibited without permission.

Reproduced with permission of the copyright owner. Further reproduction prohibited without permission.

UMI Number: 9942076

UMI Microform 9942076
Copyright 1999, by UMI Company. All rights reserved.

This microform edition is protected against unauthorized copying under Title 17, United States Code.

UMI
300 North Zeeb Road
Ann Arbor, MI 48103

Reproduced with permission of the copyright owner. Further reproduction prohibited without permission.

Copyright by
Marcellin Zahui
1999

Reproduced with permission of the copyright owner. Further reproduction prohibited without permission.

ACKNOWLEDGEMENTS

This work would not have been possible without the support of my dear friend Rita Ahiboh, and my son, Cameron. Also, I am deeply indebted to Dr. James Kamman and Dr. Koorosh Naghshineh for their confidence, tolerance and support during the past four years. This work could not have progressed as quickly as it did without the ideal working conditions and computational and experimental tools which Dr. James Kamman and Dr. Koorosh Naghshineh brought together and made readily accessible at the Western Michigan University Dynamics, Vibrations, Acoustic, and Controls (DVAC) Laboratory. In addition, I would like to thank all members of my doctoral committee: Dr. Dennis VandenBrink and Dr. Hossein Mousavinezhad, for their advice during the course of my research. I am thankful also to Yasmin Jones and Aie Li Ong for their typing services.

A mon père

"Qu'il est long et tortueux, le chemin du succès"

Marcellin Zahui

Reproduced with permission of the copyright owner. Further reproduction prohibited without permission.

TABLE OF CONTENTS

Reproduced with permission of the copyright owner. Further reproduction prohibited without permission.

Table of Contents-continued

CHAPTER

Reproduced with permission of the copyright owner. Further reproduction prohibited without permission.

CHAPTER

Reproduced with permission of the copyright owner. Further reproduction prohibited without permission.

Reproduced with permission of the copyright owner. Further reproduction prohibited without permission.

LIST OF TABLES

Reproduced with permission of the copyright owner. Further reproduction prohibited without permission.

LIST OF FIGURES

Reproduced with permission of the copyright owner. Further reproduction prohibited without permission.

Reproduced with permission of the copyright owner. Further reproduction prohibited without permission.

Reproduced with permission of the copyright owner. Further reproduction prohibited without permission.

List of Figures-Continued

Reproduced with permission of the copyright owner. Further reproduction prohibited without permission.

Reproduced with permission of the copyright owner. Further reproduction prohibited without permission.

INTRODUCTORY REMARKS

Introduction

The focus of this research is to extend the work presented by Mason et al. (1994) and Naghshineh & Mason (1996) to actively control the sound radiated from vibrating structures. This patented technique (Mason & Naghshineh, 1995) is based on sensing and minimizing the local volume displacement, velocity, or acceleration (assuming $e^{i\omega t}$ time dependence) of a vibrating structure. This method of canceling the volume displacement, velocity, or acceleration will be referred to herein as source strength cancellation. However, whenever structural displacement, velocity, or acceleration is measured for the purpose of cancellation of radiated sound, the terms volume displacement cancellation, volume velocity cancellation, or volume acceleration cancellation can be used, respectively.

Noise reduction is achieved by distributing an array of noise-control devices over the surface of the radiating structure. Each device is controlled independently of the other devices and consists of a motion sensor, a controller, and a loudspeaker. The loudspeaker is driven such that it reduces the volume displacement of the radiating structure within its close proximity. Because the device uses a motion sensor and an acoustic actuator, there can be very little modification of structural vibrations by the actuator. Thus, there is very little coupling between the actuator (i.e., loudspeaker)

Reproduced with permission of the copyright owner. Further reproduction prohibited without permission.

and the structural sensor. In addition, since each device is controlled independently, the controller can be very simple and made of low cost components.

The concept behind this technique has been widely accepted. Minimization of volume displacement results in lower sound radiation. Recent publications by Guigou et al. (1994), Johnson and Elliott (1993), and Charette et al. (1998) introduced the concept of the active control of sound radiated from structures by sensing and controlling the total volume displacement of the structure. This control, however, is achieved by altering the structural vibrations using structural actuators. The methodology presented in this thesis is different from the work of these authors in that acoustic actuators are used to control the local volume displacement.

The work presented by this author describes the further development of this technique on a simple, non-uniformly vibrating structure (sound radiator). The example chosen is a clamped vibrating beam. This implementation requires the development of several components. These are: (a) the experimental setup; (b) the numerical models needed to verify the experimental setup; (c) the development and implementation of a local volume displacement sensor for the beam; (d) the selection and implementation of control techniques; and (e) the cancellation experiments.

In the first step, a plywood box is made and a clamped aluminum beam is mounted inside the box such that the top of the beam is flush with the top surface of the box. The beam is excited using a shaker that is completely sealed inside the box. In the second step, the finite element method is used along with the discretization of the Rayleigh integral to compute the velocity distribution on the surface of the beam,

Reproduced with permission of the copyright owner. Further reproduction prohibited without permission.

the sound pressure, and the acoustic power radiated by the beam. In the third step, two different techniques are used to develop local volume displacement sensors for the beam. The sensors are made of Polyvinylidene Fluoride (PVDF). Also an internal pressure sensor that measures the volume displacement of the loudspeaker is devised using techniques similar to those presented by Anthony and Elliot (1991). Both the PVDF sensor (for vibrating beams) and pressure sensor (for loudspeaker) are fabricated and experimentally checked. The fourth step is focused on the development of, and experimentation with, different loudspeaker control techniques.

The controller performance is evaluated using a simple setup consisting of two loudspeakers. Each loudspeaker is equipped with an internal pressure sensor that measures its volume displacement. Thus, the volume displacement of the source loudspeaker is reduced using the second loudspeaker. A proportional and derivative controller is implemented using a PC equipped with a controller board capable of performing real-time control. In the final step, the noise cancellation experiment is performed using the controller developed in the fourth step. Two loudspeakers are used to independently cancel the volume displacements of two sections of the beam.

Thesis Organization

This thesis is articulated around the active control of the sound radiated by a baffled beam, using local volume displacement cancellation. It is composed of three major parts: (1) theoretical development, (2) numerical simulation, and (3) experimental verification. These major parts are presented in six chapters. The

Reproduced with permission of the copyright owner. Further reproduction prohibited without permission.

narration starts from a brief literature review and research motivation presented in Chapter I and ends in Chapter VI with the summary of the design process and findings. The actual design and experiments are found in Chapters II, III, IV and V.

Chapter II pertains to achieving sound power reduction through local volume displacement cancellation. It is shown that the sound power radiated from a baffled beam that is excited by external sources can be reduced drastically by driving a set of actuators (loudspeakers) placed around it with prescribed volume displacements. The beam is divided into sections so that for each section, a loudspeaker immediately next to it is driven with negated volume displacement of that section. This type of active noise control is referred to as local volume displacement cancellation. The study presented in Chapter II uses a baffled beam and several baffled pistons representing loudspeakers. First, a theoretical development is presented, followed by a numerical simulation. This numerical experiment is based on the finite element analysis of the baffled beam and the discretization of the Rayleigh integral. The results, presented in the last section, show that the acoustic power of a baffled beam can be minimized by canceling its local volume displacement.

The local volume displacement cancellation concept development of Chapter II makes no mention of how the volume displacement of the section of the beam is measured. It assumes that the local volume displacement of the beam is known or can be measured. Chapter III discusses the measurement of the volume displacement of a beam and a loudspeaker. The design and the numerical verification of PVDF sensors are presented. This sensor development follows the three major design paths

Reproduced with permission of the copyright owner. Further reproduction prohibited without permission.

mentioned earlier. Theoretical development using two different approaches (modal expansion and quadratic form) is presented, followed by numerical simulation. This design methodology is also used for the design of volume displacement sensors for the loudspeakers.

Finally, Chapter IV presents the experimental verification of the PVDF sensors (for the beam) and internal pressure sensors (for the loudspeakers). The baffled beam is built. Using an Active Noise Control Package (ANCPACK) program, specially written for this thesis, the baffled and clamped end conditions of the beam are checked. Then, the volume displacement sensors are fabricated and verified.

Chapter V concludes this research work by achieving the prescribed goal. The noise radiated by a baffled beam is reduced using local volume displacement cancellation. The cancellation experiment is performed using two loudspeakers placed next to each half of the beam respectively.

Reproduced with permission of the copyright owner. Further reproduction prohibited without permission.

CHAPTER I

RESEARCH OVERVIEW

Research Motivation

The attenuation of sound radiated by vibrating structures is traditionally achieved by energy absorbing materials, vibration isolation, detuning, and vibration absorbers. This method of controlling sound is called passive control. Passive noise control has two major problems. The first drawback is that it is only effective for medium and high frequency sound. The second problem is the weight of the absorbing material. The thickness of the material must increase with decreasing frequency. Real-time control of sound using actuators is therefore suggested as a solution to control low frequency noise. The amount of research toward this new technique, referred to as Active Noise Control (ANC), has rapidly increased in the last two decades. The introduction of fast processors with high computational power contributed to that development.

A number of successful active noise control techniques have been demonstrated (Warnaka, 1982; Ffowes-Williams, 1984). These techniques can be divided into two categories. Active Acoustic Control (AAC), and Active Structural Acoustic Control (ASAC) (Fuller, 1987; Naghshineh & Koopmann, 1992). The first, AAC, uses acoustic actuators (loudspeakers) as sources of sound cancellation. The second, ASAC, uses force actuators to alter the vibration pattern of the structure in

Reproduced with permission of the copyright owner. Further reproduction prohibited without permission.

such a way that it becomes a weak radiator (Crawley & De Luis, 1987; Dimitriadis et al, 1989). The common problem of these two techniques is the complexity of the control systems. The controllers draw upon the information gathered by multiple sensors and drive many actuators (multi-input/multi-output) (Elliot & Nelson, 1986; Zuroski & Roe, 1995). Therefore, they require huge computational power and are very expensive (Clark & Fuller, 1992a; Scott et al., 1992).

It has become clear that for its practical implementation, there is a need for more research in the area of active noise control. Cost and simplicity are the major factors that will move active noise control from the laboratory to the industrial platform. Therefore, it is imperative to develop a new strategy to simplify the control system. A candidate control strategy should have two principal characteristics. First, the controller has to be simple enough to be built using low-cost components. Second, the controller must work on a broad band of frequencies. Mason and Naghshineh (1995) used a uniformly vibrating disk to prove that local volume acceleration cancellation leads to the design of a simple and inexpensive noise reduction device.

The goal of this thesis is to extend this technique to a non-uniformly vibrating structure such as a beam. The major advantage of this method is the fact that when multiple noise reduction devices are required, each device is controlled independently. The controller can therefore be very simple and made of low-cost components. The second advantage is that the device uses a motion sensor and an acoustic actuator. The control system is further simplified because there is very little coupling from the (acoustic) actuator to the (structural) sensor. Coupling is defined as

Reproduced with permission of the copyright owner. Further reproduction prohibited without permission.

the feedback from the control (secondary) actuators to the sensors. Significant coupling can result in control instability. This becomes a major problem when using acoustic control actuators (loudspeakers) along with microphone sensors. In this research, coupling is minimized in two ways. First, by the use of structural sensors along with acoustic actuators. Second, by the choice of structures that are not easily excited by sound radiated from the control loudspeakers.

Summary of Related Research

This thesis is centered on the use of acoustic actuators (loudspeakers) to control the noise radiated by a vibrating structure. The sound attenuation is obtained by minimizing the local volume displacement of the structure. The cancellation device consists of a motion sensor, a pressure sensor and a loudspeaker. Therefore, in reviewing the research related to this strategy, one should review (a) the use of loudspeakers in active noise cancellation, (b) the control strategy, and (c) the measurement of volume displacement. Each of the following sections details the above research.

Active Acoustic Control

Active acoustic control (AAC) refers to the cancellation of sound using acoustic actuators (loudspeakers) (Deffayet & Nelson, 1988). This is made possible by two basic physical phenomena: superposition and sound source coupling. The first phenomenon relies on the principle of destructive interference between sound

Reproduced with permission of the copyright owner. Further reproduction prohibited without permission.

fields. The original (primary) sound field is superimposed with an electroacoustically generated secondary (control) field of opposite phase. As one source pushes the air surrounding it outward, the other source is pulling its surrounding air inward. With the two sources spaced by about one-third of a wavelength, the density of the air surrounding both of them stays nearly constant, preventing the formation of acoustic pressure waves. The second phenomenon is the acoustic impedance coupling between the active source and the noise source. Two sound sources of constant source strength are coupled when they are separated by less than about one-third of a wavelength or are connected by a waveguide such as a duct (Swanson, 1989).

The concept of AAC, described above will be applied in this thesis. The primary source is the structure (beam) and the cancellation sources are loudspeakers. The strategy relies on the principle of superposition, which applies in any linear system. The propagation of an acoustic wave with amplitude up to that corresponding to an extremely loud noise is a very linear process (Elliott & Nelson, 1993), but non-linearity in the control systems is often introduced by the dynamics of the loudspeaker. Therefore, care should be given to the selection and use of the loudspeaker.

Control Strategy

The noise of a physical source may be reduced to some degree if the principle of superposition can be applied and the cancellation source and the radiating source are located (coupled) less than about one-third of the wavelength of the maximum

Reproduced with permission of the copyright owner. Further reproduction prohibited without permission.

frequency component. Both superposition and active reduction of radiation impedance can be artificially created with high-speed electro-acoustic control systems. This technique was first patented by Lueg in 1936. However, theoretical treatment of active noise control started in the 1960's (Jessel, 1966). The first technical demonstration installation of this technique was reported in the 1980's (Swimbanks, 1982; Ross, 1981). Commercial products were available around 1987 (Erikson & Allie, 1987).

This relatively slow growth of active noise control between 1930 and 1980 is due to a poor understanding of the problem from an acoustic and control systems point of view as well as the lack of necessary technology to deal with the design of successful ANC systems. The design difficulties range from the broad band nature of the sound and distributed noise sources to the characteristics of transducers and other electronic equipment used. Recent advances in control systems technology, which include the development of active filters and adaptive controls, made active control of noise more attractive and feasible. The result is a rapid increase of research into reducing noise and vibration of structures. The accelerating interest is reflected by the large number of conferences, publications, and patents on active noise control.

The control systems theory, for active noise control is usually derived using the acoustic power (Nelson et al., 1987) or the source strength (Johnson & Elliott, 1995). When the acoustic power theory is used, the control law is obtained from the minimization of the sound power. Nelson et al. (1987) explained this concept using two monopole sources operating at the same frequency ω. If q_p and q_s represent

Reproduced with permission of the copyright owner. Further reproduction prohibited without permission.

the complex source strength of the primary and secondary sources respectively, and p_p and p_s are the complex acoustic pressure at the positions of the primary and secondary sources respectively, the acoustic power outputs of the primary and secondary sources can be written as

$$W_p = \frac{1}{2} R_e\left(q_p^* p_p\right), \tag{1.1}$$

$$W_s = \frac{1}{2} R_e\left(q_s^* p_s\right), \tag{1.2}$$

where the superscript * denotes complex conjugation, and R_e denotes the real part of the bracketed quantity. The total power output of the two acoustic sources is given by

$$W_t = W_p + W_s, \tag{1.3}$$

where W_p and W_s are the acoustic power radiated by the primary and secondary sources respectively. Equation (1.3) is a quadratic function of the real and imaginary parts of q_s. It has a minimum value of W_t associated with a unique secondary source strength. In practice the sound pressure is measured by an array of microphones. The signals from the microphones are used by the controller to compute the source strength of the secondary sound source. The controller then drives the secondary source (cancellation source) with the computed source strength.

An entirely different strategy of active control emerges if, instead of minimizing the total power output of the source pair, the net source strength is minimized. Equation (1.1) can be written as

Reproduced with permission of the copyright owner. Further reproduction prohibited without permission.

$$W_p = \frac{S}{2} R_e\left(\dot{x}_p^{*} p_p\right), \tag{1.4}$$

or

$$W_p = \frac{S}{2} R_e\left\{\left(\int \ddot{x}_p dt\right)^{*} p_p\right., \tag{1.5}$$

where x is the surface displacement, S the surface area of the source, and $\dot{x}$ and $\ddot{x}$ the surface velocity and acceleration respectively. From the above equation, it is clear that reducing the displacement, velocity or acceleration of a source will result in the reduction of radiated acoustic power. In other words, the noise radiated by a given vibrating structure can be reduced by simply reducing its surface displacement, velocity or acceleration (Burdisso & Fuller, 1992; Sung & Jan, 1997). This method of control, as mentioned earlier, is active structural acoustic control (Clark & Fuller, 1992b) and is beyond the scope of this work.

Rather than reducing the structural displacement, velocity or acceleration of a monopole, as mentioned in the above case, the net source strength of a dipole will be minimized. This will result, in the reduction of the radiated noise. The combined source strength of the primary and secondary source can be written as

$$Q = q_p + q_s, \tag{1.6}$$

a secondary source strength can be defined so that Q is zero, that is

$$q_p = -q_s. \tag{1.7}$$

This type of control is applied by measuring the volume displacement, velocity or acceleration of the structure and by driving several loudspeakers so that the net source

Reproduced with permission of the copyright owner. Further reproduction prohibited without permission.

strength of loudspeakers and structure is minimized. The technique is referred to as total source strength cancellation.

Considering both control strategies, power minimization and source strength cancellation, Nelson et al. (1987) showed that power minimization is the best method of quieting a vibrating structure, because it reduces the sound pressure level over the whole control surface at any frequency. This is in contrast with source strength cancellation which only works at low frequency and can sometimes enhance acoustic power at some points on the control surface (Johnson & Elliott, 1995). Even though power minimization is more effective, it is associated with a large number of sensors and therefore requires an expensive multi-channel controller. This makes acoustic power minimization less appealing than source strength cancellation. Johnson and Elliott (1995) demonstrated that, unlike power minimization, source strength cancellation yields simpler controllers. Many others have followed this path to actively control the noise radiated from a beam or a plate (Fuller, 1991; Oppenheim et al., 1992). In these experiments the control law is applied to the whole structure. This type of control still requires a slightly complex control system because one actuator alone cannot control the noise generated by the vibration of a wide-area structure. Thus, the control strategy involved in this method needs to be further simplified.

Naghshineh and Mason (1996) introduced a new technique based on sensing and minimizing the local source strength of the vibrating structure. The vibrating surface is divided into smaller patches and each patch is treated as an individual

Reproduced with permission of the copyright owner. Further reproduction prohibited without permission.

radiator of sound. Reduction of the volume displacements of the individual patches results in an overall reduction of the structural volume displacement that in turn results in a quiet structure. This is because at low frequencies, successful reduction of source strength results in direct reduction of total radiated acoustic power. This thesis extends the concept involved in local source strength cancellation to a vibrating baffled beam.

Volume Displacement Sensor

Previous experiments focused on actively quieting uniformly vibrating bodies (e.g., disk or loudspeaker cone) by canceling their volume displacement, velocity, or acceleration. A single accelerometer mounted on the vibrating surface measured the volume acceleration of those structures (Naghshineh & Mason, 1996). In this work, two different types of structures are used: a loudspeaker, which is modeled as a baffled piston and a beam which is a non-uniformly vibrating body.

The sensing problem becomes much more complicated for the beam. Balas (1978) and many other authors have investigated the use of discrete point sensors to control the vibrations of flexible structures and found that these control strategies suffer from spillover. The spillover due to residual (uncontrolled) modes is found to lead to control instabilities. In addition, to accurately measure local volume displacement of a non-uniformly vibrating structure using point sensors would necessitate an increase in the number of sensors utilized per controller (and require more preprocessing of the sensor data before it is passed to the controller).

Reproduced with permission of the copyright owner. Further reproduction prohibited without permission.

Alternatively, one could resort to an increase in the number of single-input/single-output cancellation devices (e.g., many single-accelerometer/single-loudspeaker devices required to cancel the volume acceleration of a large number of small radiating areas). Both of the above alternatives would represent a less efficient control scheme. Therefore, discrete point sensors were not considered in this work.

Recent publications by Johnson and Elliott (1993), Guigou et al. (1994), and Charette et al. (1998) have introduced the concept of the active control of sound radiated from structures by sensing and controlling the total volume displacement of the structure. These researchers have made use of a single continuous sensor made of Polyvinylidene Fluoride (PVDF) which can be shaped so that it provides a measurement of total volume displacement of a vibrating beam. In the work presented here, techniques (similar to those described by these authors for sensing total volume displacement of a vibrating beam) are developed to measure the local volume displacement corresponding to each (arbitrary) section of a vibrating beam.

In this work, feedback control is used. Therefore, the feedforward sensor and the feedback sensor must measure the same entity. The PVDF sensors on the beam measure its local volume displacement. Thus, in order to match the output of the PVDF sensor, either a volume displacement sensor for the loudspeaker must be developed or, if a cone accelerometer is used (as in the work by Mason and Naghshineh, 1995) the accelerometer output must be converted into volume displacement. This would result in a more complex controller. Therefore, a volume

Reproduced with permission of the copyright owner. Further reproduction prohibited without permission.

displacement sensor for the loudspeaker is devised using techniques similar to those described by Anthony and Elliott (1991).

Reproduced with permission of the copyright owner. Further reproduction prohibited without permission.

CHAPTER II

ACHIEVING SOUND POWER REDUCTION THROUGH LOCAL VOLUME DISPLACEMENT CANCELLATION

Introduction

The objective of this chapter is to show that sound power attenuation can be obtained through local volume displacement minimization. The study will be based on a vibrating baffled beam. The beam is divided into several sections. For each section, a loudspeaker immediately next to it is driven so that the total net volume displacement of the section and the loudspeaker is reduced. The reduction of the volume displacement of the individual sections results in an overall reduction of the beam volume displacement. Consequently, the acoustic power radiated by the baffled beam is reduced.

The approach used is, first to derive the basic equations of sound pressure and sound power radiated by the baffled beam. Second, each loudspeaker is modeled as a baffled piston. The equation of the sound pressure and sound power of a baffled piston are therefore formulated. Then the beam is divided into sections. The volume displacement of an arbitrary section of the beam is calculated. This volume displacement is used to demonstrate the concept of local volume displacement cancellation. The volume displacement of the loudspeaker immediately next to a section is chosen to be equal and opposite of the volume displacement of that

Reproduced with permission of the copyright owner. Further reproduction prohibited without permission.

section. Using superposition, the total acoustic pressure radiated by each beam section and its adjacent cancellation loudspeaker are derived. A numerical simulation is used to show that the acoustic pressure and the acoustic power radiated by the combined system of the beam and the control loudspeakers is less than the acoustic pressure and the acoustic power radiated by the beam alone. Therefore, the sound produced by the vibrating baffled beam is reduced.

Theoretical Development

The goal of this study is to prove that minimizing the local volume displacement of a finite beam in an infinite baffle will result in the reduction of the acoustic power radiated by the beam. The volume displacement cancellation is achieved by using loudspeakers mounted in the same baffle, as shown in Figure 1. Thus, the pressure radiated is found using the Rayleigh integral. The acoustic power is then approximated using plane wave theory (Temkin, 1981). The volume displacement equations are also presented in this section and the concept of local volume displacement is explained.

Power Radiated by a Baffled Beam

Consider a baffled beam of length ℓ, and width b within a light fluid such as air, as shown in Figure 2. The pressure P_b at any observation point B (represented by the vector $\vec{r}$) with respect to the beam due to the beam's normal surface velocity $V_z(\vec{r})$ can be written using the Rayleigh integral (Rayleigh, 1945) as

Reproduced with permission of the copyright owner. Further reproduction prohibited without permission.

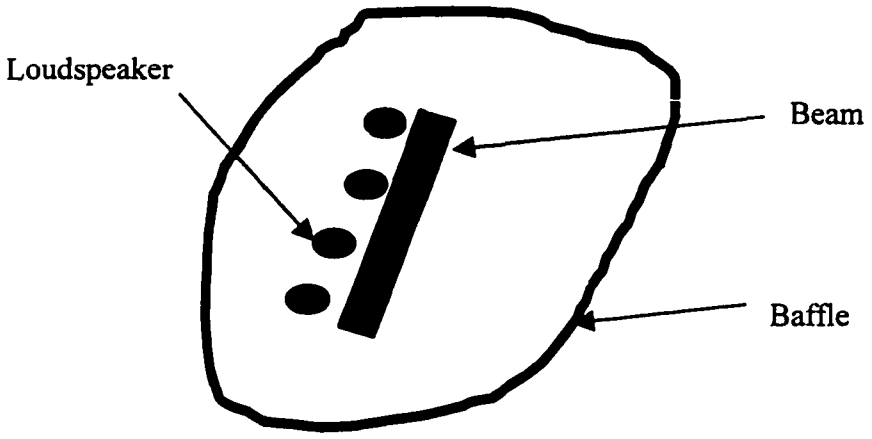

Figure 1. A Finite Beam and Loudspeakers in an Infinite Baffle.

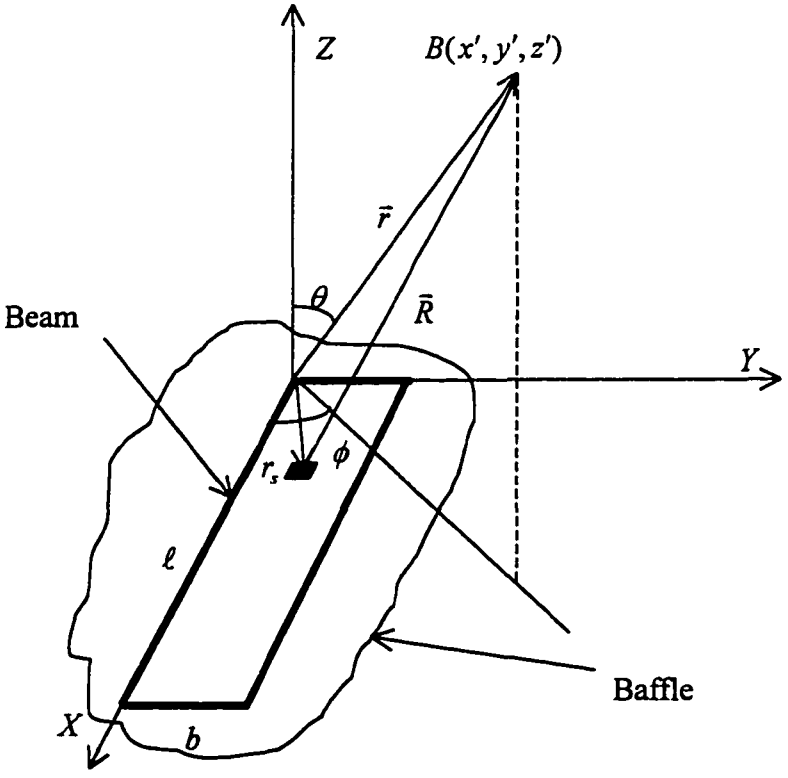

Figure 2. A Finite Beam in an Infinite Baffle.

Reproduced with permission of the copyright owner. Further reproduction prohibited without permission.

$$P_b(\vec{r}) = \frac{-i\omega\rho}{2\pi}\int_s V_z(\vec{r})\frac{e^{ikR}}{R}ds, \tag{2.1}$$

where ρ is the density of air, ω is the frequency, k is the wave number of beam vibration, $i = \sqrt{-1}$, and $R = |\vec{r} - \vec{r}_s|$. The source is defined by $\vec{r}_s$ and will be described by the coordinates x, y, and z and the receiver $\vec{r}$ (observation point), by the coordinates x', y', and z'. Therefore, the magnitude of the vector $\vec{R}$ can be written as

$$R = \sqrt{(x-x')^2 + (y-y')^2 + (z-z')^2} \ . \tag{2.2}$$

The acoustic intensity at any point $\vec{r}$ is given by

$$I(\vec{r}) = \frac{1}{2}R_e\left(P_b V_b^*\right), \tag{2.3}$$

where V_b is the particle velocity at the point $\vec{r}$. If S' is a surface defined above the baffle and enclosing the beam, the acoustic power radiated by the beam can be defined as

$$W = \frac{1}{2}\int_{S'} R_e\left(P_b V_b^*\right)ds' \ . \tag{2.4}$$

In this work, the acoustic power is calculated in the far field. Therefore, the intensity can be approximated (Kinsler et al., 1982) as

Reproduced with permission of the copyright owner. Further reproduction prohibited without permission.

$$I_b = \frac{|P_b(\vec{r})|^2}{2\rho c}, \tag{2.5}$$

where c is the speed of sound. Choosing S' as a hemisphere, the acoustic power becomes

$$W_b = \int_0^{2\pi}\int_0^{\pi/2} \frac{|P_b(\vec{r})|^2}{2\rho c} r^2 \sin\theta d\theta d\varphi . \tag{2.6}$$

Power Radiated by a Baffled Piston

As mentioned before, loudspeakers are used to cancel the volume displacement of the baffled beam. The face of the loudspeaker cone is assumed to have uniform motion, therefore, each loudspeaker is modeled as a baffled piston. Consider a baffled piston of radius a within a light fluid such as air, as shown in Figure 3. The pressure $P_L(\vec{r})$ at any observation point $\vec{r}$ with respect to the piston due to the piston normal surface velocity $V_z(\vec{r})$ can be written using the Rayleigh integral

$$P_L(\vec{r}) = \frac{-i\omega\rho}{2\pi}\int_s V_z(\vec{r}_s)\frac{e^{ikR}}{R} ds, \tag{2.7}$$

where ρ is the density of air, ω is the frequency of piston vibration, k is the wave number, and $R = |\vec{r} - \vec{r}_s|$.

The elemental surface ds considered on the disk is

Reproduced with permission of the copyright owner. Further reproduction prohibited without permission.

$$ds = r_s d\phi_s dr_s \,, \tag{2.8}$$

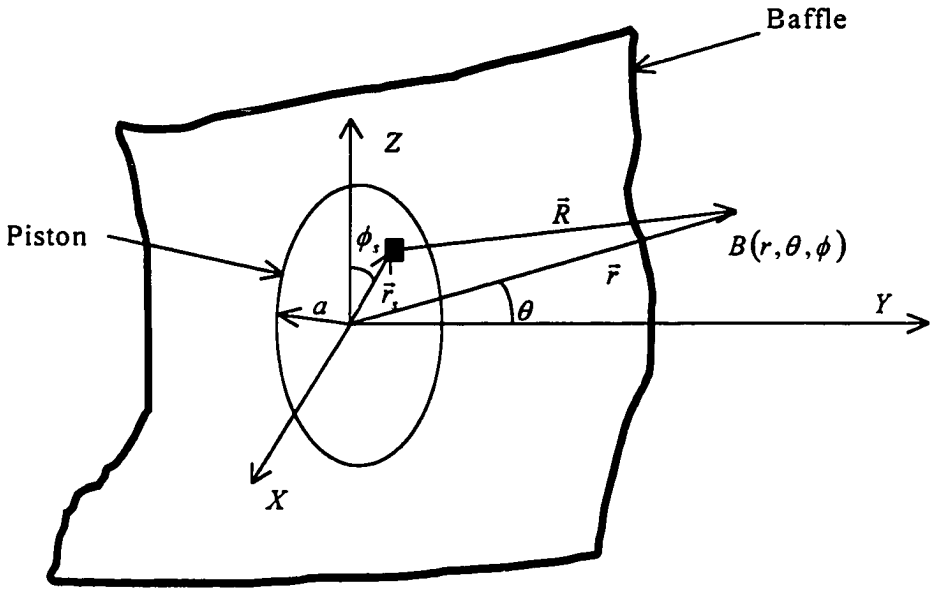

Figure 3. A Piston (Loudspeaker) in an Infinite Baffle.

replacing ds in Equation 2.7 yields

$$P_L(r,\theta,\phi) = \frac{-i\omega\rho}{2\pi}\int_0^a\int_0^{2\pi} V_z(\vec{r}_s)\frac{e^{ikR}}{R} r_s d\phi_s dr_s \,, \tag{2.9}$$

where ϕ_s and r_s define the coordinates of the source point and r, θ, and ϕ define the coordinates of the observation point, as shown in Figure 4. The vectors $\vec{r}$ and $\vec{r}_s$ can be expressed as

$$\vec{r} = r\sin\theta\cos\phi\,\vec{i} + r\sin\theta\sin\phi\,\vec{j} + r\cos\theta\,\vec{k}, \tag{2.10a}$$

$$\vec{r}_s = r_s\cos\phi_s\vec{i} + r_s\sin\phi_s\vec{j} \,, \tag{2.10b}$$

Reproduced with permission of the copyright owner. Further reproduction prohibited without permission.

which yields

$$R = \left[r^2 + r_s^2 - 2rr_s \sin\theta \cos(\phi - \phi_s)\right]^{\frac{1}{2}}. \tag{2.11}$$

In the far field, the above quantity is approximated by (Wallace, 1972)

$$R \cong r - r_s \sin\theta \cos(\phi - \phi_s), \tag{2.12}$$

in the exponential term and as $R \cong r$ in the $1/R$ term of Equation 2.9 (Junger and Feit, 1972). Substituting these approximations in Equation 2.9 yields the following far-field approximation for the sound pressure radiated from a baffled piston

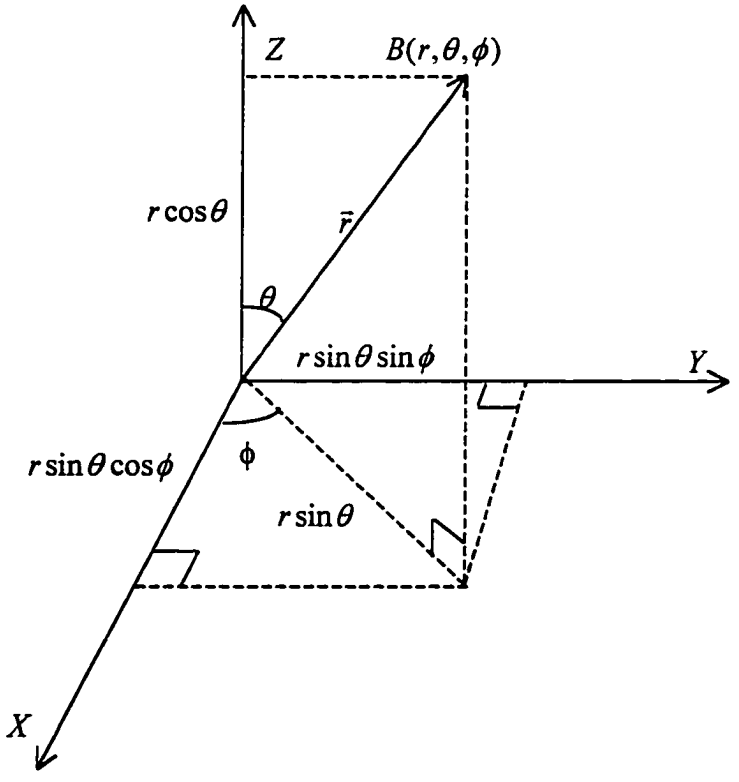

Figure 4. Observation Point B Coordinates.

Reproduced with permission of the copyright owner. Further reproduction prohibited without permission.

$$P_L(r,\theta,\phi) \cong \frac{-i\omega\rho}{2\pi} V_z \frac{e^{ikr}}{r} \int_0^a \int_0^{2\pi} \sin\theta \cos(\phi - \phi_s) r_s d\phi_s dr, \tag{2.13}$$

which can be written as

$$P_L(r,\theta) \cong \frac{-i\omega\rho}{(k\sin\theta)^2} V_z \frac{e^{ikr}}{r} \int_0^{ka\sin\theta} \tau J_0(\tau) d\tau, \tag{2.14}$$

where $\tau = kr_s \sin\theta$ and J_0 represents the Bessel function of the first kind. Using the equality $\int \tau J_0(\tau) d\tau = \tau J_1(\tau)$, the above equation reduces to

$$P_L(r,\theta) \cong \frac{i\omega\rho e^{-ikr}}{r} V_z a^2 \frac{J_1(ka\sin\theta)}{ka\sin\theta}. \tag{2.15}$$

As in the case of the beam, the acoustic power is approximated by

$$W_L \cong \int_0^{2\pi} \int_0^{\pi/2} \frac{|P_L(\vec{r})|^2}{2\rho c} r^2 \sin\theta d\theta d\varphi. \tag{2.16}$$

Local Volume Displacement Cancellation

To demonstrate the local volume displacement concept, the beam is divided into two sections, as shown in Figure 5. The volume displacement of each section is defined as the integral of its displacement over the surface such that

$$D_b = b \int_{x_1}^{x_2} z(x) dx, \tag{2.17}$$

Reproduced with permission of the copyright owner. Further reproduction prohibited without permission.

where $z(x)$ is the displacement distribution along the segment defined by x_1 and x_2 . For the first section, $x_1 = 0$ and $x_2 = \ell/2$ and for the second section, $x_1 = \ell/2$ and $x_2 = \ell$. The volume displacement of a loudspeaker is defined by the quantity D_L. To cancel the volume displacement of a section of the beam, the net volume displacement of the combined beam-section and loudspeaker is set to zero

$$D_b + D_L = 0, \tag{2.18}$$

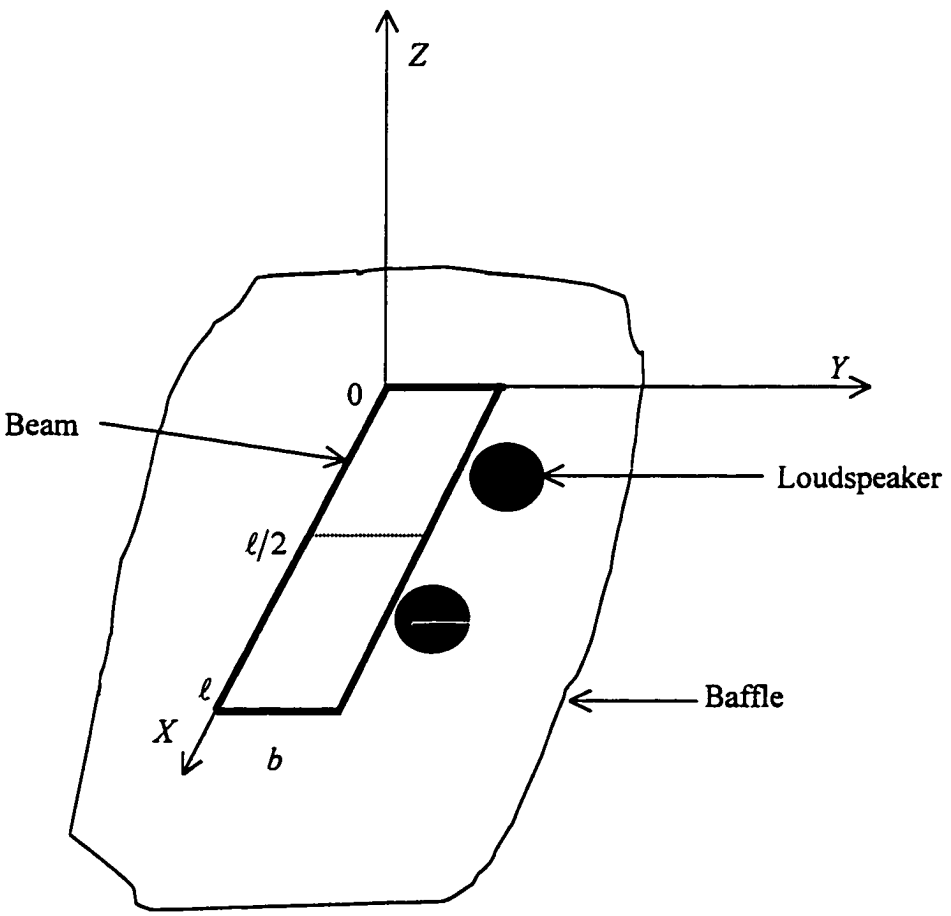

Figure 5. Baffled Beam With Two Loudspeakers.

Reproduced with permission of the copyright owner. Further reproduction prohibited without permission.

or

$$D_L = -D_b. \tag{2.19}$$

Thus, for each loudspeaker, the volume displacement will be

$$D_L = -b\int_{x_1}^{x_2} z(x)\,dx, \tag{2.20}$$

where D_L represents the volume displacement of the loudspeaker immediately next to the section defined by x_1 and x_2. In the system depicted in Figure 5, coupling between the loudspeakers themselves and the loudspeakers and the beam is neglected. This is due to the fact that the vibration and radiation of the beam do not affect the loudspeakers and vice versa. Under these conditions, the total acoustic pressure at an observation point B is

$$P = P_b + P_L. \tag{2.21}$$

This will normally result in pressure reduction at some points in the field and pressure enhancement at other points (Johnson & Elliott, 1993). However, there will be a reduction in the average acoustic pressure of the noise field above the beam. The numerical simulation detailed in the next section shows that the total average acoustic pressure P due to the cancellation loudspeakers and the beam is less than the acoustic pressure P_b radiated by the beam alone. Equation 2.6 shows that if the

Reproduced with permission of the copyright owner. Further reproduction prohibited without permission.

pressure is reduced throughout the field, then the acoustic power is also reduced. Therefore, the beam radiates less noise when control is applied to the loudspeakers.

Numerical Implementation

The acoustic pressure and power radiated by a baffled beam are computed. The results are used to simulate the local volume displacement cancellation concept. First, the finite element method is used to determine the vibration modes and the vibration response of the beam. Using a discretized form of the Rayleigh integral along with the vibration response, the sound pressure radiated by the beam is calculated. Then, the acoustic power is evaluated on a hemisphere above the baffle. The hemisphere, which encloses the beam, is divided into small patches. The pressure and the intensity are calculated at the center of each patch. The acoustic power is found by taking the sum of the intensity at the center of each patch multiplied by the area of the patch. The same technique is used to calculate the acoustic power radiated by the loudspeaker modeled as a baffled piston. Finally, the numerical experiment of local volume displacement cancellation is carried out.

Finite Element Analysis

The beam is divided into small elements (beam element) of equal length, as shown in Figure 6. Each element is considered an element of the beam, with nodal points located at each end of an element. The elements lay end to end and span the entire length of the beam, sharing nodes with adjacent elements. The motion or

Reproduced with permission of the copyright owner. Further reproduction prohibited without permission.

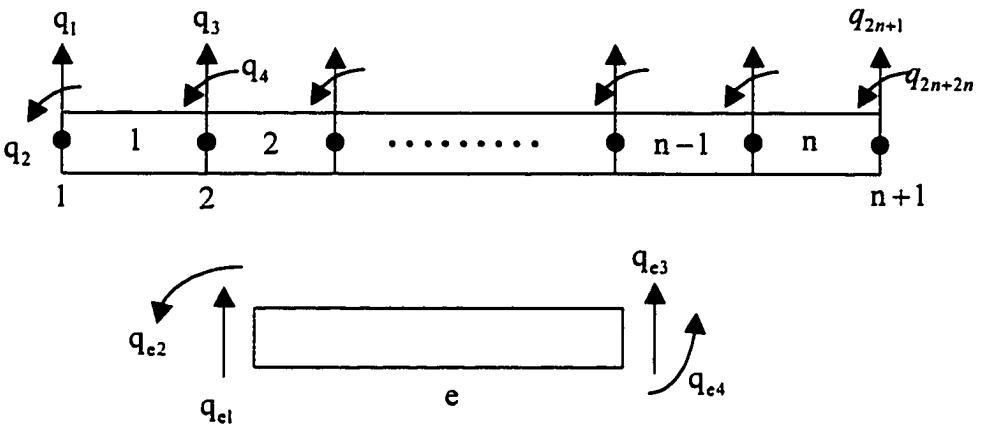

Figure 6. Finite Element Analysis of a Beam.

degrees of freedom imposed at the end of each element will determine the type of element displacement function to be used. For beam bending, the governing equation is a second order differential equation. Therefore, continuity through the first derivative must be satisfied. In this work, the degrees of freedom of node i are q_{2i-1} and q_{2i}. The degree of freedom q_{2i-1} is transverse displacement and q_{2i} is slope or rotation. The vector $\{q_e\}$ represents the local degrees of freedom and can be written as

$$\{q_e\} = [q_{e1}, q_{e2}, q_{e3}, q_{e4}]^T . \tag{2.22}$$

The Hermitian interpolation polynomials, which satisfy nodal value and slope-continuity, are used to represent the element displacement function (Chandrupatla & Belegundu, 1991). Each of the shape functions is of cubic order represented by

$$h_i = a_i\xi^0 + b_i\xi^1 + c_i\xi^2 + d_i\xi^3 \qquad (i = 1,2,3,4), \tag{2.23}$$

Reproduced with permission of the copyright owner. Further reproduction prohibited without permission.

where ξ is the natural coordinate which ranges between –1 to +1 within each element. The coefficients a_i, b_i, c_i, d_i are obtained by imposing the limiting conditions. Thus, the Hermite shape functions shown in Figure 7 are

$$
\begin{aligned}
h_1 &= \frac{1}{4}\left(2 - 3\xi + \xi^3\right) \\
h_2 &= \frac{1}{4}\left(1 - \xi - \xi^2 + \xi^3\right) \\
h_3 &= \frac{1}{4}\left(2 + 3\xi - \xi^3\right) \\
h_4 &= \frac{1}{4}\left(-1 - \xi + \xi^2 + \xi^3\right)
\end{aligned}
\tag{2.24}
$$

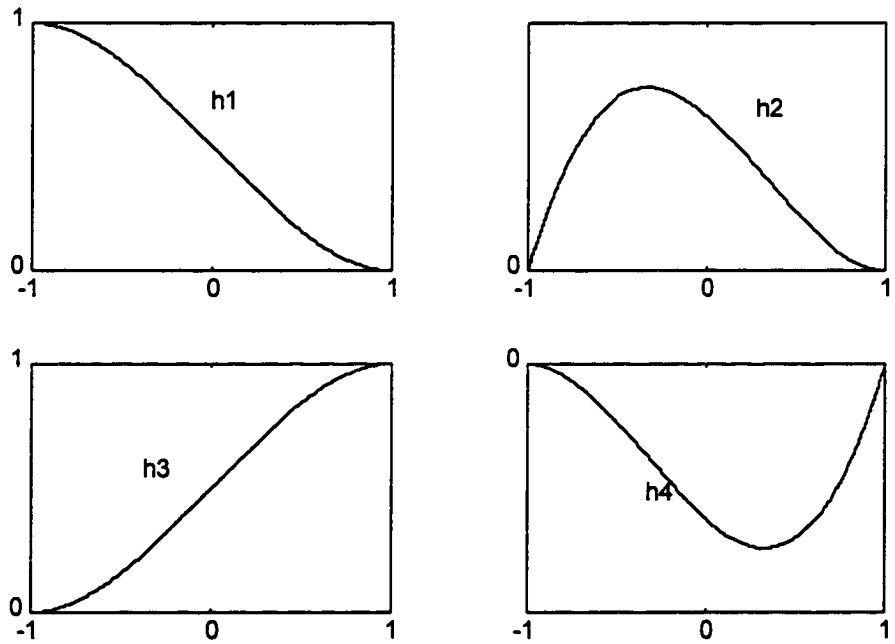

Figure 7. Hermite Shape Functions.

Reproduced with permission of the copyright owner. Further reproduction prohibited without permission.

These functions can be used to write the deflection $u(\xi)$ of the centroidal axis at ξ, in the form

$$u(\xi) = h_1 u_1 + h_2 \left(\frac{du}{d\xi}\right)_1 + h_3 u_2 + h_4 \left(\frac{du}{d\xi}\right)_2, \tag{2.25}$$

The coordinates transform by the relationship

$$x = \frac{1-\xi}{2} x_1 + \frac{1+\xi}{2} x_2 = \frac{x_1 + x_2}{2} + \frac{x_2 - x_1}{2} \xi, \tag{2.26}$$

where x is the location along the element, x_1 is the x location at node 1, and x_2 is the x location at node 2. Substituting the length $\ell_e = x_2 - x_1$, and differentiating Equation 2.26 gives,

$$dx = \frac{\ell_e}{2} d\xi. \tag{2.27}$$

The chain rule $du/d\xi = (du/dx)(dx/d\xi)$ yields

$$\frac{du}{d\xi} = \frac{\ell_e}{2} \frac{du}{dx}. \tag{2.28}$$

Noting that du/dx evaluated at nodes 1 and 2 is q_{e2} and q_{e4}, respectively, Equation 2.25 can be written as

$$u(\xi) = h_1 q_1 + \frac{\ell_e}{2} h_2 q_2 + h_3 q_3 + \frac{\ell_e}{2} h_4 q_4, \tag{2.29}$$

Reproduced with permission of the copyright owner. Further reproduction prohibited without permission.

which may be denoted as

$$u = \{h\}^T \{q_e\}, \tag{2.30}$$

where

$$\{h\} = \left[h_1, \frac{\ell_e}{2} h_2, h_3, \frac{\ell_e}{2} h_4 \right]^T. \tag{2.31}$$

Derivation of the Stiffness Matrix

The element strain energy can be written using Equation 2.29, in the form

$$\Pi_e = \frac{1}{2} EI \int_e \left(\frac{d^2 u}{dx^2} \right)^2 dx, \tag{2.32}$$

where E is the Young's Modulus of the material and I is the area moment of inertia of the element. From Equation 2.28

$$\frac{d^2 u}{dx^2} = \frac{4}{\ell_e^2} \frac{d^2 u}{d\xi^2}. \tag{2.33}$$

Then, substituting with $u = \{h\}^T \{q\}$ yields the matrix

$$\left[\frac{d^2 u}{dx^2} \right]^2 = \{q\}^T \frac{16}{l_e^4} \left\{ \frac{d^2 h}{d\xi^2} \right\} \left\{ \frac{d^2 h}{d\xi^2} \right\}^T \{q\}, \tag{2.34}$$

where

Reproduced with permission of the copyright owner. Further reproduction prohibited without permission.

$$\left\{\frac{d^2h}{d\xi^2}\right\}=\left[\frac{3}{2}\xi,\frac{-1+3\xi}{2}\frac{\ell_e}{2},-\frac{3}{2}\xi,\frac{1+3\xi}{2}\frac{\ell_e}{2}\right]^T. \tag{2.35}$$

And the element strain energy becomes the following equation (Equation 2.36)

$$\Pi_e=\frac{1}{2}\{q\}^T\frac{8EI}{\ell_e^3}\int_{-1}^{+1}\begin{bmatrix} \frac{9}{4}\xi^2 & \frac{3}{8}\xi(-1+3\xi)\ell_e & -\frac{9}{4}\xi^2 & \frac{3}{8}\xi(1+3\xi)\ell_e \\ \frac{3}{8}\xi(-1+3\xi)\ell_e & \left(\frac{-1+3\xi}{4}\right)^2\ell_e^2 & -\frac{3}{8}\xi(-1+3\xi)\ell_e & \frac{-1+9\xi^2}{16}\ell_e^2 \\ -\frac{9}{4}\xi^2 & -\frac{3}{8}\xi(-1+3\xi)\ell_e & \frac{9}{4}\xi^2 & -\frac{3}{8}\xi(1+3\xi)\ell_e \\ \frac{3}{8}\xi(1+3\xi)\ell_e & \frac{-1+9\xi^2}{16}\ell_e^2 & -\frac{3}{8}\xi(1+3\xi)\ell_e & \left(\frac{1+3\xi}{4}\right)^2\ell_e^2 \end{bmatrix}d\xi\{q\}$$

Each term in the matrix is integrated. Also

$$\int_{-1}^{1}\xi^2d\xi=\frac{2}{3}\qquad\int_{-1}^{1}\xi d\xi=0\qquad\int_{-1}^{1}d\xi=2. \tag{2.37}$$

This results in the element strain energy given by

$$\Pi_e=\frac{1}{2}\{q\}^T\{K^e\}\{q\}, \tag{2.38}$$

where the element stiffness matrix $[K^e]$ is

$$[K^e]=\frac{EI}{\ell_e^3}\begin{bmatrix} 12 & 6\ell_e & -12 & 6\ell_e \\ 6\ell_e & 4\ell_e^2 & -6\ell_e & 2\ell_e^2 \\ -12 & -6\ell_e & 12 & -6\ell_e \\ 6\ell_e & 2\ell_e^2 & -6\ell_e & 4\ell_e^2 \end{bmatrix}. \tag{2.39}$$

Reproduced with permission of the copyright owner. Further reproduction prohibited without permission.

The total strain energy is the sum of the element strain energies, such that

$$\Pi = \sum_e \Pi_e = \sum_e \frac{1}{2} EI \int_e \left(\frac{d^2 u}{dx^2} \right)^2 dx , \tag{2.40}$$

using Equation 2.38, the total strain energy can be written as

$$\Pi = \sum_e \Pi_e = \sum_e \frac{1}{2} \{q_e\}^T [K^e] \{q_e\} = \frac{1}{2} \{q\}^T [K] \{q\} , \tag{2.41}$$

where $[K]$ is the global stiffness matrix and $\{q\}$ is the global nodal velocity vector.

Derivation of the Mass Matrix

A solid body with distributed mass is considered in Figure 8. The kinetic energy is given by

$$T = \frac{1}{2} \int_V v^2 \rho dV , \tag{2.42}$$

where ρ is the density of the material and v is the velocity field defined over the entire body. In the dynamic finite element method, the body is divided into elements, and in each element, v is expressed in terms of the nodal velocity vector $\{\dot{q}_e\}$, using shape functions $\{h\}$. Thus the velocity is given by

$$v = \{h\}^T \{\dot{q}_e\} . \tag{2.43}$$

Reproduced with permission of the copyright owner. Further reproduction prohibited without permission.

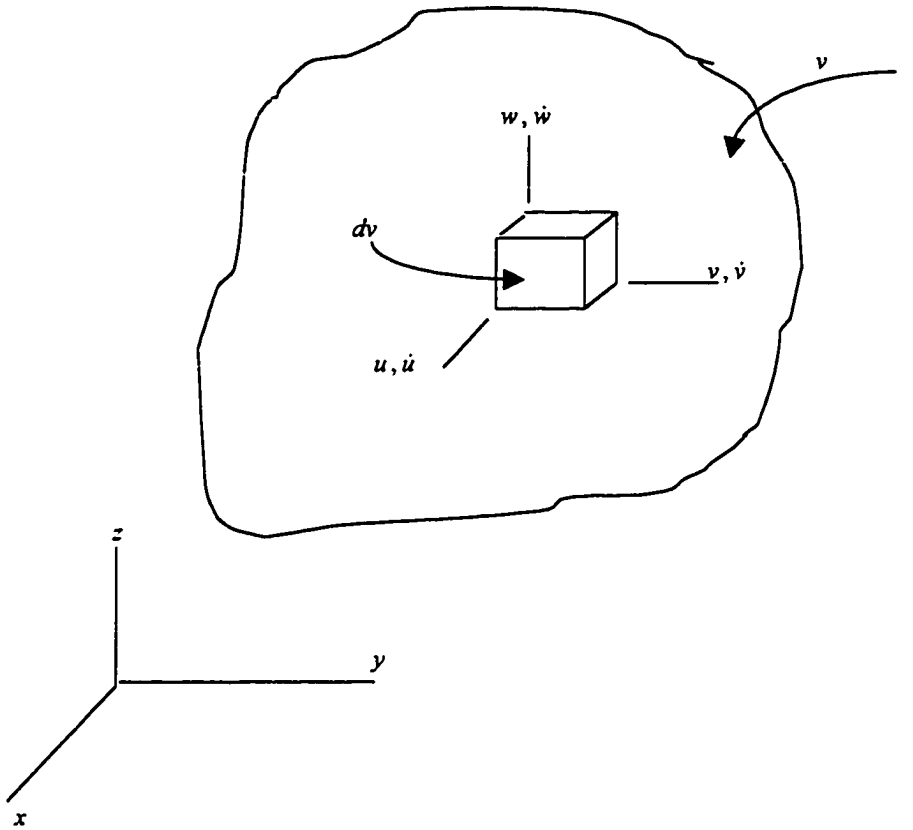

Figure 8. Body With Distributed Mass.

Substituting the above equation into the kinetic energy equation for a single element e, gives

$$T_e = \frac{1}{2}\{\dot{q}_e\}^T \left[\int_{V_e} \rho \{h\}\{h\}^T \, dV \right] \{\dot{q}_e\}, \tag{2.44}$$

where the bracketed expression is the element mass matrix

$$[M^e] = \int_{V_e} \rho \{h\}\{h\}^T \, dV \, . \tag{2.45}$$

Reproduced with permission of the copyright owner. Further reproduction prohibited without permission.

Using Equation 2.27, the above equation can be written as

$$[M^e]=\int_{-1}^{+1}\{h\}\{h\}^T\,\rho A_e\,\frac{\ell_e}{2}\,d\xi, \tag{2.46}$$

which yields

$$[M^e]=\frac{\rho A_e \ell_e}{420}\begin{bmatrix} 156 & 22\ell_e & 54 & -13\ell_e \\ 22\ell_e & 4\ell_e^2 & 13\ell_e & -3\ell_e^2 \\ 54 & 13\ell_e & 156 & -22\ell_e \\ -13\ell_e & -3\ell_e^2 & -22\ell_e & 4\ell_e^2 \end{bmatrix}. \tag{2.47}$$

This mass matrix is consistent with the shape functions chosen and is called the consistent mass matrix. The summation over all the elements yields the total kinetic energy

$$T=\sum_e T_e=\sum_e \frac{1}{2}\{\dot{q}\}^T[M^e]\{\dot{q}\}=\frac{1}{2}\{q\}^T[M]\{\dot{q}\}. \tag{2.48}$$

where $[M]$ is the global mass matrix.

Computation of Vibration Modes

The total potential energy and the total kinetic energy are given by the Equations 2.41 and 2.48 respectively. Using the Lagrangian $L=T-\Pi$, in the following LaGrange's equation,

$$\frac{d}{dt}\left(\frac{\partial L}{\partial \dot{q}}\right)-\frac{\partial L}{\partial q}=0, \tag{2.49}$$

Reproduced with permission of the copyright owner. Further reproduction prohibited without permission.

the equation of motion for free vibration of the beam is obtained as

$$[M]\{\ddot{q}\}+[K]\{q\}=0\ . \tag{2.50}$$

Assuming harmonic motion, $\{q\}=\{U\}\sin\omega t$, the above equation can be written as follows

$$[K]\{U\}=\omega^2[M]\{U\}, \tag{2.51}$$

where $\{U$ is the vector of nodal amplitude of vibration and ω is the circular frequency of vibration. This is the generalized eigenvalue problem

$$[K]\{U\}=\lambda[M]\{U\}, \tag{2.52}$$

where $\{U$ is the eigenvector, representing the vibration mode, corresponding to the eigenvalue $\lambda=\omega^2$.

Computation of Vibration Response

The focus of this section is the response of the beam to an excitation. In general the response of a structure to an external force $\{f\}$ can be determined using the equation:

$$\{v\}=[Y(\omega)]\{f\}, \tag{2.53}$$

Reproduced with permission of the copyright owner. Further reproduction prohibited without permission.

where $\{v\}$ is the velocity vector and $[Y]$ the mobility. It can be shown – although not very easily! – that the mobility matrix is given(Ewins,1984) by

$$[Y]=\sum_{j=1}^{N}\frac{i\omega\{\phi_j\}\{\phi_j\}^T}{\omega_j^2-\omega^2+i\eta_j\omega_j^2}, \tag{2.54}$$

where ω is the frequency of excitation, $\{\phi_j\}$ is the mass normalized eigenvector corresponding to the j^{th} mode, ω_j is the eigenvalue corresponding to the j^{th} mode, $i=\sqrt{-1}$, and η_j is the damping ratio corresponding to the j^{th} mode.

Discretization of the Pressure Expression

The pressure expression given in Equation 2.1 can be discretized using a variety of techniques. The most obvious and the easiest to implement is one where the length of the beam is broken into elements of equal length and the beam surface velocity is approximated to be constant within each element. Another technique is one where the variation of the velocity within each element is approximated to be linear along the length of the element. Both of these techniques have a strong disadvantage. The constant velocity approximation results in a velocity profile that exhibits discontinuity of both velocity and its slope at the element boundaries (nodes) and the linear velocity approximation results in a velocity profile that exhibits discontinuity of slope at the element boundaries. Since the goal of this project is to find velocity profiles that are realistic enough, the continuity of both the velocity and its slope are to be maintained.

Reproduced with permission of the copyright owner. Further reproduction prohibited without permission.

Therefore, the discretization technique commonly used in modeling the vibration behavior of beams using the finite element concepts is used. This technique approximates the variations of the velocity and its slope using cubic Hermitian polynomials to maintain their continuity across element boundaries (Chandrupatla & Belegundu, 1991). The length of the beam is divided into n equal elements as shown in Figure 6. Each element has two nodes with two degrees of freedom at each node (normal velocity and its slope).

The surface source along the length of the beam ℓ is then expressed in terms of natural coordinate ξ which ranges between -1 to +1 within each element. The Hermite shape functions from Equation 2.24 are used. Substituting Equation 2.43 in Equation 2.1 yields

$$p(x',y',z') = \frac{-i\omega\rho_f b}{2\pi} \sum_{e_i}^{n} \int_{-1}^{+1} \{h\}^T \{v_i\} \frac{e^{ikR}}{R} \frac{\ell_e}{2} d\xi, \tag{2.55}$$

where $\{v_e\} = \{\dot{q}_e$ from Equation 2.24. Taking $\{v_i$ out of the integral

$$p(x',y',z') = \frac{-i\omega\rho b}{2\pi} \sum_{e_i}^{n} \left[\int_{-1}^{+1} \{h\}^T \frac{e^{ikR}}{R} \frac{\ell_e}{2} d\xi \right] \{v_i\}. \tag{2.56}$$

The above expression can be re-written as

$$p(x',y',z') = \sum_{e_i}^{n} \{g_{ei}\}^T \{v_i\}, \tag{2.57}$$

where

Reproduced with permission of the copyright owner. Further reproduction prohibited without permission.

$$\{g_{ei}\}=\frac{-i\omega\rho b}{2\pi}\frac{\ell_e}{2}\int_{-1}^{+1}\{h\}\frac{e^{ikR}}{R}d\xi\,. \tag{2.58}$$

Thus, Equation 2.57 can be written as

$$p(x',y',z')=\{g\}^T\{v\}, \tag{2.59}$$

where $\{g\}$ is the global radiation vector and $\{v\}$ is the global velocity vector.

To demonstrate how the global vector $\{g\}$ relates to its elements, the example of a two-element beam model as shown in Figure 9, will be used where

$$p(x',y',z')=\sum_{1}^{2}\{g_{ei}\}^T\{v_i\}=\{g_{e1}\}^T\{v_1\}+\{g_{e2}\}^T\{v_2\}, \tag{2.60}$$

or

$$p(x',y',z')=\left[g_{e1}^1,g_{e1}^2,g_{e1}^3,g_{e1}^4\right]\begin{Bmatrix}v_1^1\\ \theta_1^1\\ v_1^2\\ \theta_1^2\end{Bmatrix}+\left[g_{e2}^1,g_{e2}^2,g_{e2}^3,g_{e2}^4\right]\begin{Bmatrix}v_2^2\\ \theta_2^2\\ v_2^3\\ \theta_2^3\end{Bmatrix}, \tag{2.61}$$

where the superscripts, in the radiation vector correspond to the Hermite shape function and in the velocity vector refer to the node number of the element. The subscripts correspond to the element number in both the vectors. Equation 2.60 can also be written as

Reproduced with permission of the copyright owner. Further reproduction prohibited without permission.

$$p(x',y',z')=\left[g_{e1}^{1},g_{e1}^{2},\left(g_{e1}^{3}+g_{e2}^{1}\right),\left(g_{e1}^{4}+g_{e2}^{2}\right),g_{e2}^{3},g_{e2}^{4}\right]\begin{Bmatrix}v_1\\ \theta_1\\ v_2\\ \theta_2\\ v_3\\ \theta_3\end{Bmatrix}. \tag{2.62}$$

Transformation of R from local to global coordinates is done using

$$\xi=\frac{2(x-x_j)}{\ell_e}-1, \tag{2.63}$$

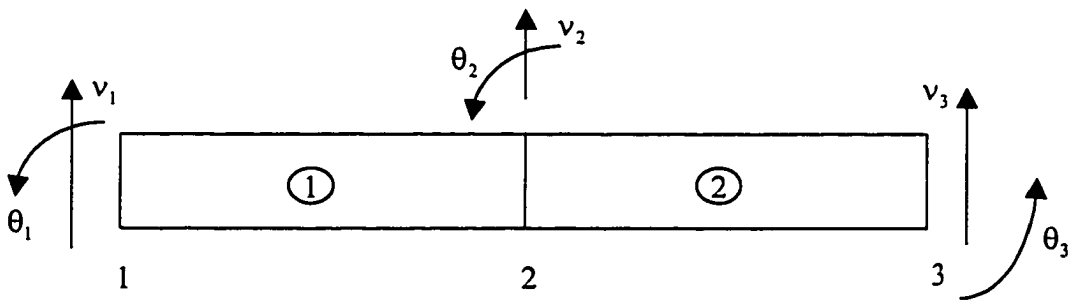

Figure 9. Two-Element Beam Model.

and

$$x=(\xi+1)\frac{\ell_e}{2}+x_j, \tag{2.64}$$

where $\ell_e=x_{j+1}-x_j$.

Reproduced with permission of the copyright owner. Further reproduction prohibited without permission.

Substituting these values in Equation 2.2 yields

$$R_j=\left[\left\{\xi\frac{(x_{j+1}-x_j)}{2}+\frac{(x_{j+1}-x_j)}{2}+x_j-x'\right\}^2+y'^2+z'^2\right]^{1/2}. \tag{2.65}$$

Equation 2.65 can be re-written as

$$R_j=\left[\left\{\xi\frac{(x_{j+1}-x_j)}{2}+\frac{(x_{j+1}-x_j)}{2}-x'\right\}^2+y'^2+z'^2\right]^{1/2}. \tag{2.66}$$

The value of R is substituted in Equation 2.58 and yields

$$\{g_{ei}\}=\frac{-i\omega\rho b}{2\pi}\frac{\ell_e}{2}\int_{-1}^{1}\{h\}\frac{e^{ik\left[\left\{(\xi+1)\frac{\ell_e}{2}+x_j-x'\right\}^2+y'^2+z'^2\right]^{1/2}}}{\left[\left\{(\xi+1)\frac{\ell_e}{2}+x_j-x'\right\}+y'^2+z'^2\right]^{1/2}}d\xi. \tag{2.67}$$

Numerical Results and Verification

An Active Noise Control Package (ANCPACK) is developed for a baffled beam and loudspeakers. The package is built using Matlab® (The MathWorks, Inc.) and is composed of four modules: vibration, radiation, control and sensor design. The first three modules are discussed in this chapter. The sensor design module is presented in Chapter III. The vibration and radiation modules are based on the finite element formulation presented in the preceding sections. The program is capable of performing a free and forced vibration analysis of a baffled beam with the commonly encountered boundary conditions such as clamped, hinged, free, clamped-free and clamped-hinged.

Reproduced with permission of the copyright owner. Further reproduction prohibited without permission.

It can also compute the acoustic pressure and power radiated by a baffled piston and a baffled beam with the boundary conditions mentioned above.

Free Vibration

The vibration module is composed of free vibration and forced vibration programs. The forced vibration is verified in Chapter IV using experimental data. The free vibration module is checked by calculating the natural frequencies of an aluminum $\left(E = 7e10Pa, \rho = 2700\text{kg/m}^3\right)$ beam of length $\ell = 1.016m$, width $b = 0.038m$, and height $h = 0.0127m$. The results are checked against those presented by Harris (1995). The results of Table 1, obtained using ANCPACK, are in agreement with the natural frequencies published by Harris. Also, the mode shapes of the first two modes of a hinged and clamped beam are presented in Figure 10. These shapes are in close agreement with those given by Harris.

Acoustic Pressure

The radiation module is checked using the rectangular rigid piston formulation given by Junger and Feit (1972). The pressure at any point in space due to a rectangular rigid piston is given as

$$p(R,\theta,\phi) = \frac{2L_x L_y \hat{a}\rho e^{ikR}}{\pi R} j_0\left(kL_x \sin\theta\cos\phi\right) j_0\left(kL_y \sin\theta\sin\phi\right), \tag{2.68}$$

where R is the radius from the center of the rectangular piston to the observation point, θ is the angle between the observation point plane and the z-axis, ϕ is the inclination of

Reproduced with permission of the copyright owner. Further reproduction prohibited without permission.

Table 1

Natural Frequencies of a Uniform Beam

Support	Modes	Frequencies (Hz)	
		Harris	ANCPACK
Hinged-hinged	1	28.41	28.41
	2	113.62	113.63
	3	255.66	255.66
	4	454.50	454.55
	5	710.15	710.34
Clamped-clamped	1	63.91	64.39
	2	177.54	177.51
	3	347.98	348.00
	4	575.22	575.32
	5	859.29	859.61
Clamped-hinged	1	44.38	44.38
	2	143.81	143.81
	3	300.04	300.05
	4	513.09	513.16
	5	782.95	783.19
Clamped-free	1	10.10	10.12
	2	63.91	63.19
	3	177.54	177.58
	4	347.98	348.00
	5	575.22	575.32
Free-free	1	Rigid body mode	Rigid body mode
	2	Rigid body mode	Rigid body mode
	3	177.54	177.55
	4	347.98	348.00
	5	575.22	575.32

the observation point with respect to the y-axis, $2L_x$ is the width of the plate along the $x-$axis, $2L_y$ is the length of the plate along the $y-$axis, $\hat{a}$ is the plate acceleration, ρ is the density of the fluid, j_o is the spherical Bessel function, and k the wave number of the of excitation frequency. The comparisons are performed for a rectangular piston

Reproduced with permission of the copyright owner. Further reproduction prohibited without permission.

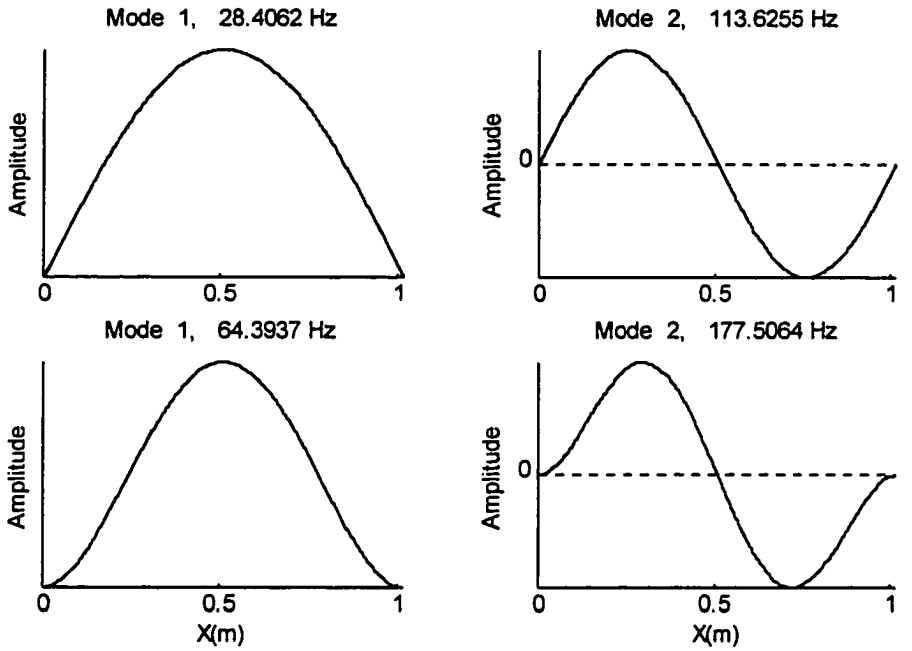

Figure 10. Mode Shapes of Hinged Beam (Top) and Clamped Beam (Bottom).

moving at velocity of $1 m/s$. The pressure is calculated at a point directly above the center of the piston $\theta = \phi = 0$. The acoustic pressure at the observation point $(R, \theta = 0, \phi = 0)$ can be written as

$$p(R, \theta = 0, \phi = 0) = \frac{2L_x L_y \hat{a} \rho e^{ikR}}{\pi R}. \tag{2.69}$$

The following values are used to calculate the pressure at different frequencies: $R = 10m$, $2L_x = 0.5m$, $2L_x = 1m$, $c = 343 m/s$, $\rho = 1.21 kg/m^3$. A plot of the values predicted from the above equation versus those predicted from the computer program (assuming uniform beam displacement) at different frequencies is shown in Figure 11.

Reproduced with permission of the copyright owner. Further reproduction prohibited without permission.

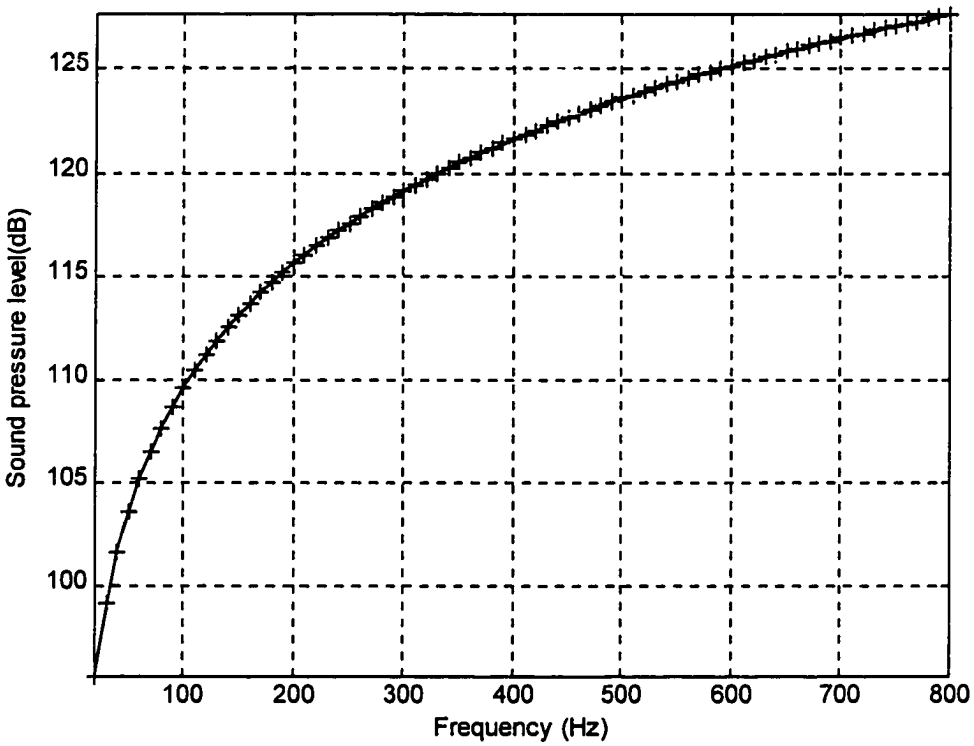

Figure 11. Plot of Values Predicted From Equation 2.59 (Solid) Versus the Analytical Values From Equation 2.69 (++++).

The pressure is computed in *Pascals* (Pa) and converted to decibel (dB) scale using the following equation

$$P(dB) = 20\log_{10}\left(\frac{p(Pa)}{2e^{-5}}\right). \tag{2.70}$$

The values obtained are in close agreement. Thus, the radiation module is reliable for predicting the sound pressure radiated from a baffled beam. This module is further checked in the next section when the acoustic power is calculated from the acoustic pressure (Equation 2.6)

Reproduced with permission of the copyright owner. Further reproduction prohibited without permission.

Acoustic Power

The acoustic power is calculated from Equation 2.6. This equation can be approximated as

$$W_b = \sum_{i=1}^{N} \frac{P_i^2 s_i}{2\rho c}, \tag{2.71}$$

where s_i is the surface area of the i^{th} patch on a hemisphere above the baffle and enclosing the beam, as shown in Figure 12, P_i is the acoustic pressure at the center of the patch and N the total number of patches on the hemisphere. To check the validity of the above technique used to calculate the sound power, the radiation efficiency is evaluated and compared to the analytical results predicted by Wallace (1972) for a hinged beam. The radiation efficiency of the baffled beam is defined by

$$\sigma(\omega) = \frac{W(\omega)}{\rho c b l} \frac{1}{\left\langle \left| U_\omega^2 \right| \right\rangle}, \tag{2.72}$$

where ω is the vibration frequency, $W(\omega)$ is the acoustic power at ω and $\left\langle \left| U_\omega^2 \right| \right\rangle$ denotes the mean-square velocity average over the surface of the beam at ω. For a hinged beam, Wallace has shown that

$$\left\langle \left| U_\omega \right|^2 \right\rangle = \frac{1}{4} U_m^2, \tag{2.73}$$

Reproduced with permission of the copyright owner. Further reproduction prohibited without permission.

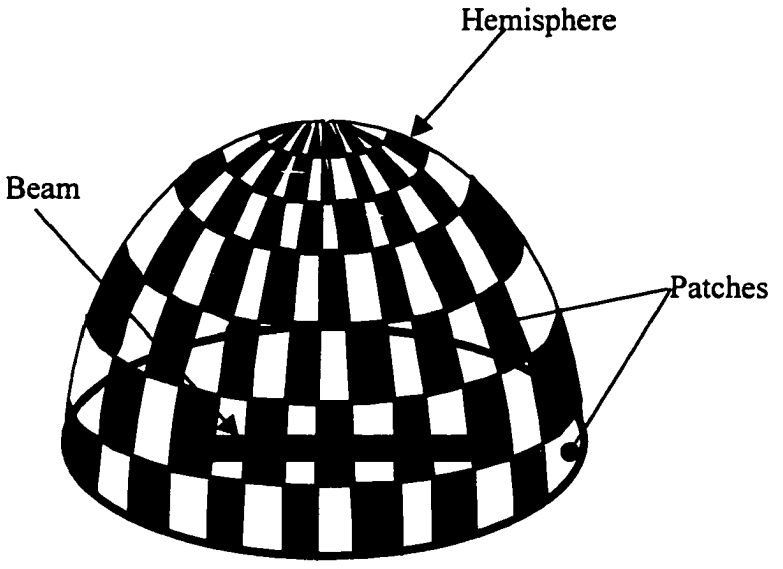

Figure 12. Hemisphere on Which the Acoustic Power is Calculated.

where U_m is the amplitude of the velocity profile of the surface of the beam. The radiation is computed and plotted against the non-dimensional frequency written as

$$\frac{k\ell}{n\pi}, \tag{2.74}$$

where k is the wave number of vibration, ℓ the length of the beam, and n the mode number. From Wallace plots, the radiation efficiency of a hinged beam with width to length ratio of 1/8 is found for $kl/n\pi = 0.1$. The radiation efficiency values are calculated by the program for the same beam ($b/\ell = 1/8$, $k\ell/n\pi = 0.1$) and compared to the values presented by Wallace in graphical form. The results presented in Table 2 show that the errors are within acceptable ranges.

Reproduced with permission of the copyright owner. Further reproduction prohibited without permission.

Table 2

Radiation Efficiency of a Hinged Beam ($b/\ell = 1/8, k\ell/n\pi = 0.1$)

Mode number	Wallace	ANCPACK	Errors (%)
1	0.0017	0.002	17
2	Not available	0.000065	-------
3	0.0015	0.00182	21
4	0.0002	0.000199	0.5
5	0.0013	0.00181	39
6	0.0004	0.000432	8
7	0.0011	0.00162	47
8	0.0006	0.00055	0.8
9	0.0009	0.001035	15
10	0.0008	0.000729	8.8

Loudspeaker Acoustic Power

Finally, the acoustic power radiated by the loudspeaker is calculated by the program and checked against the analytical value. Substituting Equation 2.15 into Equation 2.16 yields the following acoustic power expression of a baffled piston (Junger & Feit, 1972).

$$W \cong \frac{1}{2\rho c}\frac{k^2(\rho c)^2}{4}V_z^2 a^4 \int_0^{\frac{\pi}{2}} \frac{1}{r^2}\left[\frac{2J_1(ka\sin\theta)}{ka\sin\theta}\right]^2 r^2 2\pi \sin\theta d\theta . \qquad (2.75)$$

performing the above integration gives

Reproduced with permission of the copyright owner. Further reproduction prohibited without permission.

$$W \cong \frac{\rho c v^2 a^2 \pi}{2}\left[1 - \frac{J_1(2ka)}{ka}\right]. \tag{2.76}$$

Figure 13 represents the acoustic power radiated by a baffled piston using Equations 2.71 and 2.74. The plots show good agreement between the power calculated by the radiation module and the analytical values predicted by Equation 2.74. The power is calculated in *watts* (w) and converted to decibel scale using the following

$$w(dB) = 10\log_{10}\left(\frac{w\left(N/m^2\right)}{1e^{-12}}\right). \tag{2.77}$$

Local Volume Displacement Cancellation

From Equation 2.21, Johnson and Elliott concluded that the total average acoustic pressure radiated in the hemisphere S' (Figure 12) by the beam and the cancellation loudspeakers is less than the total pressure radiated by the baffled beam alone. Consequently, the average power radiated by the loudspeaker-beam system is minimized. This conclusion is numerically demonstrated in this section. A clamped baffled beam (1.016m long, 0.038m wide, 0.0127, thick) is utilized. First, the acoustic power radiated by the beam is calculated using Equation 2.71. The excitation frequency ranges from 10 to 800 Hz, including up to the fourth mode of the beam, 573.32Hz (Table 1). The local volume displacement cancellation theory is then applied.

Reproduced with permission of the copyright owner. Further reproduction prohibited without permission.

Naghshineh and Mason (1996) suggested that one cancellation device be used for each half wavelength of the structural vibrations. Therefore, four cancellation loudspeakers will be used and the beam will be divided into four sections. The

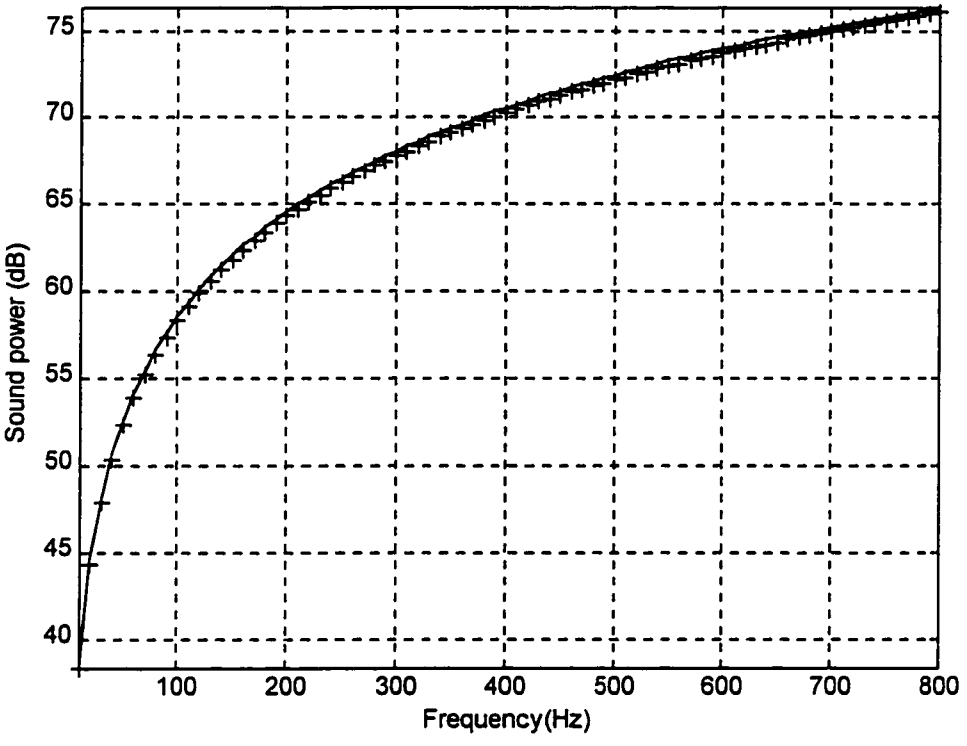

Figure 13. Plot of Values Predicted From Equation 2.71 (Solid) Versus the Analytical Values From Equation 2.76 (++++).

volume displacement of each beam section is calculated. The volume displacement of a loudspeaker in the immediate proximity of a section is chosen to be the negated volume displacement of that section. The total acoustic power of the loudspeaker-beam system is then calculated. Figure 14 shows the total acoustic power radiated by the beam alone and the total acoustic power radiated by the beam and the cancellation

Reproduced with permission of the copyright owner. Further reproduction prohibited without permission.

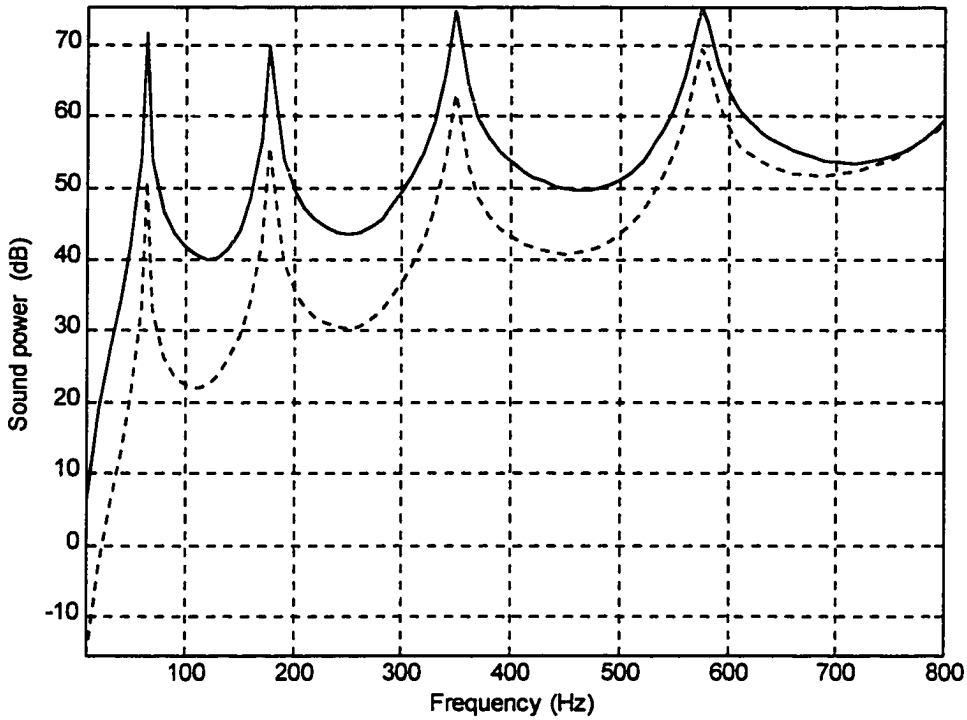

Figure 14. Total Acoustic Power Radiated by the Beam Alone (Solid) and the Total Acoustic Power Radiated by the Beam and the Cancellation Loudspeakers (Dashed).

loudspeakers. The results indicate a net reduction in the total acoustic power when control loudspeakers are used.

Summary

A method has been described for reducing the noise radiated by a beam in an infinite baffle. The strategy adopted was to divide the beam into sections. A loudspeaker (modeled as a baffled piston) was placed next to each beam-section. The volume displacement needed by the loudspeaker for successful noise cancellation was

Reproduced with permission of the copyright owner. Further reproduction prohibited without permission.

calculated (Equation 2.20) by setting the net volume displacement of the section and the loudspeaker immediately next to it to zero (Equation 2.18). Using four loudspeakers, this principle was applied to a baffled clamped beam with four sections. The volume displacements of each of the four sections of the beam were calculated and used to respectively drive the loudspeakers. The total acoustic power radiated by the beam was calculated and compared to the total acoustic power radiated by the beam and the cancellation loudspeakers. The results, presented in Figure 14, showed a significant reduction of the acoustic power radiated by the beam when its volume displacement was actively cancelled. These theoretical and numerical developments agree with the findings of Naghshineh and Mason (1996) on the local volume displacement cancellation of a wide area structure .

The local volume displacement cancellation conclusions were drawn without reference to the measurement of the control variables. It was assumed that these variables (volume displacement) were known or could be measured. The next chapter details the theoretical development and numerical simulation of sensors that will measure the volume displacement of the beam and loudspeakers.

Reproduced with permission of the copyright owner. Further reproduction prohibited without permission.

CHAPTER III

VOLUME DISPLACEMENT SENSOR DEVELOPMENT

Introduction

After showing that acoustic power attenuation can be achieved through local volume displacement cancellation, the sensing problem is addressed in this chapter. Volume displacement sensors for the beam and the loudspeaker are developed. For the beam, the goal is to design a sensor that accurately measures the volume displacement over any segment of the beam. Two approaches are used for sensing the volume displacement of a beam. The first is the adaptation of the techniques presented by Lee and Moon (1990) and Guigou et al. (1994). In the second approach, the formulation presented by Rex (1991) and Johnson and Elliott (1993) is adopted.

In the method used by Guigou et al (1994), the total volume displacement of the beam and the output charge of the PVDF are expressed in modal superposition form. The sensor shape is obtained by equating the total volume displacement of the beam to the output charge of a single PVDF sensor. The resulting equation yields a unique shape of PVDF sensor for a given set of boundary conditions. Johnson and Elliott (1993) expressed the PVDF output charge in quadratic form to measure volume displacements of a beam. Unlike the previous design, the quadratic approach gives many sensor shapes for each boundary condition. The previous researchers

Reproduced with permission of the copyright owner. Further reproduction prohibited without permission.

designed sensors to measure the volume displacement of the entire length of the beam. In this work, sensors are developed to measure the volume displacement of any arbitrary segment of the beam.

Both PVDF sensor design methodologies, modal form and quadratic form, are presented here. The sensors are checked with numerical simulation first. Then, they are fabricated and experimentally verified. The experimental verification is presented in the next chapter. Finally, the development of the volume displacement sensor for the loudspeaker is presented in the last section of this chapter.

Total Volume Displacement Sensor Development for Beams

Recent publications by Guigou et al. (1994), Johnson and Elliott (1993), and Charette et al. (1998) have introduced the concept of the active control of sound radiated from structures by sensing and controlling the total volume displacement of the structure. These researchers used a single continuous sensor made of Polyvinylidene Fluoride (PVDF) which can be shaped so that it provides a measurement of the total volume displacement of a vibrating beam. In the work presented here, techniques (similar to those described by these authors for sensing total volume displacement of a vibrating beam) are developed to measure the local volume displacement corresponding to each (arbitrary) section of a vibrating beam.

Reproduced with permission of the copyright owner. Further reproduction prohibited without permission.

Modal Expansion

Lee and Moon (1990) reported the electrical charge of an arbitrarily shaped PVDF sensor applied to a beam of length ℓ as

$$Q = -\frac{h_b + h_s}{2} e_{31} \int_0^{\ell} \int_{-F(x)}^{+F(x)} u''(x) dy dx , \tag{3.1}$$

which can be written as

$$Q = -(h_s + h_b) e_{31} \int_0^{\ell} F(x) u''(x) dx , \tag{3.2}$$

where, h_b and h_s are respectively the beam and the PVDF sensor thicknesses, e_{31} is the PVDF sensor stress/charge coefficient, $u''(x)$ is the second derivative of the beam surface displacement field $u(x)$ with respect to x, and $F(x)$represents the function describing the shape of the PVDF sensor as shown in Figure 15. This shape actually covers the beam surface between $-F(x)$ and $+F(x)$ (symmetric with respect to the center line of the beam). As indicated by Charette et al. (1998), negative values of $F(x)$ correspond to an inversion of the PVDF film polarity.

Lee and Moon (1990) approximated $F(x)$ by expanding it as a function of the second derivatives of the mode shapes of the vibrating beam as

Reproduced with permission of the copyright owner. Further reproduction prohibited without permission.

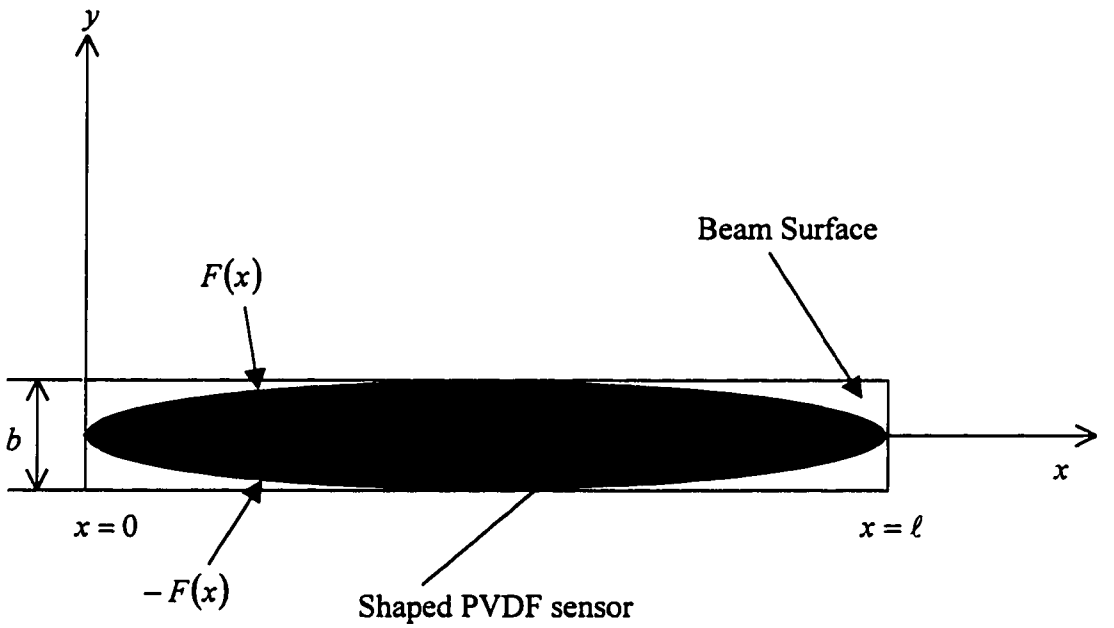

Figure 15. Top View of the Beam With Shaped PVDF Sensor.

$$F(x) \cong \sum_{i=1}^{N} \alpha_i \phi_i''(x), \tag{3.3}$$

where the α_i are unknown (sensor) shape coefficients and N is the number of modes in the approximation. Expressing the displacement field $u(x)$, using the modal expansion, we can write

$$u(x) \cong \sum_{n=1}^{N} \hat{W}_n \phi_n(x), \tag{3.4}$$

Reproduced with permission of the copyright owner. Further reproduction prohibited without permission.

where the ϕ_n are the mass-normalized modal displacement functions, the $\hat{W}_n$ are the modal participation factors, and the subscript n refers to the n^{th} mode. This equation can be expressed in the discretized form (Ewins, 1984)

$$\{u\} \cong \sum_{n=1}^{N} \frac{\{\phi_n\}\{\phi_n\}^T\{f\}}{\omega_n^2 - \omega^2 + i\eta_n\omega_n^2}, \tag{3.5}$$

where $\{\phi_n$ and $\{u\}$ are now vectors, $\{f\}$is a harmonic excitation force vector at frequency ω, the ω_n are the beam's natural frequencies, the η_n are the modal damping loss factors (obtained experimentally), and $i = \sqrt{-1}$. From the modal expansion of $u(x)$, Equation 3.2 can be written as

$$Q = -(h_b + h_s)e_{31}\sum_{n=1}^{N}\hat{W}_n\int_0^{\ell}F(x)\phi_n''(x)dx, \tag{3.6}$$

Replacing $F(x)$ with its modal expansion form yields

$$Q = -(h_b + h_s)e_{31}\sum_{i=1}^{N}\alpha_i\sum_{n=1}^{N}\hat{W}_n\int_0^{\ell}\phi_i''(x)\phi_n''(x)dx, \tag{3.7}$$

the above equation may be written in matrix form as

$$Q \cong \{\hat{w}\}^T[R]\{\alpha\} \quad \text{with} \quad R_{ni} = -(h_b + h_s)e_{31}\int_0^{\ell}\phi_i''(x)\phi_n''(x)dx, \tag{3.8}$$

Reproduced with permission of the copyright owner. Further reproduction prohibited without permission.

where $[R]$ is an N-by-N matrix with elements R_{ni} and $\{\hat{w}\}$ is the column vector of $\hat{W}_n$ and $\{\alpha\}$ is an N-by-1 vector. The volume displacement of the beam is defined as the integral of its surface displacement over the surface so that

$$D = b\int_0^{\ell} u(x)dx\,. \tag{3.9}$$

Using Equation 3.4, the above equation (Equation 3.9) becomes

$$D = b\sum_{i=1}^{N}\hat{W}_n\int_0^{\ell}\phi_n(x)dx\,, \tag{3.10}$$

The corresponding matrix formulation is

$$D \equiv \{\hat{w}\}^T\{d\} \quad \text{with} \quad d_n = b\int_0^{\ell}\phi_n(x)dx\,, \tag{3.11}$$

where b is the beam width and d_n represents the n^{th} element of the vector $\{d\}$. To construct a sensor that accurately measures the total volume displacement of the beam, set $Q = D$ for all displacement fields. This yields

$$[R]\{\alpha\} = \{d\}\,, \tag{3.12}$$

which is solved for the unknown (sensor) shape coefficients α_i. Since the beam mode shapes (and their second derivatives) are orthogonal over the length of the beam, the

Reproduced with permission of the copyright owner. Further reproduction prohibited without permission.

matrix $[R]$ is diagonal. Thus, the solution to Equation 3.12 is very simple. In addition, it can be shown that the coefficient α_1 corresponding to the first beam mode is dominant and dictates the shape of the sensor (Guigou et al., 1994). Using the above method, Guigou et al. (1994) obtained the PVDF sensor shape for different beam boundary conditions, as shown in Figure 16.

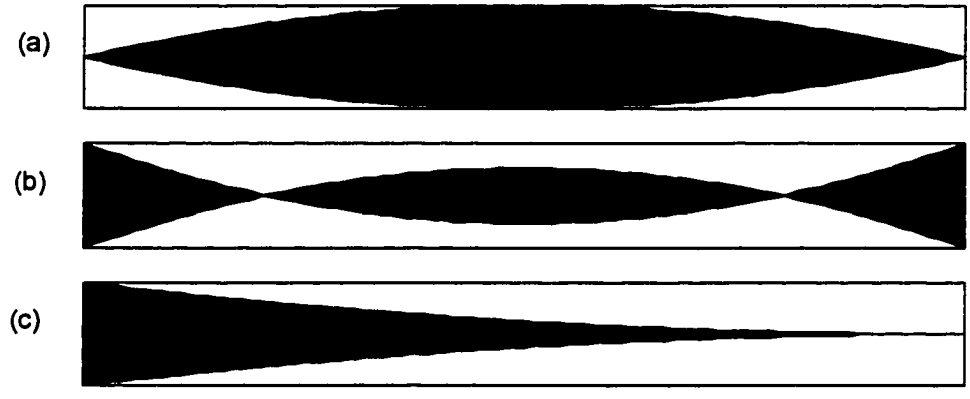

Figure 16. Total Volume Displacement PVDF Sensor for (a) Hinged, (b) Clamped, (c) Clamped-Free Beam.

Quadratic Form

In their investigation of the potential use of PVDF as a volume velocity sensor for active control of sound radiated from vibrating plates, Johnson and Elliott (1993) extended a formulation initially introduced by Rex (1991) for one-dimensional sensors. The equation of the output charge of the PVDF, Equation 3.2, is integrated by parts as follows

Reproduced with permission of the copyright owner. Further reproduction prohibited without permission.

$$Q = -(h_b + h_s)e_{31}\Big\{ \left[F(\ell)u'(\ell) - F'(\ell)u(\ell)\right] - \left[F(0)u'(0) - F'(0)u(0)\right] + \int_0^{\ell} F''(x)u(x)dx \Big\}. \quad (3.13)$$

Next, they defined the shape of the PVDF film (or its sensitivity) $F(x)$ to be quadratic in the x-direction and to be independent of y. Johnson and Elliott (1993) showed that the charge output of the PVDF sensor is a function of the integrated displacement (of the beam/plate) minus the net displacement along the $x = 0$ or $x = \ell$ edges. If the edges are not fixed, they concluded, additional transducers will be needed to measure the total displacement, but by assuming fixed edges, they simplify the problem to where only one sensor is required.

Johnson and Elliott's (1993) presentation can be expanded by writing the general expression for $F(x)$ such that $F''(x) = 2\kappa$ and

$$F(x) = \kappa x^2 + Ax + B, \quad (3.14)$$

where κ, A, and B are unknown coefficients. To measure the total volume displacement of the beam accurately, Equations 3.9 and 3.13 need to be equal $(Q = D)$ as shown in the following equation

$$b\int_0^{\ell} u(x)dx = -(h_b + h_s)e_{31}\Big\{ \left[F(\ell)u'(\ell) - F'(\ell)u(\ell)\right] - \left[F(0)u'(0) - F'(0)u(0)\right] + \int_0^{\ell} F''(x)u(x)dx \Big\}. \quad (3.15)$$

Reproduced with permission of the copyright owner. Further reproduction prohibited without permission.

For Equation 3.15 to hold true for any arbitrary displacement, $u(x)$, it can be shown that

$$b = -2(h_b + h_s)e_{31}\kappa \quad \text{or} \quad \kappa = \frac{-b}{2(h_b + h_s)e_{31}}, \tag{3.16a}$$

$$\left[F(\ell)u'(\ell) - F'(\ell)u(\ell)\right] - \left[F(0)u'(0) - F'(0)u(0)\right] = 0. \tag{3.16b}$$

Using Equations 3.14 and 3.16, the PVDF sensor shape can be determined. For a clamped beam the displacement and its slope are both zero at the beam boundaries ($u(0) = u'(0) = u(\ell) = u'(\ell) = 0$). Thus, all the terms in Equation 3.16b are zero. This leaves two known coefficients A and B. Thus, unlike the modal form, there is a lot of freedom in designing a PVDF total volume displacement sensor for a clamped beam as there are many possible solutions. Some of the simpler solutions to this problem can be obtained by setting $F(0) = F(\ell) = 0$, $F(\ell) = F'(\ell) = 0$, and $F(0) = F'(0) = 0$. For the first case $F(0) = F(\ell) = 0$, A and B are found from the following system of equations

$$\begin{cases} B = 0 \\ \kappa\ell^2 + A\ell = 0, \end{cases} \tag{3.17}$$

or

Reproduced with permission of the copyright owner. Further reproduction prohibited without permission.

$$\begin{cases} B = 0 \\ A = -\kappa\ell, \end{cases} \tag{3.18}$$

thus,

$$F(x) = \kappa\left(x^2 - \ell x\right). \tag{3.19a}$$

Applying the same procedure to the other two conditions, yields the following equations, respectively

$$F(x) = \kappa(x - \ell)^2, \tag{3.19b}$$

$$F(x) = \kappa x^2. \tag{3.19c}$$

Figure 17 shows the sensor shapes described by Equations 3.19 (a, b, c), respectively. The rectangular border area represents the beam surface area and the dark area the PVDF sensor delimited by the two curves $F(x)$ and $-F(x)$. It is important to note that there are many other possible solutions to this problem. The choice of the most suitable sensor shape can be made by taking other considerations such as those from the implementation of these sensors into account. These problems could be set up as an optimization problem with a cost function of choice to be maximized or minimized.

For a clamped-free beam, the displacement and its slope are both zero at the clamped boundary ($u(0) = u'(0) = 0$). Equation 3.16b is reduced to

Reproduced with permission of the copyright owner. Further reproduction prohibited without permission.

$[F(\ell)u'(\ell) - F'(\ell)u(\ell)] = 0$. One easy way to ensure this equality is true is to set $F(\ell) = F'(\ell) = 0$ which yields Equation 3.19b, one of the conditions that was already considered in the case of a clamped beam. For a simply supported beam, the displacement is zero at both beam boundaries ($u(0) = u(\ell) = 0$). Equation 3.16b becomes $[F(\ell)u'(\ell) - F(0)u'(0)] = 0$. By setting $F(0) = F(\ell) = 0$ this condition is

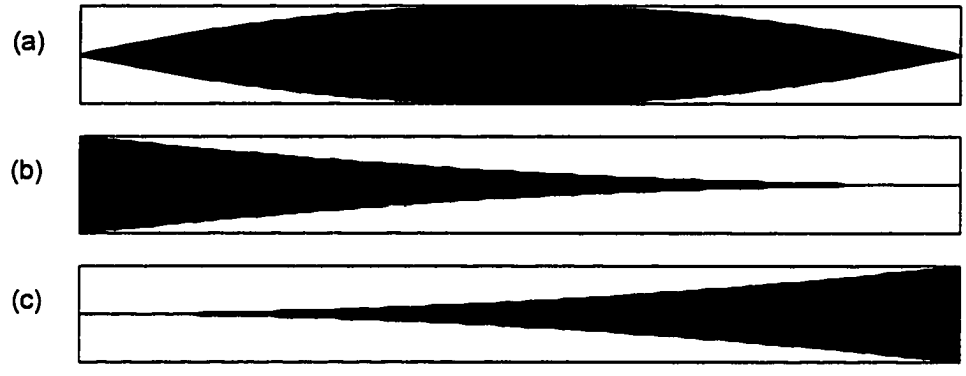

Figure 17. Total Volume Displacement Sensors for a Clamped Beam.

satisfied. This has already been considered in the case of a clamped beam and gives Equation 3.19a.

For a clamped-simply supported beam, the displacement is zero at both boundaries and the slope is zero at the clamped boundary ($u(0) = u'(0) = u(\ell) = 0$). Equation 3.16b leaves the expression $F(\ell)u'(\ell) = 0$ that can be satisfied by setting $F(\ell) = 0$. This leaves one equation and two unknowns with many possible solutions, as shown by the following equation.

Reproduced with permission of the copyright owner. Further reproduction prohibited without permission.

$$\kappa\ell^2 + A\ell + B = 0 \tag{3.20}$$

Some simple solutions can be found by introducing an additional condition. For example, setting $F'(\ell) = 0$ or $F'(0) = 0$ yields $F(x) = \kappa\left(x^2 - \ell^2\right)$, which is shown in Figure 18. On the other hand, setting $F(0) = 0$, yields the same answer as that already considered in the case of a clamped beam represented by Equation 3.19a.

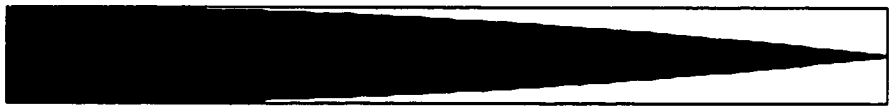

Figure 18. Total Volume Displacement Sensor for a Clamped-Hinged Beam.

It is important to note that the sensor shown in Figure 17a (obtained using quadratic form) will measure the same volume displacement as the sensor of Figure 16a (obtained using modal expansion). However, in order for their shape to look exactly alike, the curves of either one need to be shifted by half the width of the beam.

Local Volume Displacement Sensor Development for Beams

One objective of this research is to design a sensor that accurately measures the beam volume displacement over any arbitrary segment of the beam. As mentioned before, two methods are used in the design of the sensors. Each method is presented here. Before discussing individual approaches, it is important to point out a common

Reproduced with permission of the copyright owner. Further reproduction prohibited without permission.

element between these approaches. Both approaches require the use of multiple sensors, each extending over the entire length of the beam to measure the volume displacement within a segment of the beam. For example, for a beam split into three segments, three sensors are needed to measure the volume displacement of all segments. Each sensor may span the entire length of the beam, but it measures only the volume displacement of a segment of the beam. The physical explanation for the extension of each sensor to the beam boundaries lies in the fact that the PVDF transducer is a strain sensor. Strain is a local quantity. The goal is to measure volume displacement as defined by an integration of beam displacement over the beam area of interest. As such, to successfully implement PVDF as a local volume displacement sensor, it has to be extended to at least one zero-displacement beam boundary. It is also important to note that although the examples given in this work are all for a beam divided into equal-length segments, this technique does not require the vibrating surface to be divided equally.

Modal Expansion

Using a sensor that spans the entire length of the beam, Equation 3.12 may be rewritten for local volume displacements as

$$[R]\{\hat{\alpha}\} = \{\hat{d}\}\ , \tag{3.21}$$

Reproduced with permission of the copyright owner. Further reproduction prohibited without permission.

where $\{\hat{\alpha}\}$ and $\{\hat{d}\}$ are N-by-1 vectors, $[R]$ is as defined previously in Equation 3.8, and $\hat{}$ denotes a local quantity. The elements of $\{\hat{d}\}$ are defined as

$$\hat{d}_n = b\int_a^c \phi_n(x)dx, \tag{3.22}$$

where a and c are the coordinates of the two ends of the beam segment defined by $a \le x \le c$ as shown in Figure 19. The matrix $[R]$ is diagonal (as before), so Equation 3.21 is easily solved for the new (sensor) shape coefficients $\hat{\alpha}_i$ $(i = 1, \cdots, N)$. The shape of the local volume-displacement sensor is then defined over the entire length of the beam by using the $\hat{\alpha}_i$ in place of the α_i in Equation 3.3.

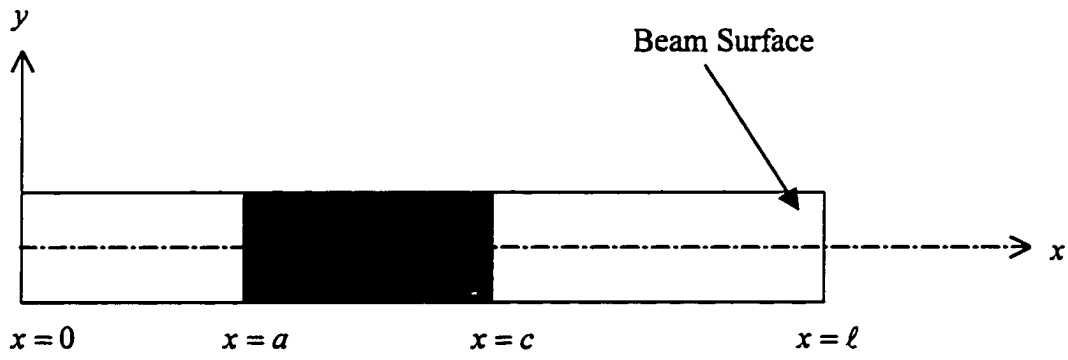

Figure 19. Top View of the Beam Where the Darker Section Represents the Segment of the Beam Whose Volume Displacement Is Being Sought.

Reproduced with permission of the copyright owner. Further reproduction prohibited without permission.

Quadratic Form

The formulation presented in the total volume displacement sensor development section is extended to develop a one-dimensional local volume displacement sensor. Following the logic presented in the above section, to measure the beam local volume displacement within any arbitrary beam segment from $x = a$ to $x = c$, as shown in Figure 19, a single sensor is required that would extend the full length of the beam. Such a sensor is assumed to consist of three distinct segments ($0 \le x \le a, a \le x \le c$, and $c \le x \le \ell$) while maintaining the continuity of sensor shape and slope at $x = a$ and $x = c$.

The charge generated by such a sensor is written as the sum of charges generated by individual segments of the sensor as

$$Q = Q_1 + Q_2 + Q_3, \tag{3.23}$$

where the subscripts 1, 2, and 3 refer to the sensor segments $0 \le x \le a, a \le x \le c$, and $c \le x \le \ell$, respectively. Using Equation 3.2 the equation of Q_1, Q_2 and Q_3 can be written as

$$Q_1 = -(h_b + h_s)e_{31}\int_0^a F_1(x)u''(x)dx, \tag{3.24a}$$

Reproduced with permission of the copyright owner. Further reproduction prohibited without permission.

$$Q_2 = -(h_b + h_s)e_{31}\int_a^c F_2(x)u''(x)dx, \tag{3.24b}$$

$$Q_3 = -(h_b + h_s)e_{31}\int_c^\ell F_3(x)u''(x)dx, \tag{3.24c}$$

Integration by parts of each of the above equations yields

$$Q_1 = -(h_b + h_s)e_{31}\Big\{ [F_1(a)u'(a) - F_1'(a)u(a)] - [F_1(0)u'(0) - F_1'(0)u(0)] + \int_0^a F_1''(x)u(x)dx \Big\}, \tag{3.25a}$$

$$Q_2 = -(h_b + h_s)e_{31}\Big\{ [F_2(c)u'(c) - F_2'(c)u(c)] - [F_2(a)u'(a) - F_2'(a)u(a)] + \int_a^c F_2''(x)u(x)dx \Big\}, \tag{3.25b}$$

and

$$Q_3 = -(h_b + h_s)e_{31}\Big\{ [F_3(\ell)u'(\ell) - F_3'(\ell)u(\ell)] - [F_3(c)u'(c) - F_3'(c)u(c)] + \int_c^\ell F_3''(x)u(x)dx \Big\}, \tag{3.25c}$$

where $F_1(x)$, $F_2(x)$, and $F_3(x)$ describe the sensor shape over the $0 \le x \le a, a \le x \le c$, and $c \le x \le \ell$ beam segments, respectively. If the shape

Reproduced with permission of the copyright owner. Further reproduction prohibited without permission.

functions F_1 and F_3 are assumed to be linear, then $F_1''(x)=0$ and $F_3''(x)=0$, and the integrals of Equation 3.25a and c are zero. Constraining the PVDF sensor shapes to maintain the continuity of sensor shape and its slope at the segment boundaries $x=a$ and $x=c$ yields

$$F_1(a)=F_2(a), \tag{3.26a}$$

$$F_1'(a)=F_2'(a), \tag{3.26b}$$

$$F_2(c)=F_3(c), \tag{3.26c}$$

and

$$F_2'(c)=F_3'(c). \tag{3.26d}$$

From the constraint equations, the following equations are derived

$$[F_1(a)u'(a)-F_1'(a)u(a)]=[F_2(a)u'(a)-F'(a)u(a)], \tag{3.27a}$$

$$[F_2(c)u'(c)-F_2'(c)u(c)]=[F_3(c)u'(c)-F'(c)u(c)]. \tag{3.27b}$$

Substituting Equations 3.27 (a, b) in Equation 3.23 yields

$$Q=-(h_b+h_s)e_{31}\Big\{\ -[F_1(0)u'(0)-F_1'(0)u(0)]+$$

Reproduced with permission of the copyright owner. Further reproduction prohibited without permission.

$$[F_3(\ell)u'(\ell) - F_3'(\ell)u(\ell)] + \int_a^c F_2''(x)u(x)dx \Big\}. \tag{3.28}$$

Assuming a quadratic sensor shape for the $a \le x \le c$ beam segment (i.e., $F_2''(x) = 2\kappa$), the above equation can be written as

$$Q = -(h_b + h_s)e_{31}\Big\{ -[F_1(0)u'(0) - F_1'(0)u(0)] + [F_3(\ell)u'(\ell) - F_3'(\ell)u(\ell)] + \kappa\int_a^c u(x)dx \Big\}. \tag{3.29}$$

To accurately measure the local beam volume displacement over an arbitrary section $a \le x \le c$, the above equation should equal to the following expression

$$\hat{D} = \int_a^c u(x)dx. \tag{3.30}$$

Thus, for $\hat{D} = Q$ for any arbitrary $u(x)$, it is required that the following two conditions be satisfied

$$b = -2(h_b + h_s)e_{31}\kappa, \quad \text{or} \quad \kappa = -b/2(h_b + h_s)e_{31}, \tag{3.31a}$$

and

$$\left[\overbrace{F_1'(0)u(0)}^{(1)} - \overbrace{F_1(0)u'(0)}^{(2)} + \overbrace{F_3(\ell)u'(\ell)}^{(3)} - \overbrace{F_3'(\ell)u(\ell)}^{(4)}\right] = 0, \tag{3.31b}$$

Reproduced with permission of the copyright owner. Further reproduction prohibited without permission.

It is important to note that the combination of two linear (F_1 and F_3) and one quadratic (F_2) functions necessitates the determination of 7 unknown coefficients. Equation 3.31a provides the means to determine the coefficient for the x^2 term in the quadratic polynomial $F_2(x)$, which represents the PVDF shape for the beam segment whose volume displacement is to be measured. Thus, the number of unknown coefficients will be reduced to six

$$F_1(x) = A_1 x + B_1, \tag{3.32a}$$

$$F_2(x) = \kappa\, x^2 + A_2 x + B_2, \tag{3.32b}$$

$$F_3(x) = A_3 x + B_3, \tag{3.32c}$$

where Equation 3.31b places further constraints (in addition to Equation 3.26) on the shape of PVDF sensors in the beam segments whose volume displacement is not being measured ($F_1(x)$ and $F_3(x)$).

Three commonly encountered beam boundary conditions are considered here, namely clamped, simply supported, and free. These boundaries may appear at either end of the beam, yielding six combinations as shown in Table 3. To satisfy Equation 3.31b it becomes necessary to consider when the beam displacement and its slope are zero at each of its boundaries. In the case of a clamped boundary condition, the

Reproduced with permission of the copyright owner. Further reproduction prohibited without permission.

displacement and its slope are both zero ($u|_{b.c.} = u'|_{b.c.} = 0$ where b.c. represents the boundary conditions (either $x = 0$ or $x = \ell$). Thus, for a clamped beam, Equation 3.31b is completely satisfied since all its four terms are zero. This yields an under-determined system of equations given by Equation 3.26 (6 unknown polynomial

Table 3

Beam Boundary Conditions

		x = ℓ		
		Clamped	Hinged	Free
x = 0	Clamped	(1),(2),(3),(4)=0 No additional equation 4 equations 6 unknowns	(1),(2),(4)=0 $F_3(\ell) = 0$ 4 equations 6 unknowns	(1),(2)=0 $F_3(\ell) = F_3'(\ell) = 0$ No F_3 sensor 6 equations 6 unknowns
	Hinged	(2),(3),(4)=0 $F_1(0) = 0$ 5 equations 6 unknowns	(2),(4)=0 $F_1(0) = F_3(\ell) = 0$ 6 equations 6 unknowns	
	Free	(3),(4)=0 $F_1(0) = F_1'(0) = 0$ No F_1 sensor 6 equations 6 unknowns		

Reproduced with permission of the copyright owner. Further reproduction prohibited without permission.

coefficients and 4 equations). There are many possible solutions to this set of equations. The selection of the PVDF sensor shape in this case can take the form of an optimization procedure depending on the cost and fabrication constraints involved.

As a demonstration, some of the many shapes that the PVDF sensor can take for a clamped beam are given in Figure 20. In each case, the functions F_1, F_2, and F_3 and the functions $-F_1$, $-F_2$, and $-F_3$ are plotted to obtain the sensor envelope. The PVDF sensor is represented by the area surrounded by these two curves. The sensor corresponding to $F_1(0 \le x \le a)$ is given in gray shaded area followed by the sensor defined by $F_2(a \le x \le c)$ in darker shade and $F_3(c \le x \le \ell)$ in gray shade. All incidences of the (F_1, F_2, F_3) and the $(-F_1, -F_2, -F_3)$ curves crossing each other represent a reversal in PVDF film polarity (e.g., Figure 20b). The rectangular border represents the beam surface.

To obtain Figures 20 a-i, all the possibilities of pairs of unknown polynomial coefficients A_1, B_1, A_2, B_2, A_3, and B_3 being set equal to zero are considered. In anticipation of the experiments that are to be performed using the PVDF sensor, a sensor with two additional constraints is designed. The PVDF sensor shapes are set equal to zero at the two beam boundaries (i.e., $F_1(0)=0$ and $F_3(\ell)=0$). The PVDF sensor shape is given in Figure 20j. This sensor shape is thought to be most practical considering the sensor fabrication techniques used in this work. In the experimental apparatus considered here, only a beam divided into two equal segments is used.

Reproduced with permission of the copyright owner. Further reproduction prohibited without permission.

Thus, the PVDF sensors are also sought for the case where $x = a$ is set equal to zero, as shown in Figure 21.

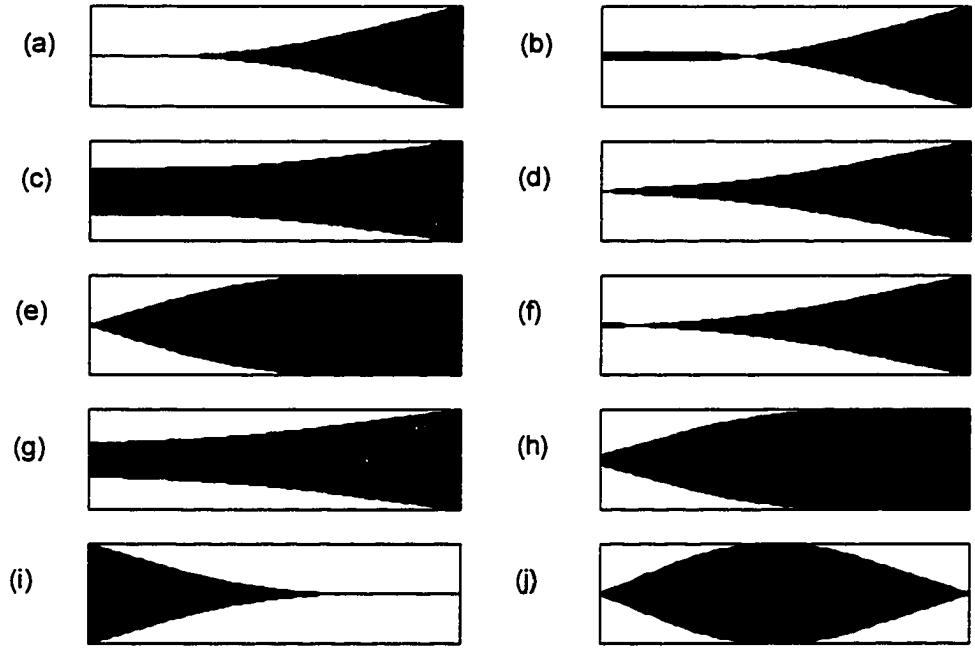

Figure 20. Different Possible PVDF Sensor Shapes for a Clamped Beam Divided Into Three Sections Where the Darker Area Represents the Segment of the Beam Whose Volume Displacement Is Being Sought.

For a clamped-simply supported boundary condition, terms (1), (2), and (4) of Equation 3.31b are zero. However, the only way for term (3) of this equation to be equal to zero is to set $F_3(\ell) = 0$. This yields a system of 5 equations and 6 unknowns. As in the case of the clamped beam, there are many possible solutions that would satisfy this problem. Figure 22 illustrates a few of these sensor shapes.

Reproduced with permission of the copyright owner. Further reproduction prohibited without permission.

In the case of a free boundary, neither the beam displacement nor its slope is zero. Again, for example, if the free boundary is located at $x = \ell$, then neither of the two terms in Equation 3.31b corresponding to this boundary is zero. To satisfy the condition of Equation 3.31b, it is necessary to have $F_3'(\ell)u(\ell) - F_3(\ell)u'(\ell) = 0$ which

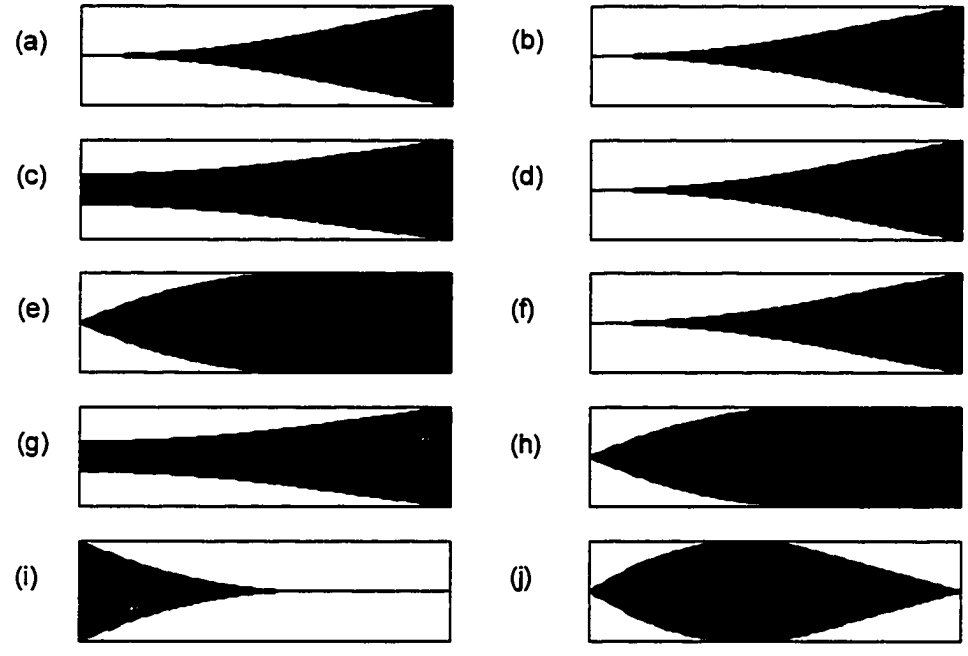

Figure 21. Different Possible PVDF Sensor Shapes for a Clamped Beam Divided Into Two Sections Where the Darker Area Represents the Segment of the Beam Whose Volume Displacement Is Being Sought.

can be met by setting $F_3'(\ell) = F_3(\ell) = 0$. The shape of the PVDF strip on this beam segment has already been assumed to be linear, the most obvious solution would be

Reproduced with permission of the copyright owner. Further reproduction prohibited without permission.

for $F_3(x)=0$, i.e., no sensor is required on the $c \le x \le \ell$ segment. It turns out that this case represents one of the cases already considered for a clamped beam and was shown in Figures 20j and 21j.

In the case of two simply supported boundaries, it is only the displacement that is zero at the boundaries ($u|_{b.c.}=0$). In this case, one of the two terms in Equation 3.29b corresponding to this boundary is not necessarily zero. For example, if the beam boundary at $x=0$ is simply-supported, then $F_1'(0)u(0)=0$. However, for

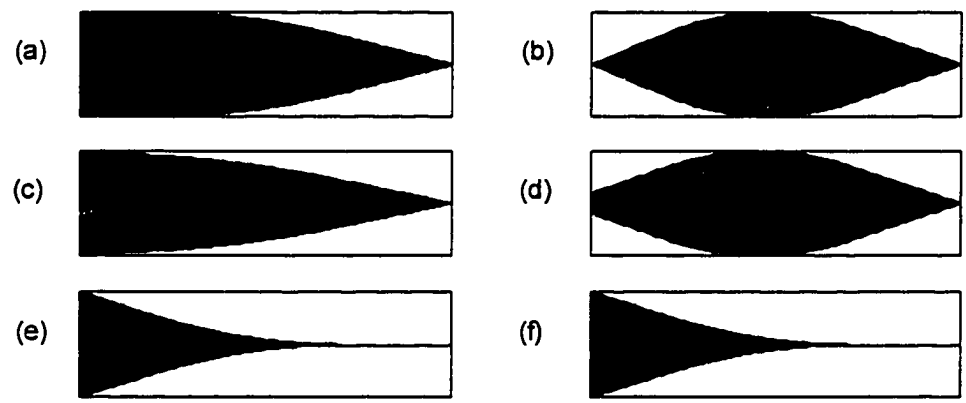

Figure 22. Different Possible PVDF Sensor Shapes for a Clamped-Hinged Beam Divided Into Three Sections Where the Darker Area Represents the Segment of the Beam Whose Volume Displacement Is Being Sought.

$F_1(0)u'(0)$ to be equal to zero, it is necessary for $F_1(0)$ to be equal to zero since $u'(0)\neq 0$. Thus, the PVDF strip covering this segment of the beam can be determined by solving a system of 6 equations for 6 unknown coefficients. As before, it turns out

Reproduced with permission of the copyright owner. Further reproduction prohibited without permission.

that this case has already been considered for a clamped beam and is shown in Figures 20j and 21j.

Numerical Simulation

Discretization of the Sensor Equation

The output charge of the PVDF sensor given by Equation 3.2 is now discretized. The process involves the discretization of the PVDF shape function $F(x)$ and the beam deflection function $u(x)$. The deflection is derived from Equation 2.30 such that

$$u(x)=\sum_{i=1}^{N} u_i(\xi) \ , \tag{3.33}$$

where $u_i(\xi)$ is the deflection of the i^{th} element and is given by Equation 2.29. The beam displacement represented by Equation 3.33 is calculated using the finite element method. The Hermite cubic shape functions are used in the finite element analysis in order to insure the continuity of both the displacement and its slope. Therefore, the shape function $F(x)$ will be discretized so that its displacement and slope are also continuous. Hermite shape functions will be utilized as described in the next paragraph.

Reproduced with permission of the copyright owner. Further reproduction prohibited without permission.

The natural coordinate ξ, defined in Equation 2.23 is used aiong with Equation 2.27 to write the output charge of a PVDF sensor measuring the volume displacement of an element of the beam as

$$Q_e = -(h_b + h_s)e_{31}\int_{-1}^{+1} F(\xi)u''(\xi)\frac{\ell}{2}d\xi \quad , \tag{3.34}$$

where

$$u''(\xi) = \frac{d^2u(\xi)}{dx^2}, \tag{3.35}$$

with u defined by Equation 2.29. The above derivation can be written as

$$u''(\xi) = \frac{d^2u(\xi)}{d\xi^2}\left(\frac{d\xi}{dx}\right)^2 . \tag{3.36}$$

Using Equation 2.27, the preceding equation becomes

$$u''(\xi) = \frac{4}{\ell^2}\frac{d^2u(\xi)}{d\xi^2}, \tag{3.37}$$

but the second derivative of Equation 2.30 with respect to ξ is

$$\frac{d^2u(\xi)}{d\xi^2} = \frac{d^2\{h\}^T}{d\xi^2}\{q_e\} \ . \tag{3.38}$$

Substitution in Equation 3.37 yields

Reproduced with permission of the copyright owner. Further reproduction prohibited without permission.

$$\frac{d^2u(\xi)}{dx^2} = \frac{4}{\ell^2}\frac{d^2\{h\}^T}{d\xi^2}\{q_e\}\,, \tag{3.39}$$

where

$$\frac{\mathrm{d}^2\{h\}}{d\xi^2} = \left[\frac{3}{2}\xi, \frac{-1+3\xi}{2}\frac{\ell}{2}, \frac{-3}{2}\xi, \frac{1+3\xi}{2}\frac{\ell}{2}\right]^T \quad . \tag{3.40}$$

Using the same procedure, $F(x)$ can be written as

$$F(\xi) = \{h\}^T\{F_e\}\,, \tag{3.41}$$

where

$$\{F_e\} = [F_1, S_1, F_2, S_2]^T\,. \tag{3.42}$$

F_1 and F_2 are the values of $F(x)$ at x_1 and x_2 respectively, and S_1 and S_2 the slopes of the sensor shape function $F(x)$ at x_1 and x_2 respectively. Substituting Equation 3.38, Equation 3.40, and Equation 3.41 into Equation 3.34 yields

$$Q_e = -(h_b + h_s)e_{31}\frac{2}{\ell}\int_{-1}^{+1}\{h\}^T\{F_e\}\frac{d^2\{h\}^T}{d\xi^2}\{q_e\}d\xi\,. \tag{3.43}$$

The term $\{h\}^T\{F_e\}$ is a scalar, thus

$$\{h\}^T\{F_e\} = \left(\{h\}^T\{F_e\}\right)^T = \{F_e\}^T\{h\}, \tag{3.44}$$

Reproduced with permission of the copyright owner. Further reproduction prohibited without permission.

and Equation 3.41 can be written as

$$Q_e = -(h_b + h_s)e_{31}\{F_e\}^T\left(\frac{2}{\ell}\int_{-1}^{+1}\{h\}\frac{d^2\{h\}^T}{d\xi}d\xi\right)\{q_e\}\,, \tag{3.45}$$

or in a matrix form as

$$Q_e = -(h_b + h_s)e_{31}\{F_e\}^T\left[\hat{h}\right]\{q_e\}\quad. \tag{3.46}$$

The 4-by-4 matrix is defined as

$$\left[\hat{h}\right] = \frac{2}{\ell}\int_{-1}^{+1}\{h\}\frac{d^2\{h\}^T}{d\xi}d\xi\,. \tag{3.47}$$

Carrying out the integration in the above equation gives

$$\left[\hat{h}\right] = \begin{bmatrix} -6/5\ell_e & -11/10 & 6/5\ell_e & -1/10 \\ -1/10 & -2\ell_e/15 & 1/10 & \ell_e/30 \\ 6/5\ell_e & 1/10 & -6/5\ell_e & 11/10 \\ -1/10 & \ell_e/30 & 1/10 & -2\ell_e/15 \end{bmatrix}. \tag{3.48}$$

The total charge from the entire length of the sensor can be written in terms of a summation of its segments as

$$Q = \sum_{i=1}^{N} Q_{ei}\,. \tag{3.49}$$

Reproduced with permission of the copyright owner. Further reproduction prohibited without permission.

Replacing Q_{ei} with Equation 3.45 in the above yields

$$Q = -(h_b + h_s)e_{31}\sum_{i=1}^{N}\{F_i\}^T\left(\frac{2}{\ell}\int_{-1}^{+1}\{h\}\frac{d^2\{h\}^T}{d\xi^2}d\xi\right)\{q_e\} \ . \tag{3.50}$$

In global matrix terms,

$$Q = -(h_b + h_s)e_{31}\left(\{F\}^T\left[\hat{H}\right]\{y\}\right) \ , \tag{3.51}$$

where $\{y\} = [q_{e1}, q_{e2}, \ldots, q_{eN}]^T$, $\left[\hat{H}\right]$ is the assembled matrix from $\left[\hat{h}\right]$, and $\{F\}$ is the assembled matrix of $\{F_e\}$.

Simulation

Equation 3.51 is simulated in the sensor design module of ANCPACK. The simulation program uses the forced vibration module to calculate the velocity distribution on the surface of the beam. Assuming harmonic excitation, this velocity is converted into displacement to get the vector $\{y\}$ of Equation 3.51. First, the simulation module computes the matrix $\left[\hat{H}\right]$, which only depends on the length of each beam element and its connectivity. Then, the vector $\{F\}$ is simply calculated from $F(x)$ and $F'(x)$ at the nodes of each beam element. Finally, the output charge of the PVDF sensor is calculated. The result is compared to the volume displacement

Reproduced with permission of the copyright owner. Further reproduction prohibited without permission.

of the beam computed from the discretized form of Equation 3.9. The volume displacement of the beam element is given as

$$D_e = b\int_{-1}^{+1} u(\xi)\frac{\ell_e}{2}d\xi \,. \tag{3.52}$$

Substituting Equation 2.30 into the above equation yields

$$D_e = b\int_{-1}^{+1} \{h\}^T \{q_e\}\frac{\ell_e}{2}d\xi \,, \tag{3.53}$$

which may be written as

$$D_e = b\left(\int_{-1}^{+1} \{h\}^T \frac{\ell_e}{2}d\xi\right)\{q_e\} \,, \tag{3.54}$$

or in matrix form as

$$D_e = b\{\bar{h}\}^T\{q_e\} \,, \tag{3.55}$$

where $\{\bar{h}\} = \int_{-1}^{+1}\{h\}\frac{\ell_e}{2}d\xi$.

Integrating the above equation yields

$$\{\bar{h}\} = \left[\frac{\ell_e}{2},\ \frac{\ell_e^2}{12},\ \frac{\ell_e}{2},\ \frac{-\ell_e^2}{12}\right]^T. \tag{3.56}$$

Reproduced with permission of the copyright owner. Further reproduction prohibited without permission.

The volume displacement of the entire beam may be written as

$$D = \sum_{i=1}^{N} D_{ei} = b\{\overline{H}\}^T \{y\} \ , \tag{3.57}$$

where $\{\overline{H}\}$ is the global matrix from $\{\overline{h}\}$ and $\{y\}$ is as defined by Equation 3.51.

The simulation is performed for a clamped beam. The PVDF output charge calculated from Equation 3.51 is compared to the beam volume displacement obtained from Equation 3.57. The measurement of the total volume displacement is numerically implemented using the sensor shape shown in Figure 17a. The results of this simulation are shown in Figure 23. Local volume displacement measurement is implemented for a clamped beam divided into two sections. The sensor shape used is shown Figure 24 and the results in Figure 25. The findings of the numerical experiment presented here show that the total volume displacement and local volume displacement of a beam can be accurately measured using PVDF sensors. It is important to note that the local volume displacement sensor senses mode 1 at approximately 64 Hz and mode 2 at approximately 177 Hz. The total volume displacement sensor does not sense mode 2 at all because the total volume displacement of that mode is zero.

Reproduced with permission of the copyright owner. Further reproduction prohibited without permission.

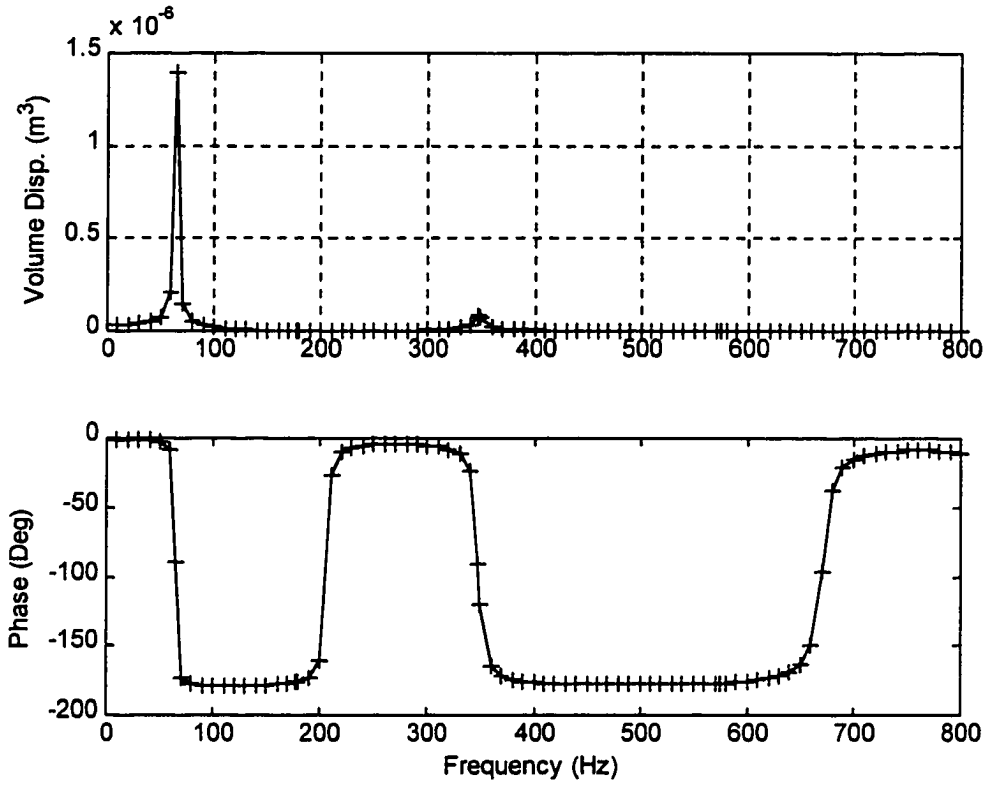

Figure 23. Total Volume Displacement of a Clamped Beam Measured by the PVDF Sensor (solid) and Predicted (++++).

Volume Displacement Sensor Development for a Loudspeaker

As mentioned before, the objective of this work is to actively cancel the volume displacement of a vibrating baffled beam using loudspeakers. The preceding sections show that the volume displacement of the beam can be accurately measured using PVDF sensors. From the output of the sensor, the volume displacement necessary for successful cancellation is calculated and fed to the loudspeaker. This describes an open-loop system. To implement a closed-loop system, as is the case in

Reproduced with permission of the copyright owner. Further reproduction prohibited without permission.

Figure 24. PVDF Sensor Shapes Implemented on a Clamped Beam Divided Into Two Sections Where the Darker Area Represents the Segment of the Beam Whose Volume Displacement Is Being Sought.

this work, the volume displacement of the loudspeaker must be measured. This is achieved by implementing one of the methods described by Anthony and Elliott (1991). They described three procedures to measure the volume velocity of an acoustic source. In their work, they proposed the use of laser velocimetry, the measurement of the internal source pressure, or the use of a moving-coil loudspeaker as an output transducer. In this thesis, the internal source pressure measurement is adopted.

The source is a loudspeaker modeled as a baffled piston of radius a, housed in an acoustically sealed enclosure, as shown in Figure 26. Changes in the internal pressure within the sealed enclosure are used to represent the volume displacement radiation of the piston. Assuming harmonic excitation, the displacement is converted into velocity by multiplying its expression by $i\omega$ (where ω is the frequency of vibration). As the piston vibrates, it causes changes, dP and dV, in the total internal pressure P and the nominal volume V of the box respectively.

Reproduced with permission of the copyright owner. Further reproduction prohibited without permission.

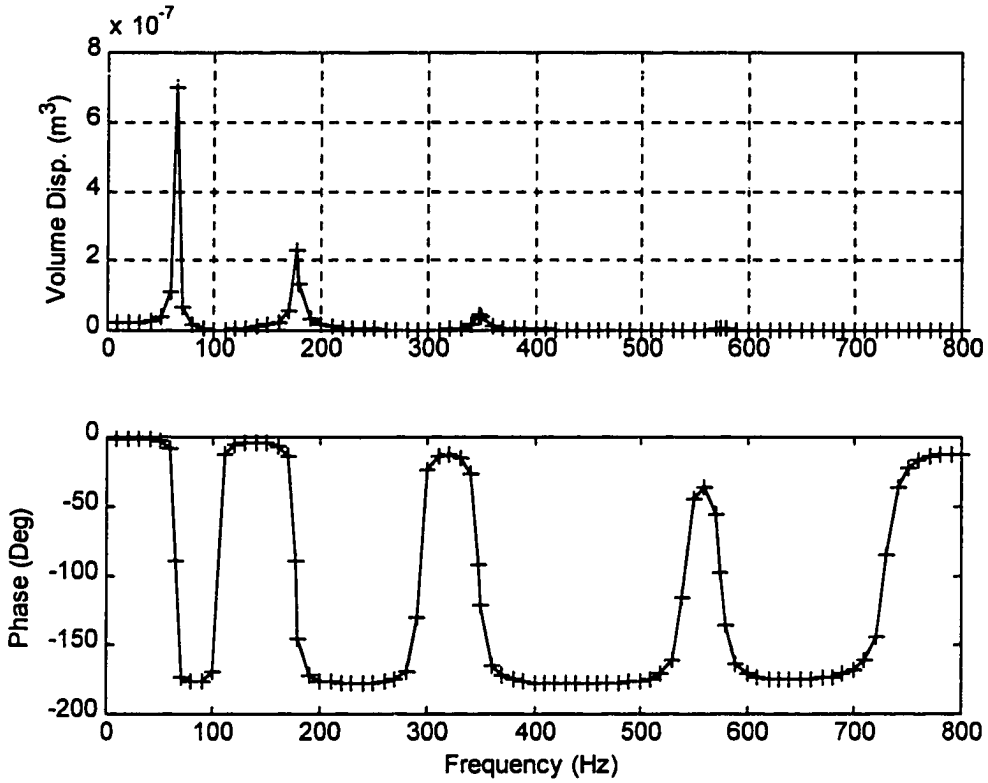

Figure 25. Total Volume Displacement of a Clamped Beam Measured by the PVDF Sensor (Solid) and Predicted (++++).

Assuming the air in the enclosure acts as a perfect gas, the heat energy dQ, gained by changes in the volume (at constant pressure) and changes in the pressure (at constant volume) is determined (Morse, 1986) as

$$dQ = T\left(C_P \frac{dV}{V} + C_V \frac{dP}{P}\right) , \tag{3.58}$$

Reproduced with permission of the copyright owner. Further reproduction prohibited without permission.

where C_V and C_P are the specific heats of the gas at constant pressure and constant volume respectively, and T is the absolute gas temperature. Assuming adiabatic compression, no heat transfer takes place and dQ is zero. Thus, Equation 3.58 yields

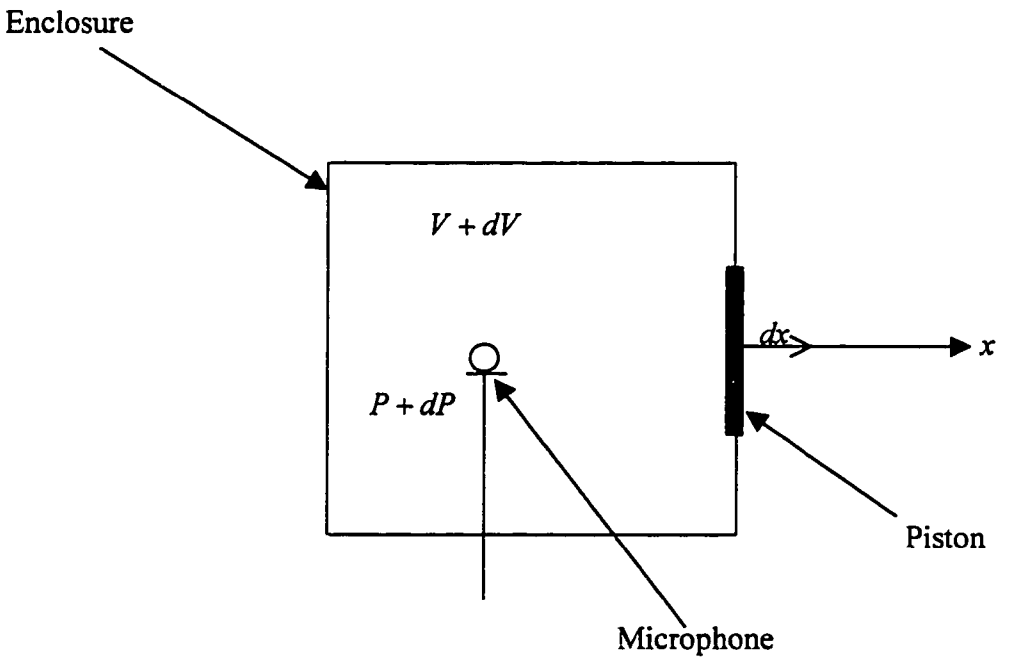

Figure 26. Baffled Piston Housed in an Acoustically Sealed Enclosure.

$$C_P \frac{dV}{V} + C_V \frac{dP}{P} = 0 \quad , \tag{3.59}$$

or

Reproduced with permission of the copyright owner. Further reproduction prohibited without permission.

$$dP = -\frac{C_P}{C_V} P \frac{dV}{V} = \frac{-\rho c^2 dV}{V} , \tag{3.60}$$

where ρ is the air density, and c is the speed of sound. The volume change can be written as

$$dV = s dx , \tag{3.61}$$

where s is the cross-section of the cylindrical enclosure and dx, is the displacement of the piston. Thus, dV is the volume displacement of the piston for $s = \pi a^2$, which is derived from Equation 3.60 and given by

$$dV = -\frac{V dP}{\rho c^2} . \tag{3.62}$$

From the above equation, the volume displacement radiated by the source can be determined by a simple pressure measurement inside the enclosure. This analysis assumes that the wavelength of the pressure wave radiated is much larger than the size of the enclosure. Therefore, there is no formation of standing waves inside the enclosure. The next chapter details the size of the enclosure and the frequencies used in the experimental verification of Equation 3.62.

Summary

The most important element of a successful active noise control strategy resides in the sensing of the control variables. As a result, this chapter is the most

Reproduced with permission of the copyright owner. Further reproduction prohibited without permission.

important in this dissertation. A methodology for sensing the volume displacement of beams and loudspeakers has been developed. Using modal expansion and quadratic form, an integrating sensor was developed. A shaped piezoelectric film (PVDF) was utilized to fabricate a sensor that measured the volume displacement of any arbitrary section of a beam. It has been proven through numerical simulation that the PVDF sensor can accurately measure the local volume displacement of a beam. A sensor for measuring the volume displacement of a loudspeaker was also developed. Pressure variation measured by an internal microphone placed in a loudspeaker enclosure was converted into volume displacement by simply multiplying it by a constant. This constant depends only on the geometry of the enclosure (Equation 3.62) and the sensitivity of the microphone. These conclusions about the sensors were experimentally verified, as described in the next chapter.

Reproduced with permission of the copyright owner. Further reproduction prohibited without permission.

CHAPTER IV

EXPERIMENTAL SETUP AND VERIFICATION

Introduction

In the previous chapter, theoretical analysis and numerical simulation are used to show that: (a) the acoustic power radiated by a vibrating baffled beam can be reduced by locally canceling its volume displacement using loudspeakers, (b) the total or local volume displacement of a beam can be accurately measured using PVDF sensors, and (c) the volume displacement of a loudspeaker can be accurately measured using internal pressure sensors. In this chapter, experimental verification of each of the above conclusions will be presented.

First, the experimental apparatus is built and checked. An aluminum beam clamped at both ends is mounted in a baffle. Using the ANCPACK, the vibration response and the radiation of the beam are predicted. The vibration modes of the beam are measured and compared with the theoretical results. Next, the acoustic pressure is measured above the baffled beam and compared to the pressure calculated using the discretized form of the Rayleigh integral. These experiments validate the clamped boundary conditions and the baffled beam assumptions.

Second, the PVDF volume displacement sensors are fabricated and experimentally verified. Accelerometer measurements are used as benchmark to check the output of the PVDF sensor. The same procedure is used to validate the

Reproduced with permission of the copyright owner. Further reproduction prohibited without permission.

output of the internal pressure sensor mounted inside the loudspeaker enclosure. The following sections detail the experimental setup, procedure and results.

Experimental Analysis of Beam Vibration and Radiation

In this section, details of the actual beam used for the experiment, the experimental measuring apparatus, the measurement procedure, and the test results are presented and discussed. A beam with clamped ends is considered. First, the beam vibration modes and the velocity response are measured. Next, the sound pressure radiated from the beam is measured. Finally, comparisons of the measurement results with the analytical predictions are presented. The discussion will begin with a brief summary of some of the basics of modal testing.

Overview of Modal Testing

This section covers some of the basic theory behind modal testing. For a detailed treatment of the topic, there are many references available. Ewins (1984) and Allemang and Brown (1987) provide a detailed discussion of modal analysis theory.

There are numerous methods for extracting the desired modal properties from a structure. In general, the displacement, velocity, and acceleration can be obtained through the acquisition of the Frequency Response Functions, FRF's, at discrete points on the structure. The FRF is a transfer function in the frequency domain and is defined by its magnitude and phase components. For the modal test, both an input quantity and an output quantity must be measured. The input is usually a force, but

Reproduced with permission of the copyright owner. Further reproduction prohibited without permission.

the output can be displacement, velocity, or acceleration. For the experiments of this analysis, the acceleration is measured with an accelerometer. Assuming harmonic excitation ($e^{i\omega t}$ dependence), the velocity and displacement can easily be found from the measured acceleration.

The FRF is unique for each pair of input and output points on the structure. To do a modal test, the structure must be divided into a discrete number of points. The number of points used determines the accuracy of the test and its resolution when viewing the mode shapes. For higher order modes, a finer mesh is needed. Discretizing the structure in this manner limits the highest frequency for which mode shapes can be calculated. When a structure is discretized into n points, only n measurements need to be taken to fully determine the modal response. Either, the response point can be fixed and the force input moved or the force input point can be fixed and the response point moved. For the tests of this analysis, the latter method is utilized.

Random signal noise can have a detrimental effect on experimental data, therefore it is always prudent to perform simple checks to ensure that the FRF data are accurate. The impact of random noise can be greatly reduced through averaging. Averaging takes the FRF's from several impacts at the same point and combines them into a net FRF. The coherence function is the most important measure of how "good" this net FRF is. Coherence shows the correlation between the output response and the input force. Perfect correlation has a coherence of one, while no correlation has zero coherence. Dips in coherence typically occur at anti-resonance's, where the signal to

Reproduced with permission of the copyright owner. Further reproduction prohibited without permission.

noise ratio is low. It is most important to have good coherence at and around the modal frequencies, since this is where the modal parameters are calculated.

Experimental Setup

The discretized beam used in testing is shown in Figure 27. The beam is made of aluminum and is supported by rectangular blocks on each end, which are rigidly bolted down. A more detailed schematic of the support conditions is shown in Figure 28. The supports constrain the vertical, horizontal, and rotational degrees of freedom of the beam at both ends. The beam (density $\rho = 2700 kg/m^3$ and elastic modulus $E = 6.89e^{10}\ N/m^2$) is 1.219 m long, 0.038 m wide and 0.0127 m thick. Although the length of the beam is 1.219 m, the effective length of the beam suspended between the end supports is 1.016 m. The extra portion of the beam is rigidly clamped to the rectangular blocks. This beam is excited using a shaker placed at a point 0.1524 m (node 3) away from its left boundary as shown in Figure 28.

The primary excitation is provided by the shaker (LDS Model V-203). The effective shaker force on the beam is measured using a force gage (PCB Model 208A03) placed between the shaker and the beam. The vibration response of the beam due to the action of the shaker is then measured at points 50.8 mm apart using an accelerometer (PCB model U353B16). The mass loading effect due to the weight of the accelerometer is considered negligible since the particular accelerometer used in this case weighed only 2 grams.

Reproduced with permission of the copyright owner. Further reproduction prohibited without permission.

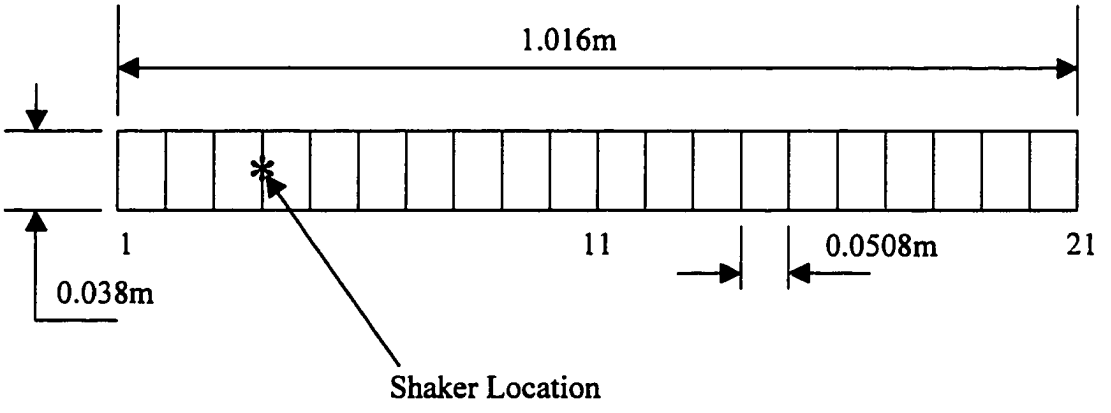

Figure 27. Discretized Rectangular Beam With 20 Elements and 21 Nodes.

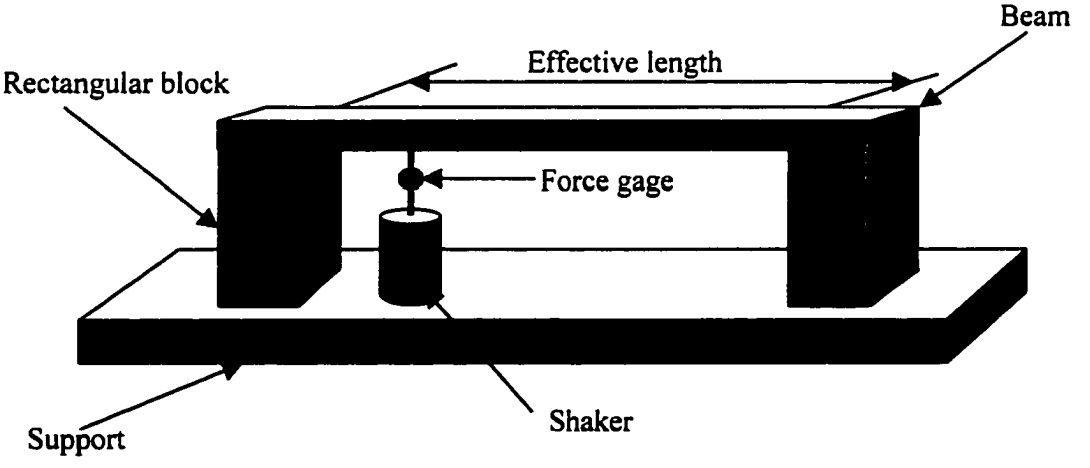

Figure 28. Beam Setup With Support Conditions.

Reproduced with permission of the copyright owner. Further reproduction prohibited without permission.

For measurement of sound radiated from this beam, the experimental setup including the wooden enclosure and the measuring devices, is shown in Figure 28. The enclosure is made of 0.019 m thick plywood which is 1.524 m long, 0.3175 m high, and 0.9144 m wide. The beam setup is mounted inside the enclosure such that the top surface of the beam is flush with the top surface of the box and seals the air that could escape from beneath the beam (similar to a large loudspeaker). This setup is made to closely simulate the boundary conditions and the baffled-beam assumption considered in the theoretical analysis. The air gap between the beam and the box top surface is covered with tape to avoid any air from escaping from under the beam to interfere in the sound measurements. Most of the empty space in the box is filled with sound absorbing foam. Vibration isolators are placed under the beam setup and the shaker, as shown in Figure 29 in order to minimize the vibration of the enclosure.

Experimental Procedure

The first step is to check the ratio of the acceleration response between the beam and the box surface. For sound pressures measured to be mainly due to vibrations of the beam and not the box, the ratio of the acceleration response (beam to box surface) should be high. Higher response values indicate that the vibration of the box surface is much smaller than the beam vibration. To check these ratios, the beam is excited using the shaker at frequencies 50, 64, 100, 174 Hz. In each case, the ratio of the response is measured with respect to nodes 4, 7, 11, 15, 20. The accelerometer on the beam is fixed at each of these nodes while the accelerometer on the box

Reproduced with permission of the copyright owner. Further reproduction prohibited without permission.

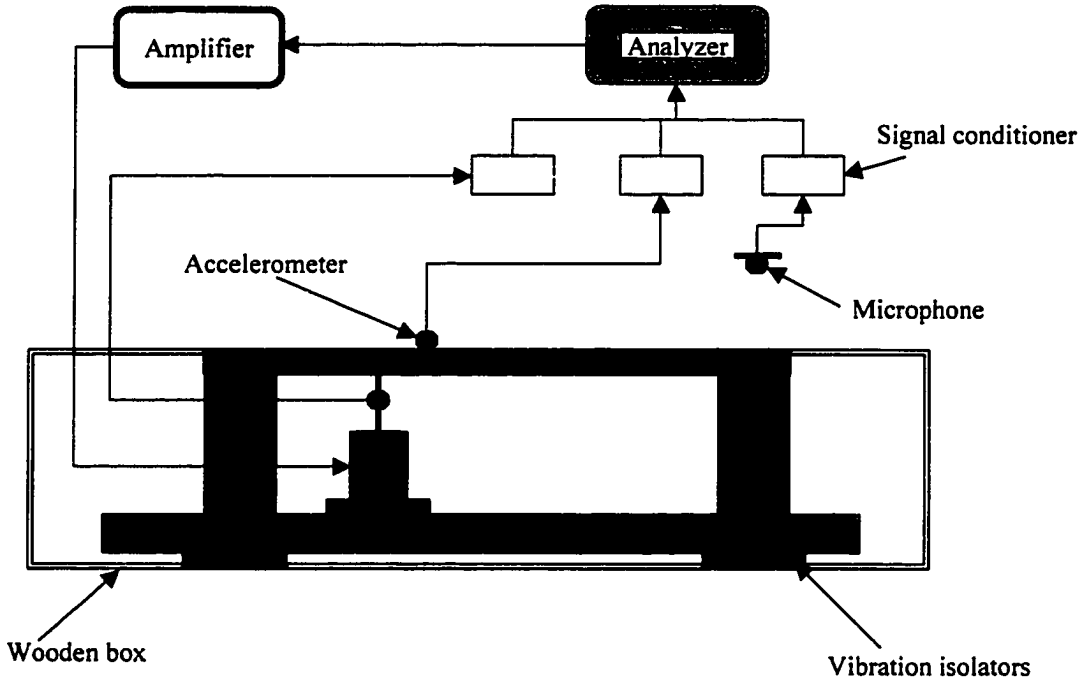

Figure 29. Experimental Setup Showing the Measuring Devices.

surface is located at different points along the y-axis. Figure 30 shows the various measurement points on the surface of the beam and the box. The ratio presented in Table 4 is simply the ratio of accelerometer outputs converted into decibel scale, as shown by the following equation

$$Ratio = 20\log_{10}\left(\frac{beam\ acceleration}{box\ acceleration}\right). \tag{4.1}$$

The results of this experiment are discussed in the next section.

Next, the vibration response of the beam is measured at 21 equally spaced points along the length of the beam. The response is the measure of the ratio of acceleration (output) to the force (input). To find the sound pressure at a particular

Reproduced with permission of the copyright owner. Further reproduction prohibited without permission.

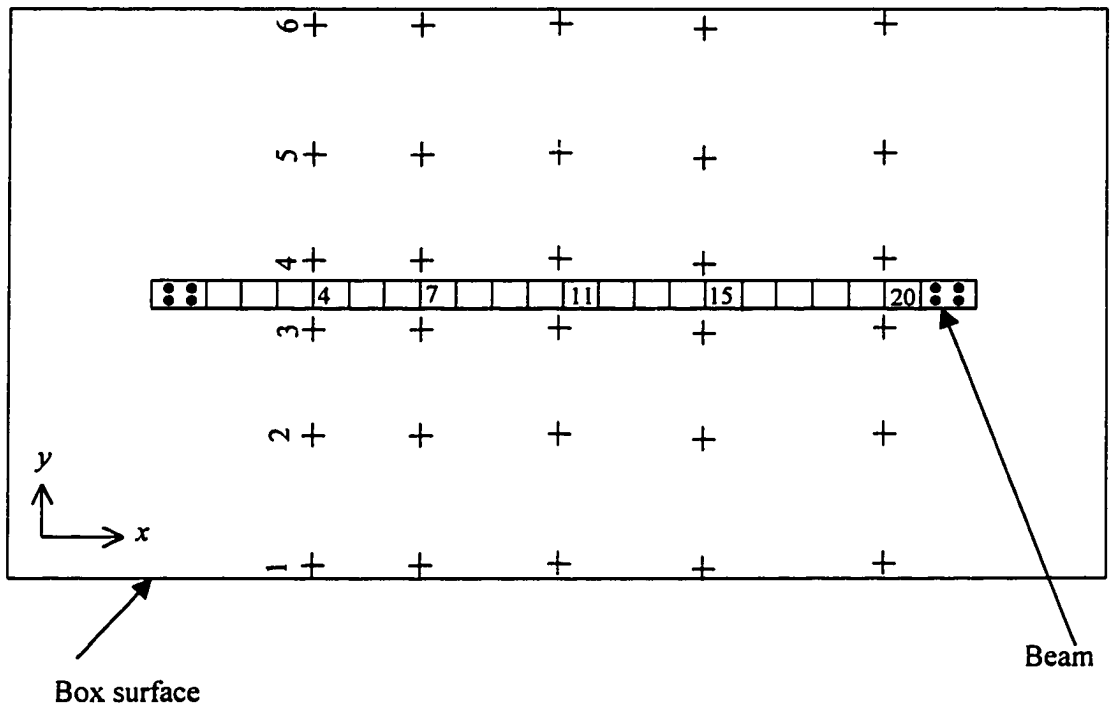

Figure 30. Beam to Box FRF Measurement Points where + Indicates Accelerometer Locations on the Box and the Node Number Indicates the Accelerometer Location on the Beam.

point in space around the beam, there must be good agreement between the analytical and experimental vibration response of the beam. For this, the resonance frequencies of the beam and their corresponding damping factors are determined experimentally and used in Equation 2.53 to calculate the velocity distribution on the surface of the beam. The calculated velocity distribution is then used to compute the sound pressure given by Equation 2.59.

The beam deflection curves shown in Figure 31 through Figure 35 are found from the FRF data. Assuming harmonic excitation the beam displacement is given by

Reproduced with permission of the copyright owner. Further reproduction prohibited without permission.

Table 4

Acceleration Response Ratio Between the Beam and the Box Surface in (dB)

F=50 Hz	1	2	3	4	5	6
Node 4	26	27	30	22	26	27
Node 7	29	39	38	24	30	39
Node 11	30	38	43	24	31	40
Node 15	25	31	39	24	29	37
Node 20	4	7	12	2	19	12
F=100 Hz	1	2	3	4	5	6
Node 4	19	30	26	28	23	27
Node 7	2	13	12	11	8	12
Node 11	27	46	33	40	34	31
Node 15	35	33	36	27	45	33
Node 20	15	18	21	18	21	21
F=64 Hz	1	2	3	4	5	6
Node 4	27	30	31	35	30	28
Node 7	40	42	40	37	38	41
Node 11	44	46	47	37	40	45
Node 15	37	40	44	37	40	46
Node 20	15	18	21	18	21	21
F=174 Hz	1	2	3	4	5	6
Node 4	34	41	42	44	36	47
Node 7	42	47	48	40	46	54
Node 11	12	23	20	9	20	27
Node 15	42	53	52	39	46	60
Node 20	22	35	36	20	28	41

Reproduced with permission of the copyright owner. Further reproduction prohibited without permission.

$$u(\omega) = \frac{\overline{F}}{-\omega^2} = \frac{\hat{a}}{-\omega^2 f}, \tag{4.2}$$

where $\overline{F}$ is the FRF, $\hat{a}$ is the acceleration, f is the excitation force, and ω the excitation frequency. Equation 4.2 is applied to all the 21 points of measurement such that for a given frequency ω, it can be written as

$$\{u\} = \frac{\{\overline{F}\}}{-\omega^2}, \tag{4.3}$$

where $\{u\}$ is a 1-by-21 vector of displacement u_i (displacement at node i).

The measured transfer function is typically obtained in millivolts (mV). Using the sensitivity of the accelerometer (10.2 mV/g with g = 9.81 m/s^2) and the sensitivity of the force gage (10.8 mV/lb). The conversion factor is found. The FRF data must be multiplied by the coefficient given as

$$\overline{F} = (measurement)\left(\frac{9.81\ m/s^2}{10.2mV}\right)\left(\frac{4.448N}{10.8mV}\right)^{-1} = 2.335(measurement)\ m/N.s^2 \tag{4.4}$$

The plots obtained from this experiment are discussed in the next section.

The sound pressure measurements are conducted using a microphone (ACO model 7212), which is suspended in the air at different locations above the beam. The data are collected by the dynamic signal analyzer (HP 35670A). The

Reproduced with permission of the copyright owner. Further reproduction prohibited without permission.

measurements at different points along the x-axis are made by keeping the z and y-coordinates fixed, as shown in Figure 36.

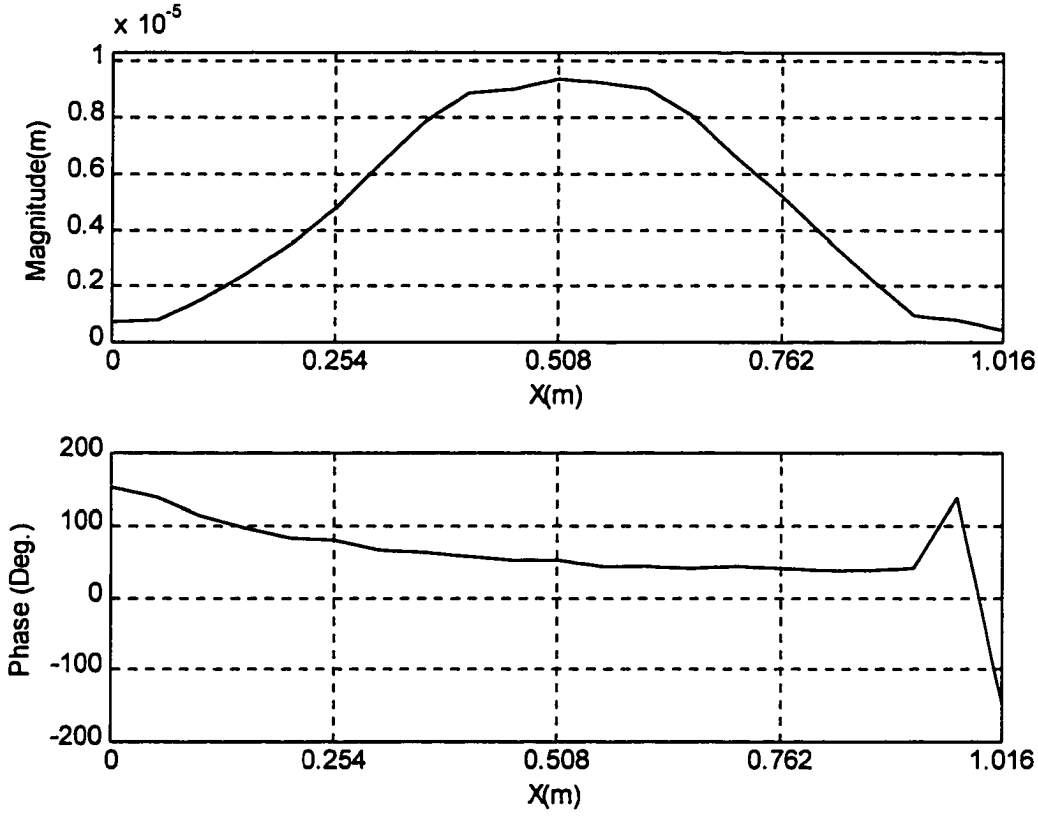

Figure 31. Plot of Beam Deflection, Mode 1 (64 Hz).

The sound pressure measured in *Pascals* (Pa) is converted to Sound Pressure Level (SPL) using the following equation

$$SPL(dB) = 20\log_{10}\left(\frac{measurement\ (Pa)}{P_{ref}}\right), \tag{4.5}$$

Reproduced with permission of the copyright owner. Further reproduction prohibited without permission.

where *ref* = 2e-5 *Pa* . The microphone sensitivity is 15.3 mV/Pa, thus

$$SPL(dB) = 20\log_{10}\left(\frac{measurement/15.3}{P_{ref}}\right). \tag{4.6}$$

The results of the sound pressure measurement at five different frequencies are presented in Figure 37 through Figure 41 along with the analytically predicted values.

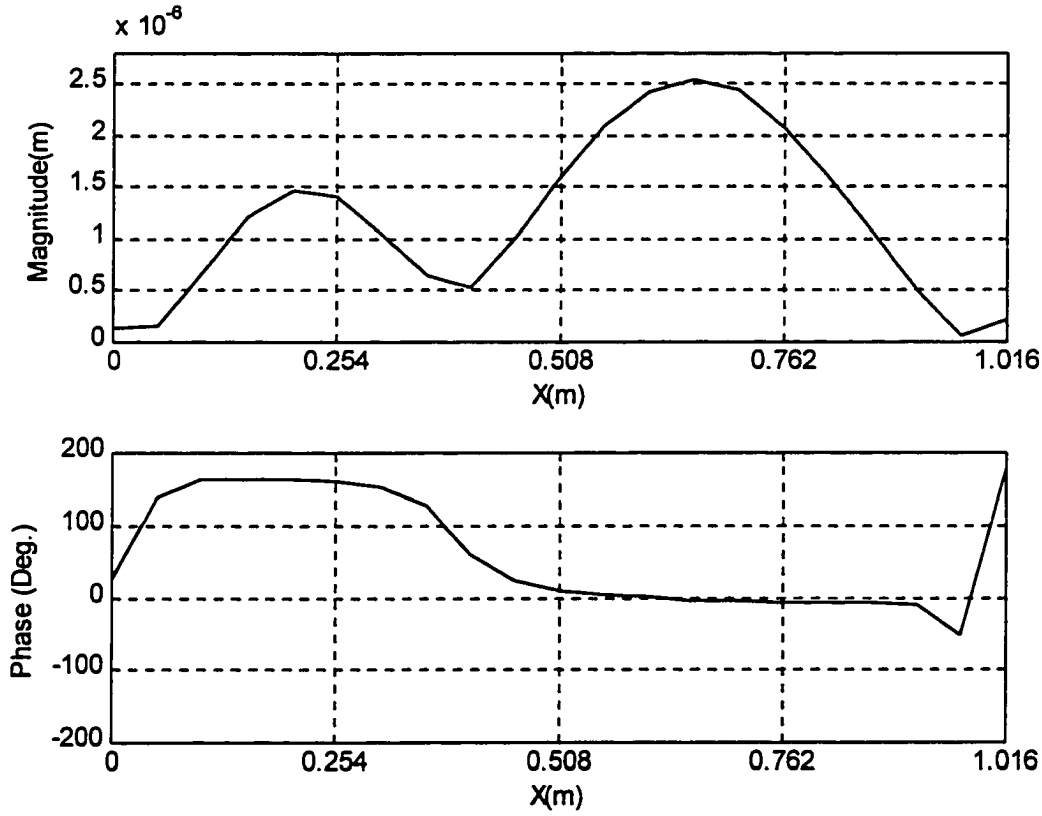

Figure 32. Plot of Beam Deflection, off Resonance (120 Hz).

Reproduced with permission of the copyright owner. Further reproduction prohibited without permission.

Discussion of Experimental Results

The ratio of the response between the beam and the box surface is measured and is found to be in the acceptable range. This is critical in sound pressure measurements since large vibration of the box surface would alter the measured sound radiated due to the vibration of the beam. Higher readings indicate that the vibration of the box surface is much less than the vibration of the beam. The values

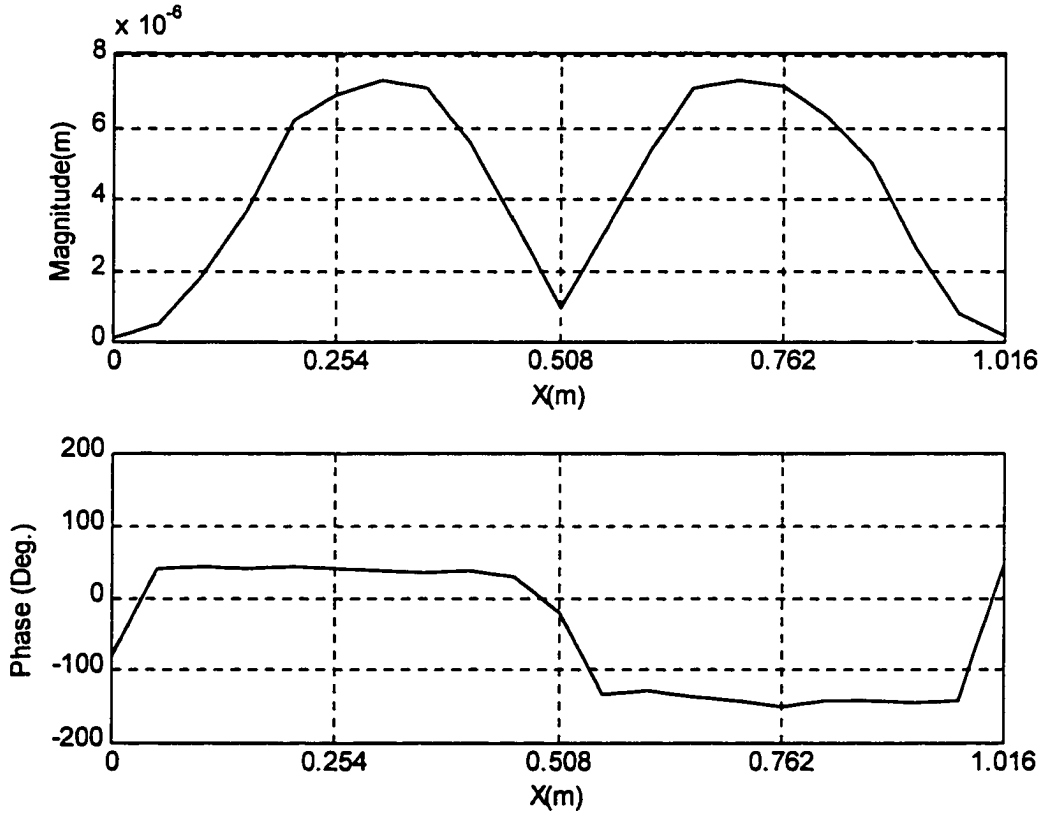

Figure 33. Plot of Beam Deflection, Mode 2 (174 Hz).

measured are found to be in the desired range (14 dB and higher) as shown in Table 4. However, measurements made at node 20 for all the frequencies, are very low

Reproduced with permission of the copyright owner. Further reproduction prohibited without permission.

since the beam displacements are low near the boundaries (clamped end) and the signal to noise ratio at that location is low.

The experimentally obtained resonances and damping factors given in Table 5 are used to find the beam vibration response (Equation 2.53) and the sound pressure radiated from the beam (Equation 2.59) analytically. The predicted first five natural

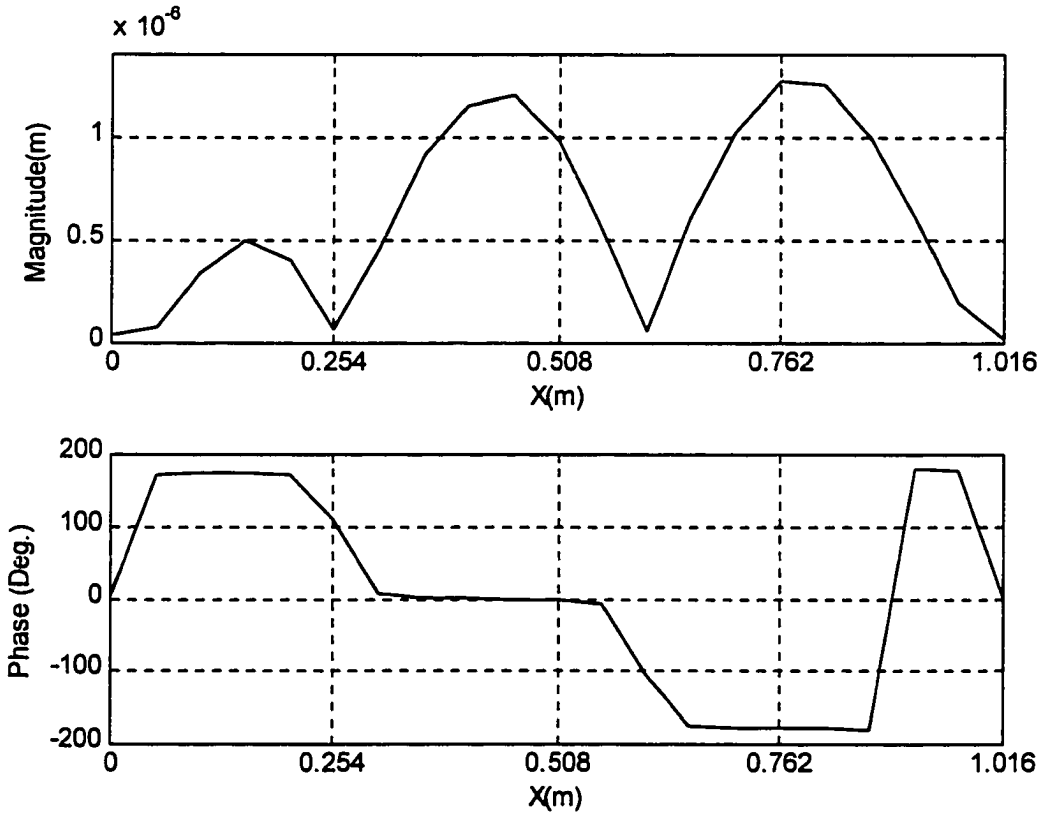

Figure 34. Plot of Beam Deflection, off Resonance (252 Hz).

frequencies of the beam obtained using the computer program, are also given in Table 5. The shaker force input is varied depending on the frequency of excitation to obtain

Reproduced with permission of the copyright owner. Further reproduction prohibited without permission.

a sound pressure level that is well above the background noise. The sound pressure measured closely matches the analytically predicted values. Thus, the clamped boundary conditions and the baffled beam assumption are validated.

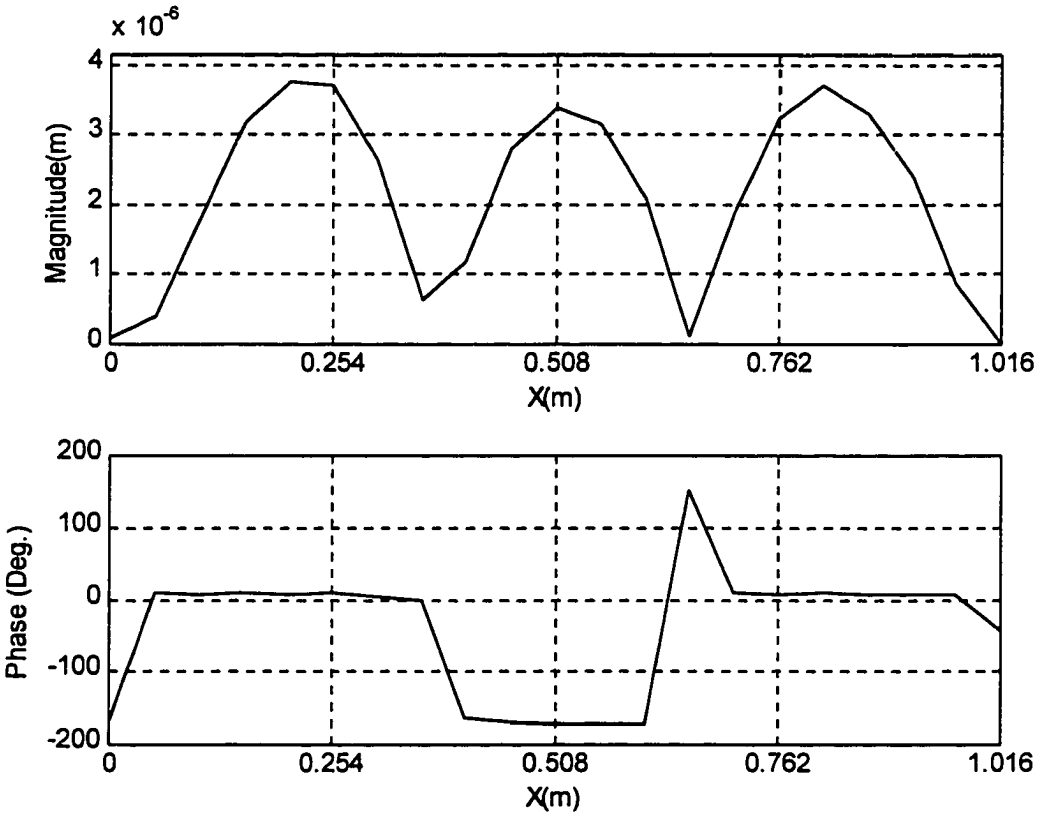

Figure 35. Plot of Beam Deflection, Mode 3 (332 Hz)

Experimental Verification of the Volume Displacement Sensors

Chapter III describes the theoretical development of volume displacement sensors. PVDF sensors are designed to measure the volume displacement of any arbitrary section of a beam. These sensors are verified using numerical simulation. The volume displacement of a beam section is calculated and compared to the output

Reproduced with permission of the copyright owner. Further reproduction prohibited without permission.

of a PVDF sensor designed for that section. The numerical simulation is further checked by a laboratory experiment as detailed in the next sections.

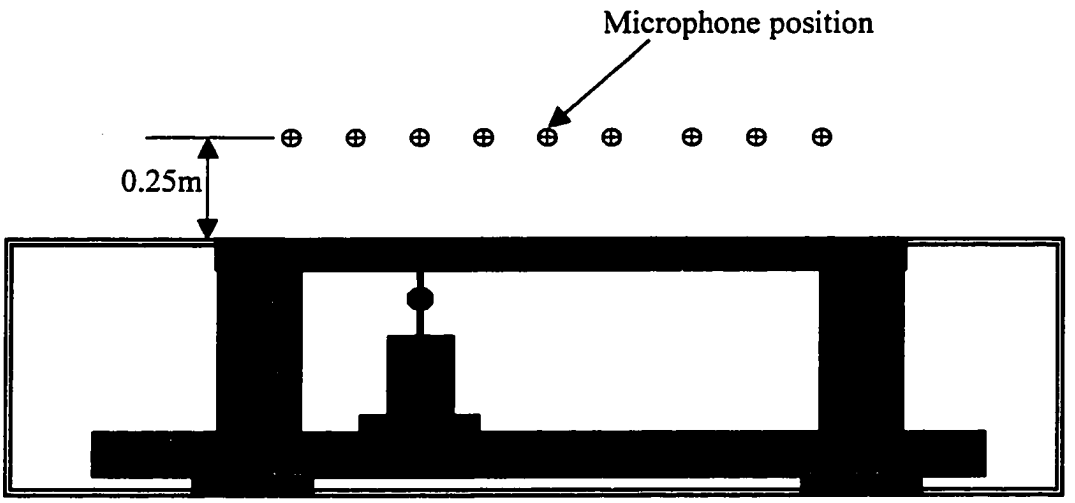

Figure 36. Sound Pressure Measurement Points Along the x-Axis (y = 0.019 m and z = 0.25 m).

The theory of loudspeaker volume displacement measurement is also presented in Chapter III. The sensor is a small microphone placed inside the loudspeaker enclosure. It measures the pressure variation inside the enclosure. Then, this measurement is converted into volume displacement by simply multiplying it by a constant. The following sections detail the experimental verification of this sensor.

Reproduced with permission of the copyright owner. Further reproduction prohibited without permission.

Volume Displacement Sensors for Beam

To verify the conclusions about sensor development, the experimental setup of Figure 29 is used. The volume displacement of each half of the beam is measured using two different methods. First, local volume displacement sensors are fabricated (using PVDF) and bonded to the surface of this beam. These sensors, which are bonded one above the other (but are electrically isolated from each other), are shown

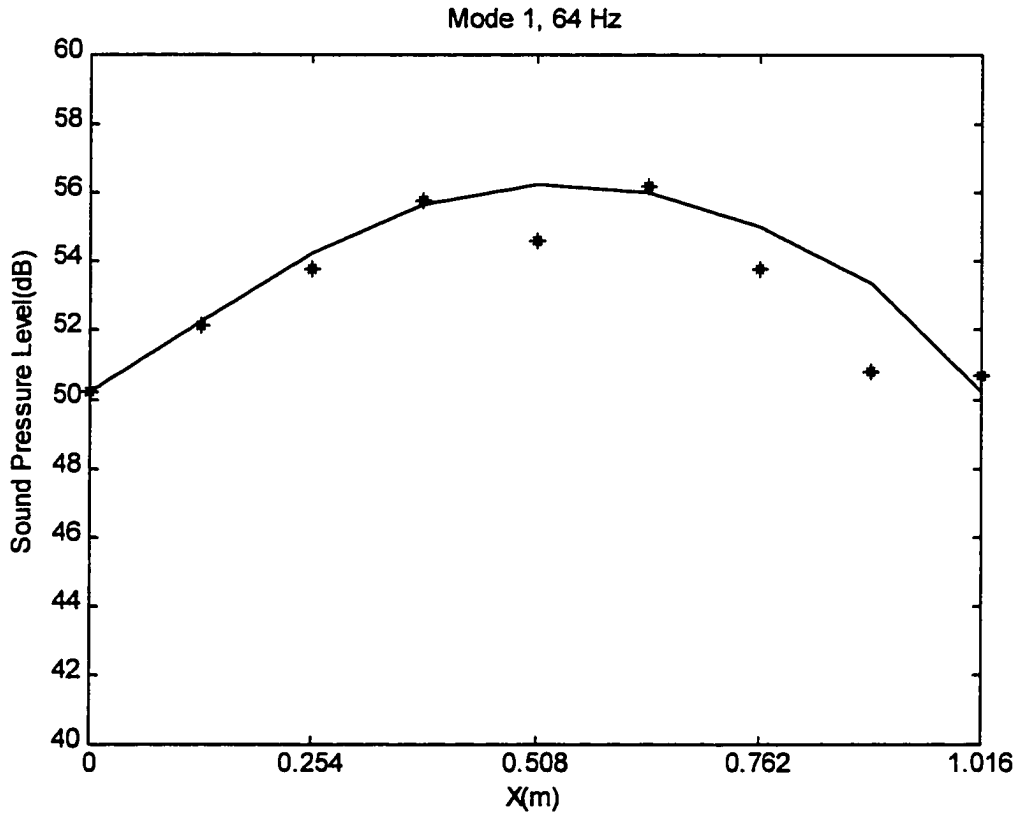

Figure 37. Plot of Sound Pressure Level Along the Beam at y = 0.019m and z =0.25m (*) = Measured, (Continuous) = Predicted With the Beam Excited at 64 Hz.

Reproduced with permission of the copyright owner. Further reproduction prohibited without permission.

in Figure 24. Using these sensors, the volume displacements of each half of the beam is measured. These measurements are then validated by computing the volume displacement of each of the beam halves using accelerometer measurements.

A single accelerometer is used to measure the acceleration of a series of points along the length of the beam subjected to a unit force over a broad band of frequencies from 0 – 800 Hz. Then, assuming the motion to be harmonic at each frequency, the beam displacements are calculated. Next, the volume displacement over each half-segment of the beam is estimated by integrating the displacements

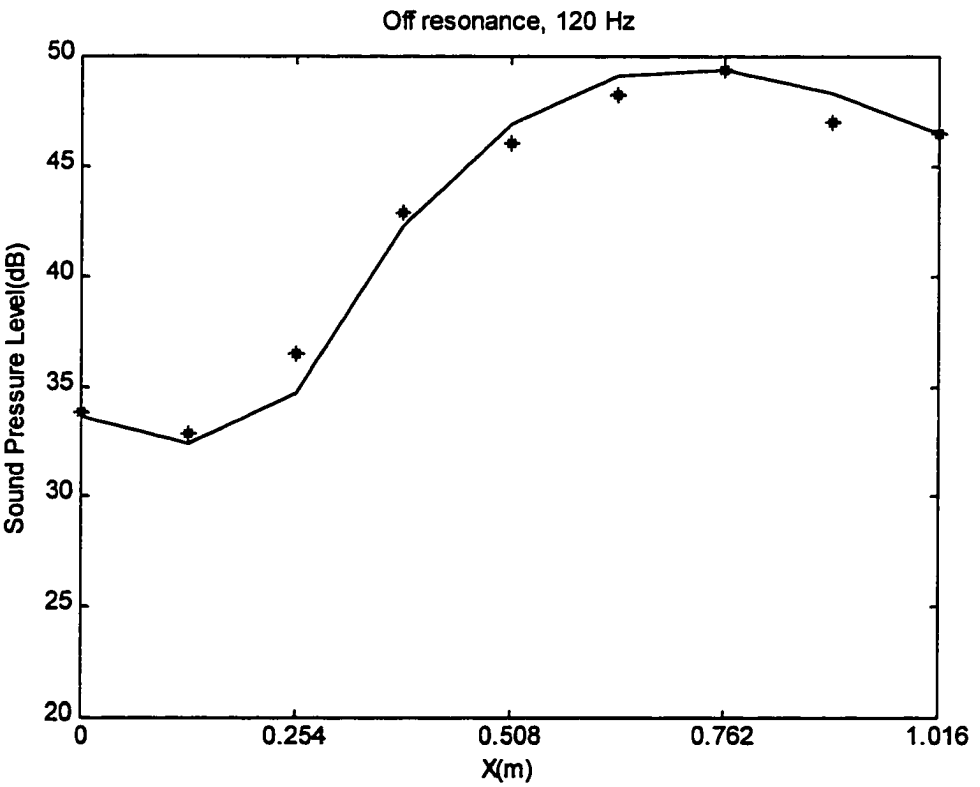

Figure 38. Plot of Sound Pressure Level Along the Beam at y = 0.019m and z =0.25m (*) = Measured, (Continuous) = Predicted With the Beam Excited at 120 Hz.

Reproduced with permission of the copyright owner. Further reproduction prohibited without permission.

over the length of that section and multiplying by the beam width. From Equation 3.9 the volume displacement of half of the beam is

$$\hat{D} = b \int_0^{\ell/2} u(x)dx \,. \tag{4.7}$$

For harmonic motion, the above equation can be written as

$$\hat{D} = b \int_0^{\ell/2} \left(\frac{-\hat{a}(x)}{\omega^2} \right) dx \,, \tag{4.8}$$

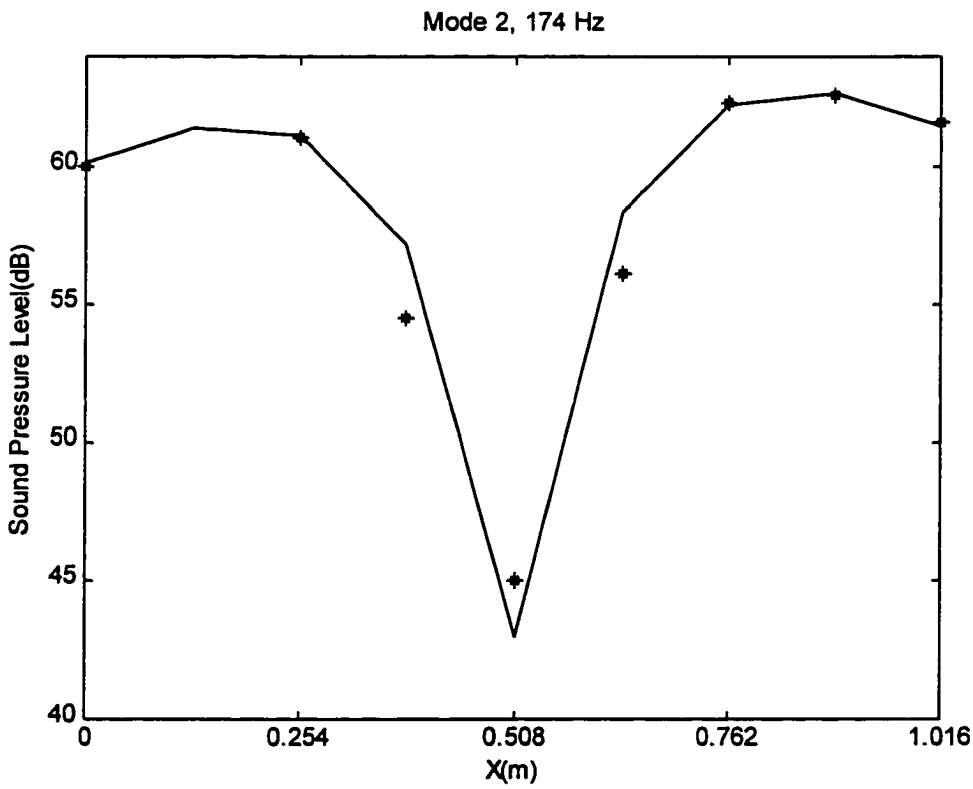

Figure 39. Plot of Sound Pressure Level Along the Beam at y = 0.019m and z=0.25m (*) =Measured, (Continuous) = Predicted With the Beam Excited at 174 Hz.

Reproduced with permission of the copyright owner. Further reproduction prohibited without permission.

where $\hat{a}(x)$ is the acceleration of the beam at position x. Equation 4.7 is approximated using the trapezoidal rule as

$$\hat{D} \cong \frac{-\ell b}{4\omega^2(n-1)}(\hat{a}_1 + 2\hat{a}_2 + ... + 2\hat{a}_{n-1} + \hat{a}_n), \tag{4.9}$$

where $n = 11$ is the total number of measurement points for half of the beam.

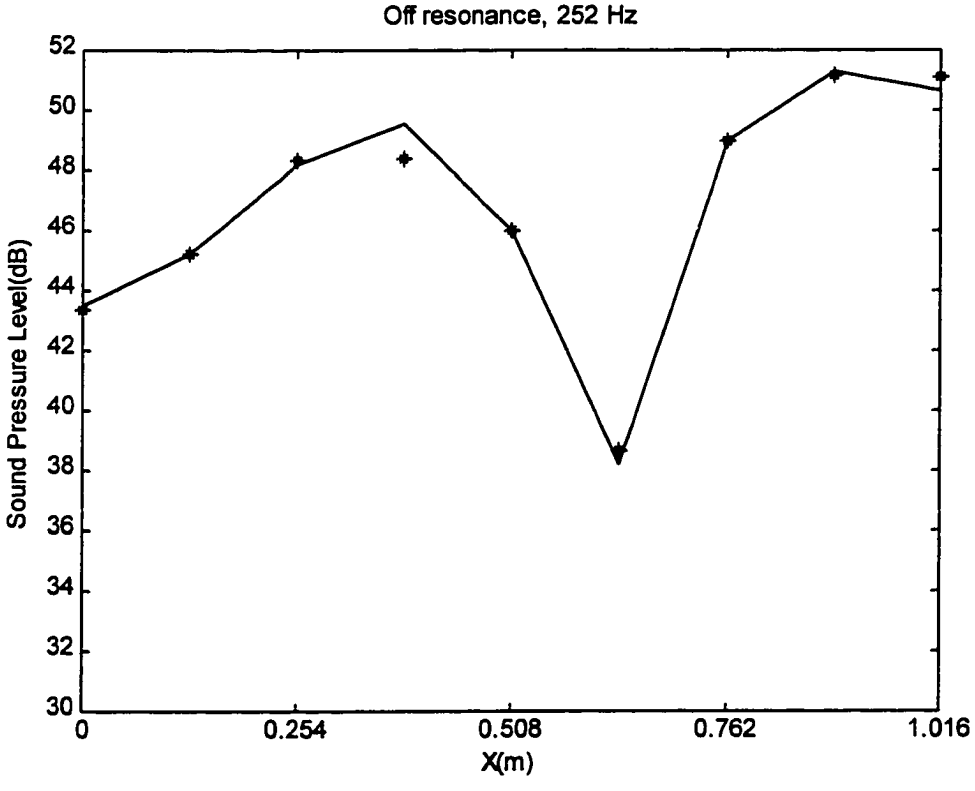

Figure 40. Plot of Sound Pressure Level Along the Beam at y = 0.019m and z =0.25m (*) = Measured, (Continuous) = Predicted With the Beam Excited at 252 Hz.

Reproduced with permission of the copyright owner. Further reproduction prohibited without permission.

Figures 42 and 43 show a comparison of the local volume displacements obtained using the accelerometer measurements and using the PVDF sensors for each of the beam halves. The PVDF measures the volume displacement accurately below 400 Hz (capturing the first three modes of the beam) for the right-half sensor that is bonded directly to the beam surface (Figure 43). The sensor accuracy, however, is decreased on the measurements of the left-half sensor that is bonded on top of the right-half sensor. As shown in Figure 42, this sensor can accurately measure the local

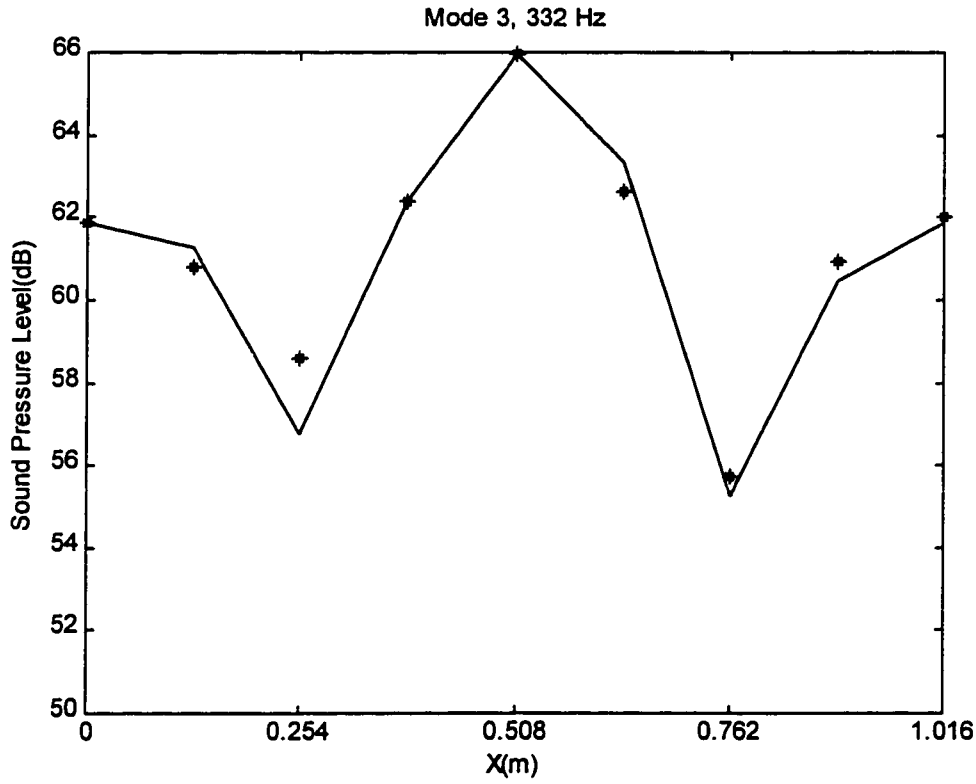

Figure 41. Plot of Sound Pressure Level Along the Beam at y = 0.019m and z =0.25m (*) = Measured, (Continuous) = Predicted With the Beam Excited at 332 Hz.

Reproduced with permission of the copyright owner. Further reproduction prohibited without permission.

volume displacement of the beam up to 300 Hz, capturing the first two modes of the beam. This difference can be attributed to the fact that ideally the sensor is to measure the beam strain, whereas by bonding a second sensor to the first sensor, the beam strain in addition to the strain in the first sensor is now being measured.

In order to facilitate the sensor development process the simulation module described in Chapter III can be utilized to predict the sensor output. The displacement vector previously measured and used in Equation 4.8 can be substituted in Equation 3.51. The results, as shown in Figure 44 and 45, closely match the actual output of the PVDF sensor. Thus, important design decisions, such as the adequacy of the output signal level, can be made before the fabrication of the PVDF sensor.

Table 5

Predicted and Experimental Values of Resonances and Damping Factors

Analytical		Experimental	
Mode Number	Frequency (Hz)	Frequency (Hz)	Damping factors
1	64	64	0.02
2	177	174	0.025
3	348	332	0.0026
4	575	534	0.042
5	860	784	0.07

It is important to note that the method of implementation of the PVDF sensors used in this work (surface bonding of each individual sensor) is not particularly well suited for applications where many (n>2) local sensors are required. Obviously, these sensors may overlap because each sensor spans the entire length of the beam. For two

Reproduced with permission of the copyright owner. Further reproduction prohibited without permission.

sensors (two beam sections) one could envision bonding sensors to the top and bottom surfaces of the beam. However, as soon as this strategy is used on a beam divided into three (or more) sections, other creative solutions must be used. One alternative may be to design narrower sensor strips and bond these sensors to the beam surface side-by-side. However, this strategy would also reach its limitations

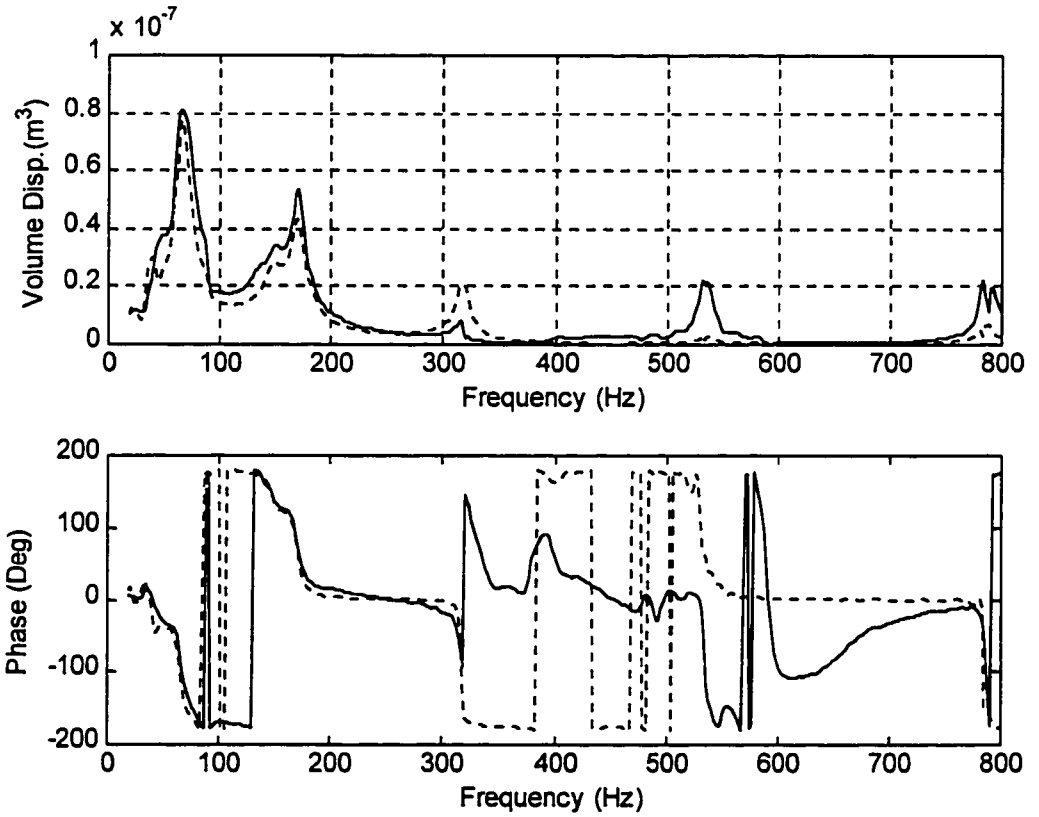

Figure 42. Local Volume Displacement of the Left Half of a Clamped Beam Measured Using Accelerometers (Dashed Lines) and PVDF Sensor Bonded to the Beam but on Top of the Right-Half Sensor (Solid Lines).

with many sections. In addition, the narrow PVDF strips would yield poor measurement accuracy. The other option, as demonstrated successfully in this thesis is to bond these sensors one on top of the other (stacked).

Reproduced with permission of the copyright owner. Further reproduction prohibited without permission.

A potentially more attractive alternative is that suggested by Lee and Moon (1990) which is referred to as 'spatial multiplexing'. In this strategy, several sensors,

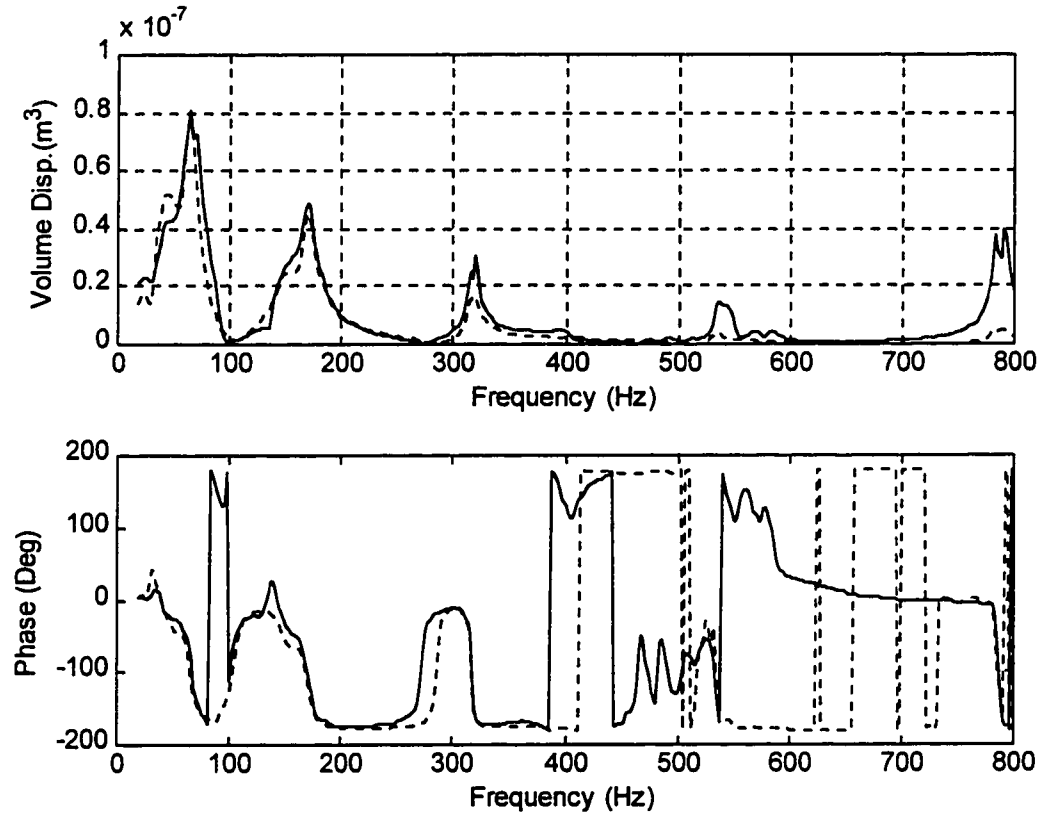

Figure 43. Local Volume Displacement of the Right Half of a Clamped Beam Measured Using Accelerometers (Dashed Lines) and PVDF Sensor Bonded to the Beam Surface (Solid Lines).

which share part of the surface, are integrated into one. An example of this strategy is given in Figure 46 for two sensors (i.e., beam divided in halves) on a clamped beam. The sum of charges generated by PVDF segments 1, 2, and 3 would provide an accurate measure of the volume displacement of the left half of the beam (Side 1). On the other hand, to measure the volume displacement of the right half of the beam

Reproduced with permission of the copyright owner. Further reproduction prohibited without permission.

(Side 2) the charges generated by PVDF segments 1, 4, and 5 have to be summed. One disadvantage of this strategy is that it can also become demanding on the data acquisition system as the number of PVDF segments becomes quite large for beams divided into many sections.

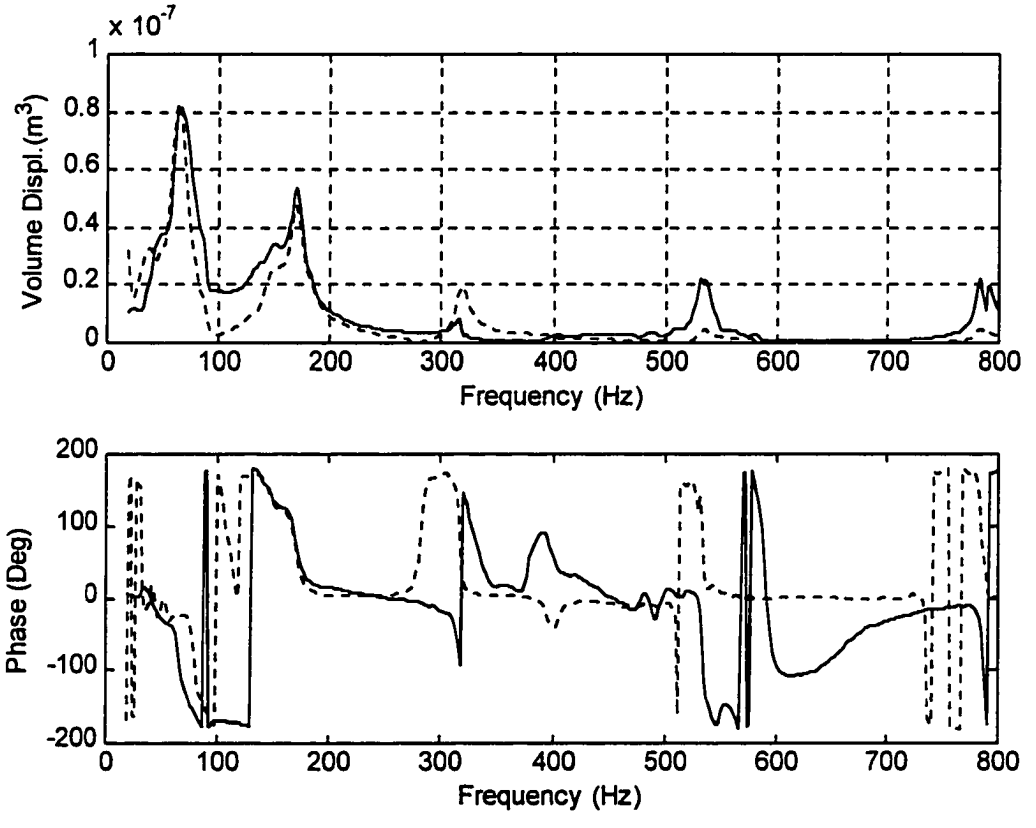

Figure 44. Local Volume Displacement of the Left Half of a Clamped Beam Simulated (Dashed Lines) and Actual PVDF Sensor Bonded to the Beam but on Top of the Right-Half Sensor (Solid Lines).

Volume Displacement Sensor for the Loudspeaker

Reproduced with permission of the copyright owner. Further reproduction prohibited without permission.

The verification of the loudspeaker volume displacement sensor (internal pressure sensor) is conducted using a single accelerometer mounted on the loudspeaker cone. The loudspeaker cone is assumed to move uniformly (i.e., simulating a piston). Acceleration measurements are integrated twice and multiplied

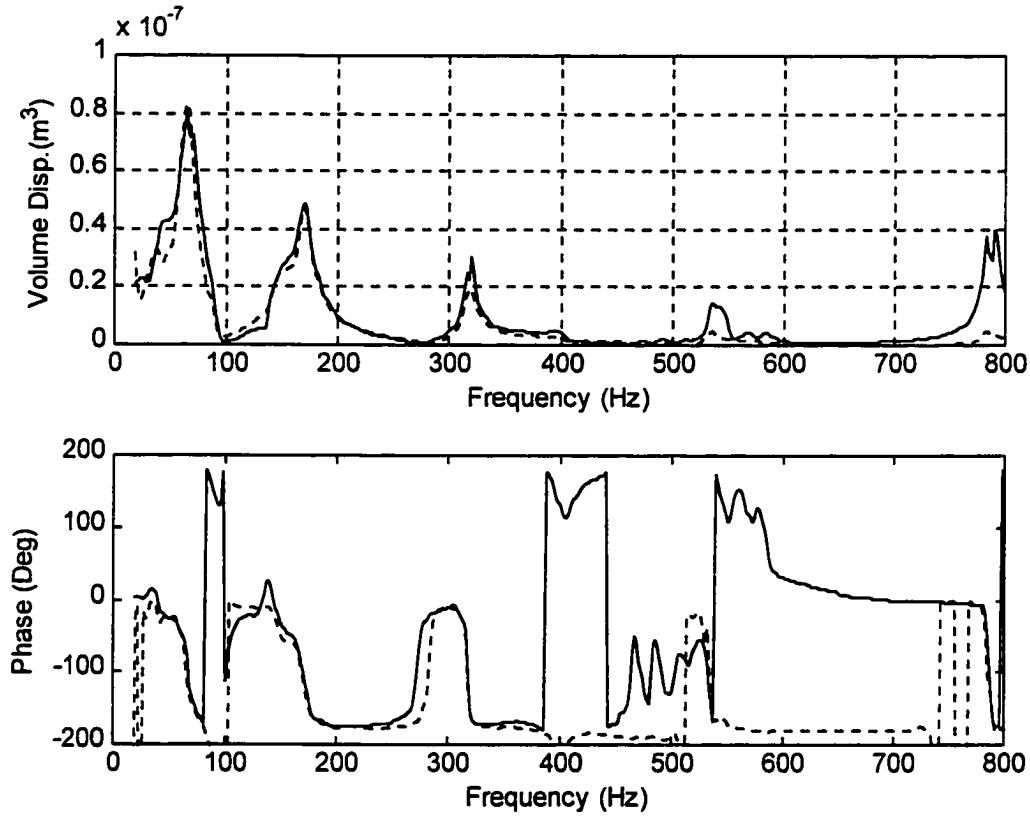

Figure 45. Local Volume Displacement of the Right Half of a Clamped Beam Simulated (Dashed Lines) and Actual PVDF Sensor Bonded to the Beam Surface (Solid Lines).

by the loudspeaker cone area to compute the loudspeaker volume displacement. The internal pressure sensor is a Radio Shack model 270-092 microphone and placed

Reproduced with permission of the copyright owner. Further reproduction prohibited without permission.

inside a sealed cylindrical loudspeaker enclosure. The loudspeaker is a Radio Shack model 40-1014A with cone diameter of 25.4 cm and the enclosure is made of 0.3175 cm thick plexiglass (24.13 cm height and 25.4 cm diameter), as shown in Figure 47.

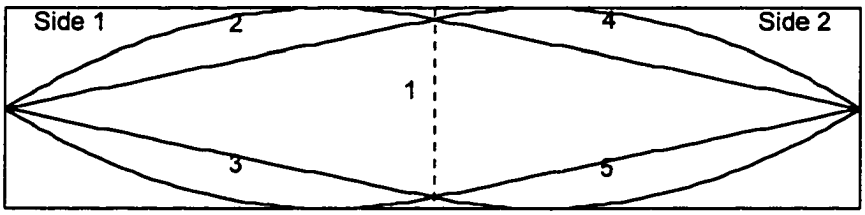

Figure 46. Integrated Sensor for Measurement of Volume Displacement of Each Half of the Beam.

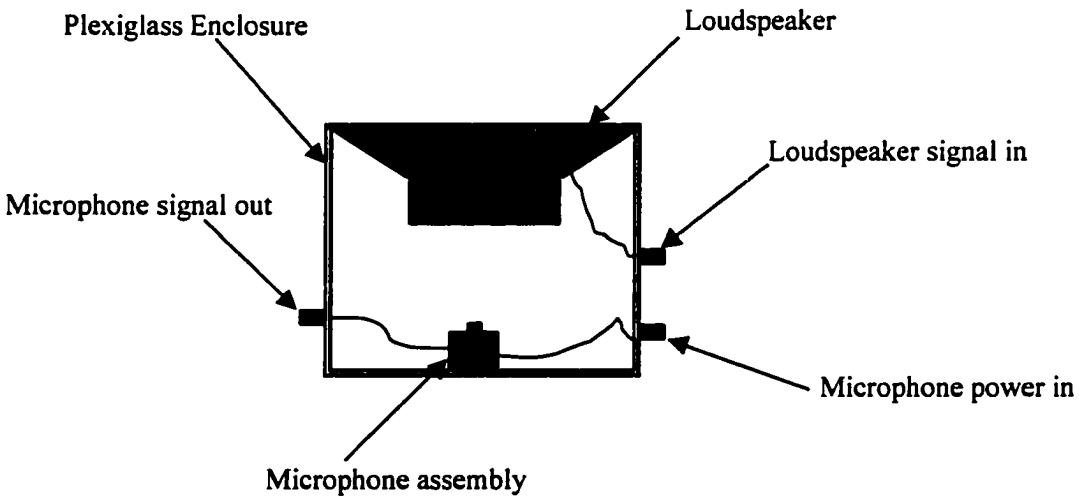

Figure 47. Loudspeaker, Internal Microphone Sensor and Enclosure Assembly.

A comparison of volume displacement values measured using the internal microphone sensor versus those measured using the cone accelerometer is shown in

Reproduced with permission of the copyright owner. Further reproduction prohibited without permission.

Figure 48. Excellent correlation is found up to 700 Hz between the volume displacement values measured using these two sensors.

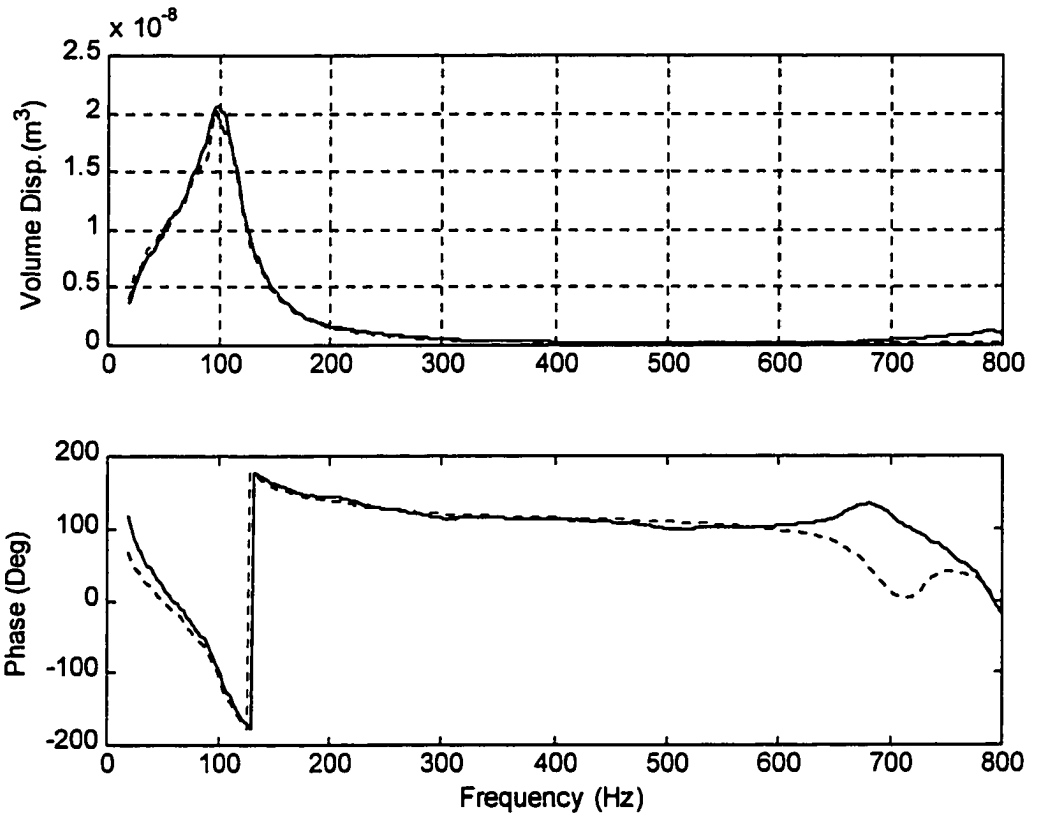

Figure 48. Comparison of Loudspeaker Volume Displacement Values Measured Using the Internal Microphone Sensor (Solid) Versus Values Measured Using a Single Accelerometer (Dashed)

Summary

In order to successfully perform the cancellation experiment, the physical model and the numerical model have to match. In this thesis, the volume displacement cancellation theory is developed around the Rayleigh integral. This assumes a baffled structure and well-defined boundary conditions. Thus, an

Reproduced with permission of the copyright owner. Further reproduction prohibited without permission.

experiment was performed to verify that the Rayleigh integral applies to the physical model. First, the natural frequencies of the beam are measured and compared to those predicted. The findings show that the clamped boundary conditions of the beam were achieved. The baffled condition was verified by measuring the sound pressure radiated by the beam and comparing it to the values predicted by the Rayleigh integral. The fact that the results were in close agreement proved that the experimental setup represented a baffled clamped beam.

An experimental verification of the volume displacement sensor was also performed. Two PVDF local volume displacement sensors were constructed, bonded to the beam and proved to accurately measure the volume displacement of the section they were designed for. Finally, the internal pressure sensor for the measurement of the volume displacement of a loudspeaker was fabricated and experimentally verified.

The experimental setup presented here seems to closely match the theoretical model used in the cancellation simulation presented in Chapter II. Thus, the noise reduction experiment can be performed. The details of this experiment is given in Chapter V.

Reproduced with permission of the copyright owner. Further reproduction prohibited without permission.

CHAPTER V

NOISE CONTROL EXPERIMENTS

Introduction

The control technique for reduction of sound radiated from vibrating structures is presented in this chapter. In Chapter II, the concept of local volume displacement cancellation is developed and numerically implemented. The experimental verification necessitates three elements: (1) the experimental setup, (2) the sensors to measure the volume displacement, and (3) the control systems. The first two elements are detailed in Chapters III and IV. The third element, control systems, is discussed in the following sections.

First, the volume displacement cancellation of a loudspeaker is performed. Two identical loudspeakers are used. One loudspeaker is the noise source. The other loudspeaker is used as the cancellation device. The internal pressure sensor developed and presented in Chapter III and IV are implemented within each loudspeaker enclosure. The signal from the source loudspeaker is fed to the cancellation loudspeaker through a controller. The details of this implementation are presented in the following sections. Next, the volume displacement of the baffled beam is cancelled. The beam is divided into two equal sections. The volume displacement of each section is measured using the PVDF sensors previously designed. The signals

Reproduced with permission of the copyright owner. Further reproduction prohibited without permission.

from these sensors are respectively fed to two separate controllers designed using the two-loudspeaker system.

Two-Loudspeaker System

The objective of this thesis is to control the local volume displacement of a baffled beam using loudspeakers. The local volume displacement of the beam, measured by PVDF sensors, is used as control input to the loudspeakers. Thus, in order to select the best and simplest control strategy possible, different control techniques are evaluated using a two-loudspeaker system. The surface of the loudspeaker is assumed to vibrate uniformly, therefore, it is modeled as a baffled piston. This makes the volume displacement cancellation of a loudspeaker ideal for the design of the controller that will be used in the beam experiment. The sound field of a baffled piston is relatively simpler to model and to control than the sound field of a baffled beam. This approach has been used by Kamman and Naghshineh (1998), to study various control techniques of the sound radiated by a loudspeaker. They used a loudspeaker cone accelerometer as the motion sensor. Thus, the sound pressure reduction was achieved by actively canceling the volume acceleration of the loudspeaker. The work presented here makes the use of internal pressure sensors to reduce the volume displacement of the loudspeaker.

Reproduced with permission of the copyright owner. Further reproduction prohibited without permission.

Physical System

The system consists of two Radio Shack model 40-1014A loudspeakers (25.4cm diameter), mounted on a cylindrical enclosure, as shown previously in Figure 47. The volume displacement of each loudspeaker is measured by a Radio Shack model 270-092 microphone placed in the enclosure. The volume displacement of the loudspeaker LS_1 (Figure 49) is fed to a computer controller that drives loudspeaker LS_2 to generate a modified noise field as detected by the microphone located roughly 0.5 m above the loudspeakers. Thus, LS_2 acts as a noise suppressor.

The controller is programmed onto a dSpace DS1102 board (mounted in a PC) using SIMULINK® (The MathWorks, Inc.) software. The analog input from the internal microphone is passed through a 16-bit Analogue to Digital (A/D) conversion unit, and the output from the digital controller is passed through a 16-bit Digital to Analogue (D/A) conversion unit. The computer controller provides an experimental platform that allows a comparison of different control strategies. The best strategy can be implemented in analog or digital circuits in its final implementation. A HP 35670A Dynamic Signal Analyzer is used to generate random noise that drives the source as well as to measure the microphone output.

System Model

Figure 50 shows a block diagram representation of the active noise control system. The transfer function in each of the blocks are defined as: (a) $LS_i (i = 1, 2)$ represent the loudspeaker/amplifier pairs, (b) volume displacement $VDS_i (i = 1, 2)$

Reproduced with permission of the copyright owner. Further reproduction prohibited without permission.

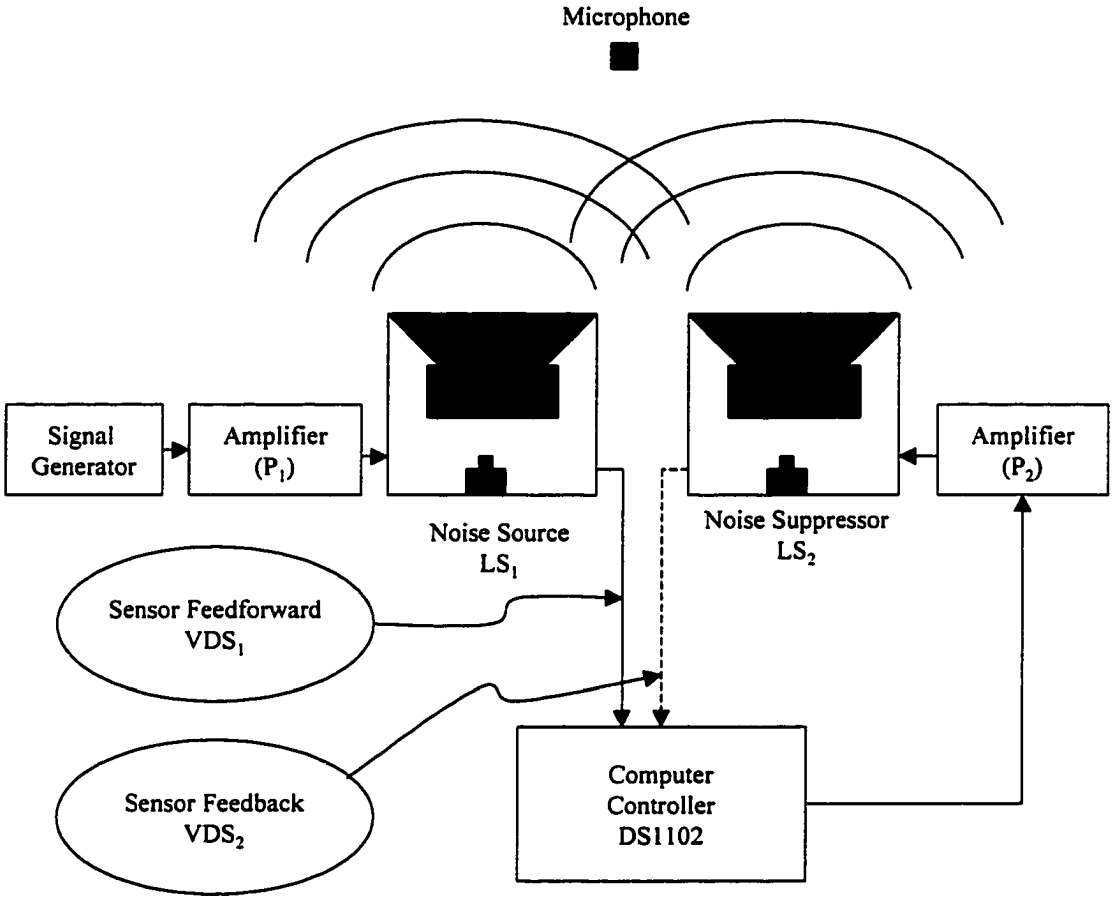

Figure 49. Two-Loudspeaker Active Noise Control System Experimental Setup.

represent the internal pressure sensor/signal conditioner pairs, and C represent the controller. The internal pressure sensor signal from the noise source (LS_1) is negated and used as a tracking signal. The output of the system as represented in Figure 50 is the net volume displacement of the two-loudspeaker system.

Reproduced with permission of the copyright owner. Further reproduction prohibited without permission.

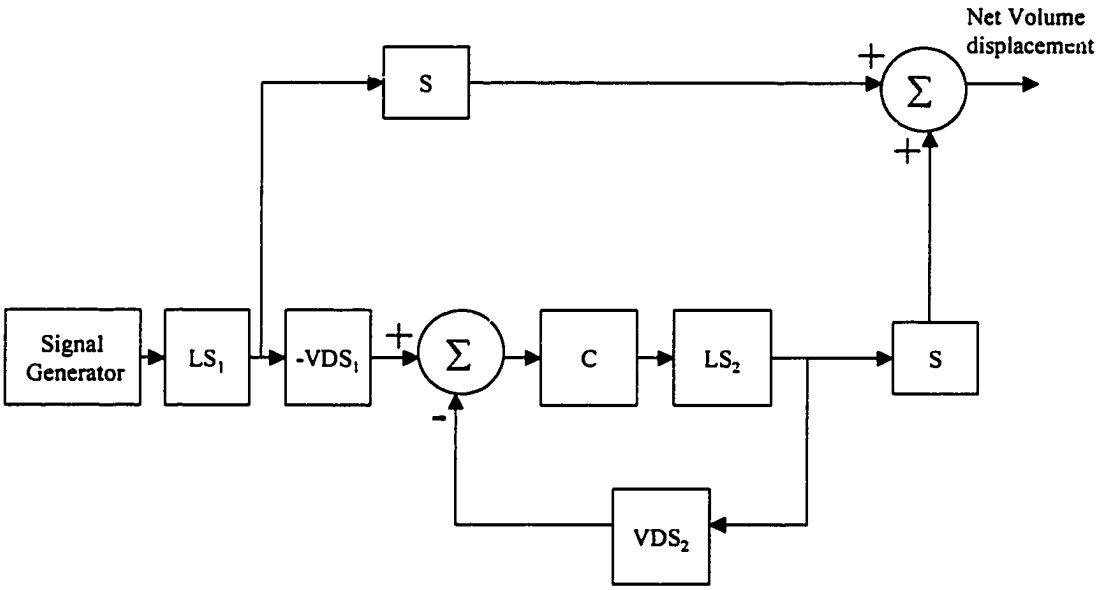

Figure 50. Block Diagram of the Two-Loudspeaker System Using Closed-Loop Control.

Controller Design

For good performance of the control system, it is important to have an accurate model of the transfer function of the loudspeaker/amplifier pairs. In this work, the interest is on the cancellation of low frequency noise. Therefore, the curve fits are focused on frequencies below 400 Hz. A z-domain transfer function with a third order numerator and fourth order denominator as shown in the following equation is found to be adequate.

$$TF_{LS} = \frac{a_3 z^3 + a_2 z^2 + a_1 z^1 + a_0}{b_4 z^4 + b_3 z^3 + b_2 z^2 + b_1 z^1 + b_0}, \tag{5.1}$$

Reproduced with permission of the copyright owner. Further reproduction prohibited without permission.

where $a_i\,(i = 0,1,2,3)$ and $b_i\,(i = 0,1,2,3,4)$ are given in Table 6. The best fit as defined by the system identification algorithm has all poles within the unit circle (stable model); two zeros fall within the unit circle and one zero outside the unit circle. Figure 51 shows a comparison of the measured and curve fit cancellation loudspeaker transfer function. Note that the fit is good from 20 to 450 Hz. The transfer function reaches a maximum at 94 Hz, which is the first resonance of the

Table 6

Transfer Function Coefficients

i	a_i	b_i
0	-2.752311130395190e-004	-1.147545735713940e-001
1	8.350463660384213e-004	4.681077943519877e-001
2	-8.232336909525310e-004	-7.167552407157837e-001
3	2.636033607394268e-004	4.882431122827351e-001
4	0	-1.248420949489856e-001

loudspeaker. This curve fit represents the model of the loudspeaker LS_2 and is used to design the controller.

A root locus analysis is used in the controller design process. Next, SIMULINK® (The Math Work, Inc.) is used to check the design for tracking capability. Then the cancellation experiment is carried out. It is important to note that the goal is to design a controller as simple as possible. Thus, a proportional feedback

Reproduced with permission of the copyright owner. Further reproduction prohibited without permission.

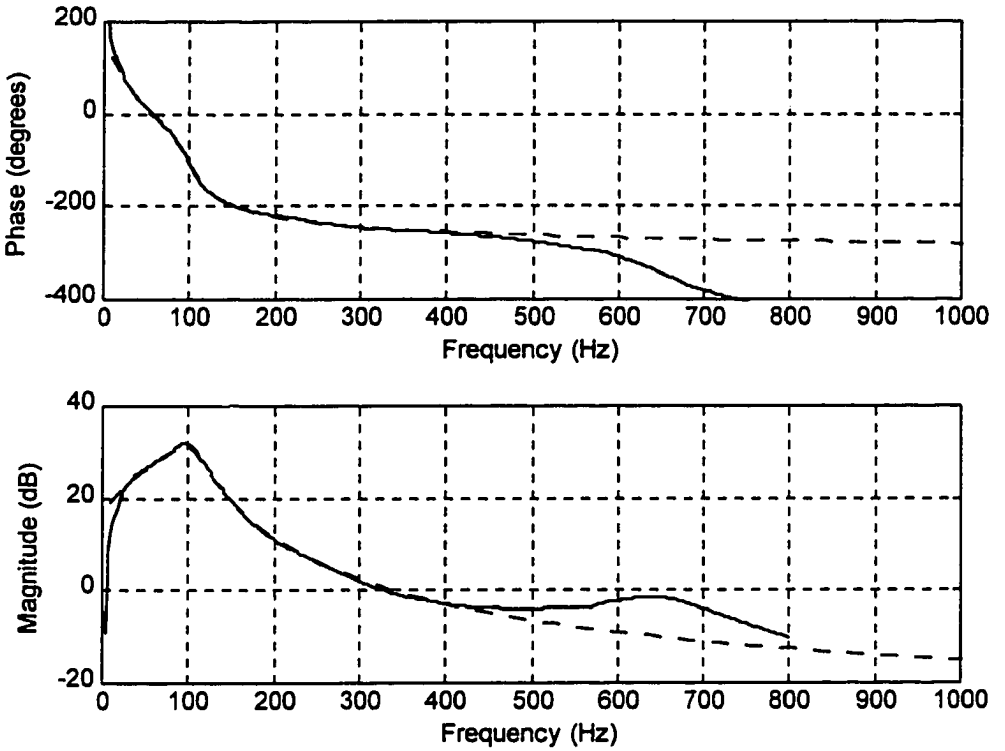

Figure 51. Comparison of Measured (Dashed) and Curve-Fit (Solid) Transfer Function of the Cancellation Loudspeaker.

controller is tested first. Poor performance of this type of controller led to the design of a Proportional and Derivative (PD) controller.

The equation of a digital PD controller is given by (Phillips, 1995) as

$$PD(z) = K_p + K_d\left[\frac{z\text{-}1}{Tz}\right], \tag{5.2}$$

where T is the sampling time, and K_p and K_d are the proportional and derivative gain respectively. This equation can be written as

Reproduced with permission of the copyright owner. Further reproduction prohibited without permission.

$$PD(z)=\left(\frac{K_pT+K_d}{T}\right)\left[\frac{z-\left(\frac{K_d}{K_pT+K_d}\right)}{z}\right], \tag{5.3}$$

or

$$PD(z)=A\left[\frac{z-B}{z}\right], \tag{5.4}$$

where

$$A=(K_pT+K_d)/T\ , \tag{5.5a}$$

and

$$B=K_d/(K_pT+K_d). \tag{5.5b}$$

Given values for A and B, K_p and K_d are found by solving the above equations simultaneously, such that

$$K_d=ABT, \tag{5.6a}$$

and

$$K_p=A(1-B). \tag{5.6b}$$

Reproduced with permission of the copyright owner. Further reproduction prohibited without permission.

A root locus analysis of the PD control, as shown in Figure 52, of loudspeaker LS_2 for various values of A shows that the system is stable up to a maximum value of A equal to 200 for B equal to 0.98. Other values of B also give a stable system but the maximum gain limit is low (for example when $B = 0.88$, $A_{max} = 15$). Therefore, the former is used in the volume displacement cancellation experiment.

Cancellation Experiment

Figure 53 represents the block diagram used in SIMULINK®. Random noise is fed to the noise source loudspeaker LS_1. The output of LS_1 is negated and tracked

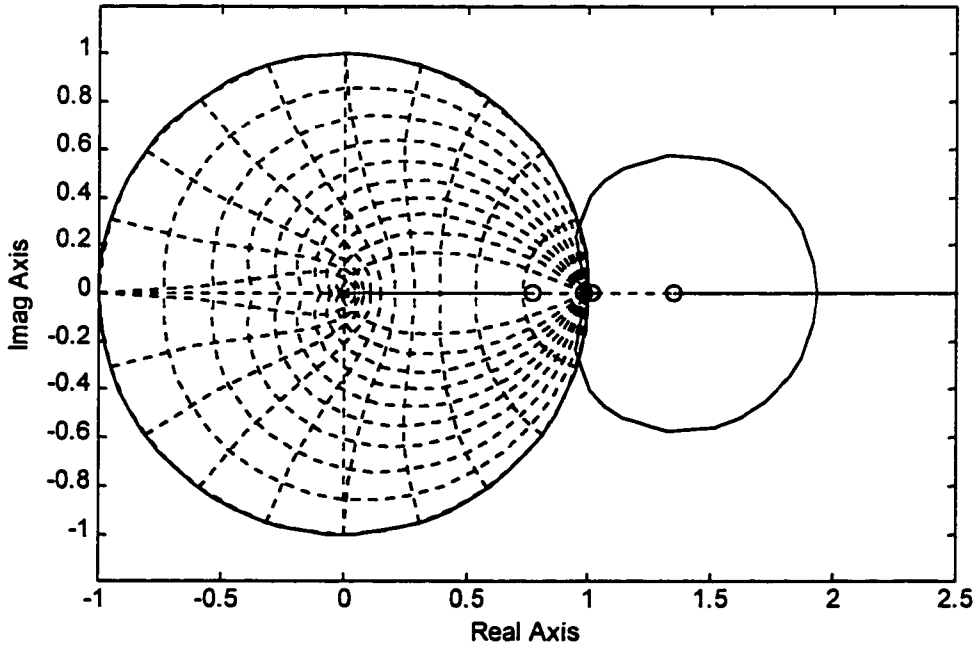

Figure 52. Root Locus Plot of the Closed-Loop Transfer Function of the System Represented by the Block Diagram of Figure 50 for $B = 0.98$ Where the Zeros are Represented by (o) and the Poles by (x).

Reproduced with permission of the copyright owner. Further reproduction prohibited without permission.

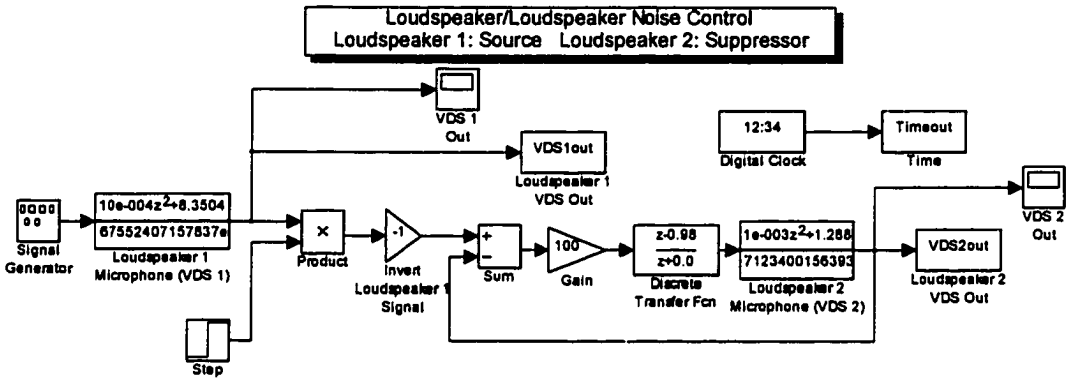

Figure 53. Simulation of Volume Displacement Cancellation Experiment.

by the cancellation loudspeaker LS_2. The outputs of the loudspeakers are shown in Figure 54. In this example, a 100 Hz sine wave is fed to the source loudspeaker LS_1. After 0.02 seconds, the output of LS_1 is negated and fed to the cancellation loudspeaker LS_2 for tracking. Thus, the signal from LS_2 would be 180 degrees out of phase with the original signal for a perfect tracking. In the actual cancellation experiment, these two signals would cancel each other provided the superposition and the impedance coupling principles apply. As mentioned in Chapter II, this would result in the attenuation of the sound pressure radiated by the source loudspeaker. The simulation experiment is fine-tuned with various values of A and B (Equation 5.4) until the phase between the two signals is about 180 degrees and their respective amplitudes are approximately the same. Then, the noise control experiment is performed. The experimental setup of Figure 49 is used. Two measurements are made. First, the noise level of the source LS_1 is measured, then the net noise level of

Reproduced with permission of the copyright owner. Further reproduction prohibited without permission.

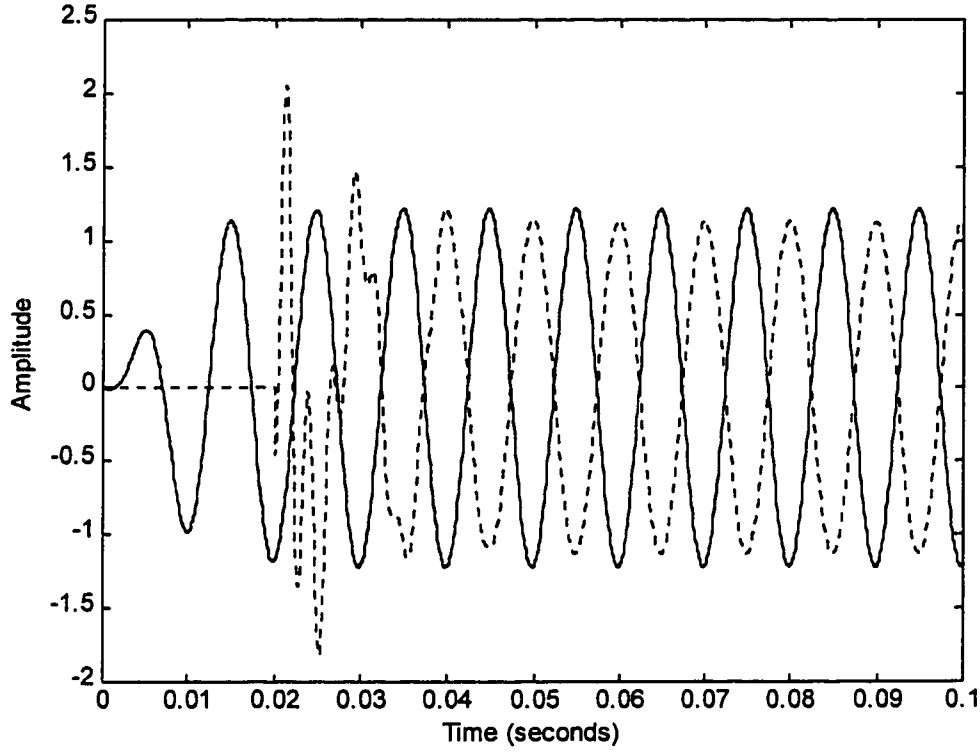

Figure 54. Simulation of Loudspeaker Volume Displacement Cancellation: the Solid Lines Represent the Source Loudspeaker Output and the Dashed Line is the Cancellation Loudspeaker Output.

the source LS_1 and the cancellation loudspeaker LS_2 is measured. Figure 55 shows a noise reduction of 5-30 dB over a range of 40-200 Hz.

Baffled Beam System

The controller developed in the two-loudspeaker system is used to actively reduce the noise radiated by the baffled beam. Two sections of the beam are used. The volume displacement of each section is measured by a PVDF local volume displacement sensor. Each sensor output is used to drive a cancellation loudspeaker.

Reproduced with permission of the copyright owner. Further reproduction prohibited without permission.

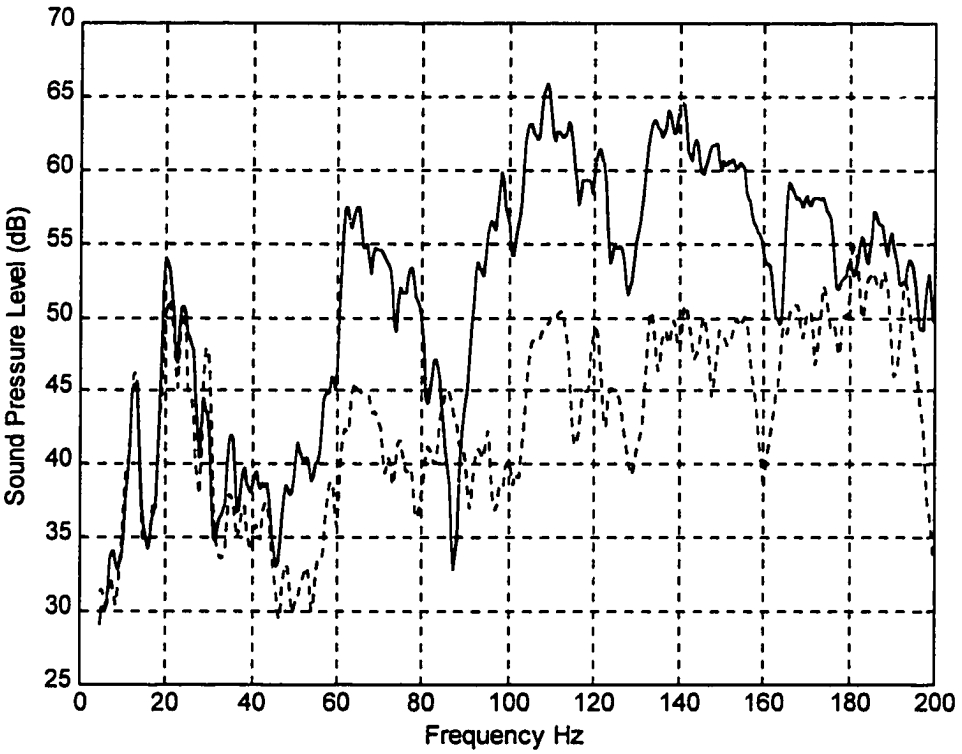

Figure 55. Sound Pressure Levels with (Dashed) and Without (Solid) Control for the Two-Loudspeaker System.

Thus, the loudspeakers are independently driven. The system used in this active local volume displacement cancellation of a baffled beam experiment is detailed in the following sections. The experimental procedure and the result of the noise reduction experiment are also presented.

Physical System

The system consists of the baffled beam described in Chapter IV and the two 25.4cm diameter Radio Shack model 40-1014A loudspeakers used in the two-

Reproduced with permission of the copyright owner. Further reproduction prohibited without permission.

loudspeaker system. The loudspeaker assembly is placed in the wooden box so that the face of the loudspeaker is flushed with the top surface of the wooden box, as shown in Figure 56. A random signal is fed to the shaker through the power amplifier P_3, causing random vibrations in the beam. These vibrations are measured in terms of volume displacements for each of the two sections of the beam. The output of each PVDF local volume displacement sensor LVD_i (i = 1, 2) is fed to the computer controllers that drive the two loudspeakers. The signal VDS_i (i =1, 2), from the internal microphones in the loudspeaker enclosure are for feedback. The loudspeakers, along with the vibrating baffled beam, generate a sound field such that the total noise radiated by the beam is reduced. The microphone placed about 0.5 m above the box is used to measure the sound pressure radiated by the beam-loudspeaker setup before and after control.

Noise Reduction Experiment

Figure 57 shows the block diagram representation of the cancellation experiment. Note that the objective is to use for each section of the beam, one PVDF sensor, one loudspeaker, and one control system. Therefore, two identical systems, each illustrated by the block diagram shown in Figure 57 are necessary for the control of the volume displacement of the entire length of the beam. The controllers are the PD controllers designed and fine-tuned in the two-loudspeaker system. Note that the controllers are designed separately for each of the loudspeakers. Two measurements

Reproduced with permission of the copyright owner. Further reproduction prohibited without permission.

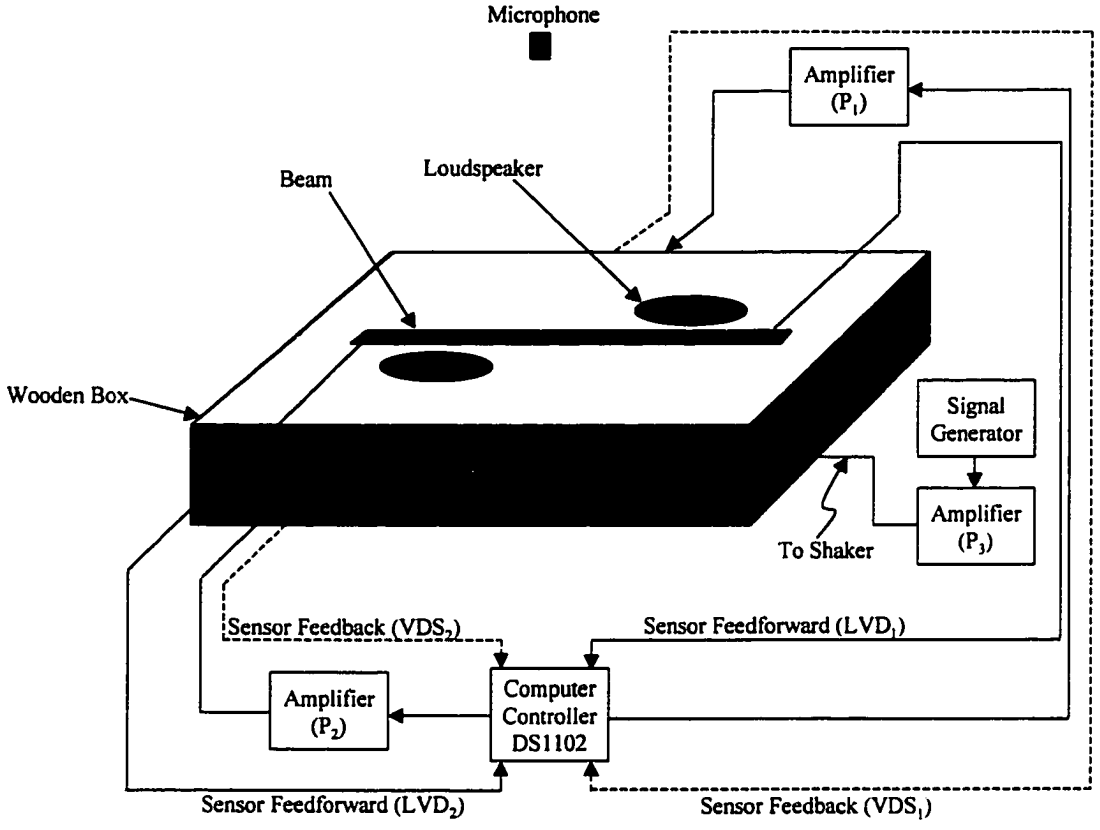

Figure 56. Baffled Beam Active Noise Control System Experimental Setup.

are made. First, the noise radiated by the beam is measured, then the net noise level of the beam and the loudspeakers is measured. Figure 58 shows that 5-15 dB noise reduction is obtained over the range 60-120 Hz. It also shows an increase in noise level above 120 Hz. Note that the region where noise reduction occurred is about half power below and above resonance (94 Hz).

Reproduced with permission of the copyright owner. Further reproduction prohibited without permission.

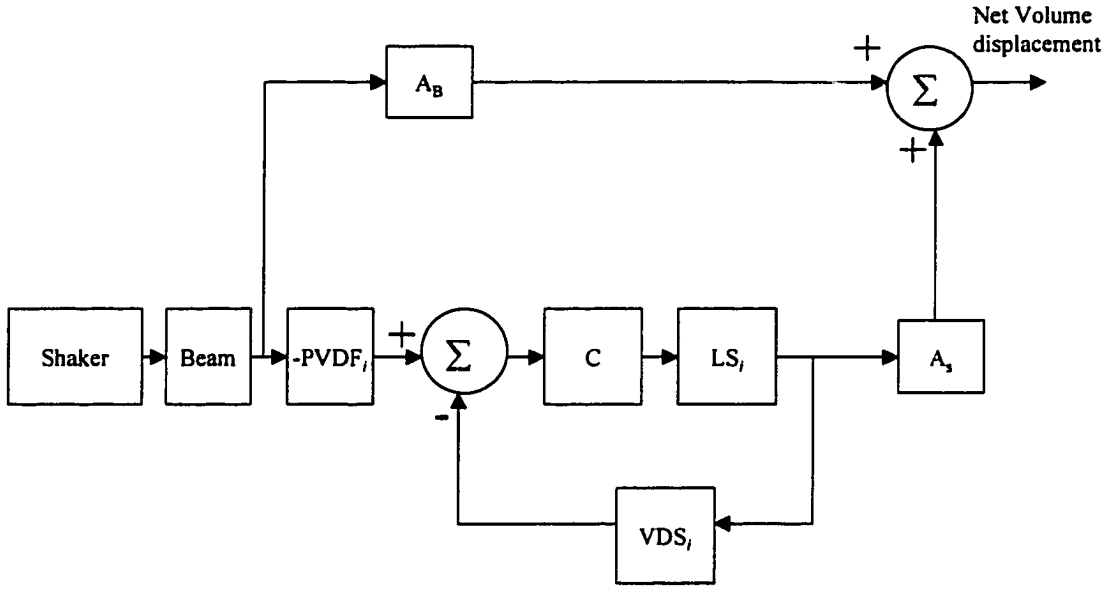

Figure 57. Block Diagram of the Baffled Beam System Using Closed-Loop Control.

Summary

Experiments have been performed to verify the reduction of sound radiated by vibrating structures, using local volume displacement cancellation. Two noise cancellation experiments were performed. The sound radiated by a loudspeaker was cancelled using an identical loudspeaker. A PD controller was used to track the negated volume displacement of the source loudspeaker. The results showed a 5 to 30 dB attenuation in sound pressure. This experiment was performed in order to design and fine tune the controller used in the beam experiment. Two loudspeakers were used to respectively cancel the volume displacement of each half of the beam. Noise reduction of 5 to 15 dB was obtained over the range of 60 to 120 Hz. Sound pressure enhancement was also recorded above 120 Hz. This limitation of the control

Reproduced with permission of the copyright owner. Further reproduction prohibited without permission.

apparatus could be attributed to several problems. One possible problem is the response of the loudspeaker. The transfer function of the loudspeakers drops rapidly on both sides of the resonance frequency, which is 94 Hz (Figure 51). Thus, the loudspeaker is not very responsive outside the frequency band around its resonance. This problem could possibly be solved by using a more sophisticated controller or switching to more responsive loudspeakers.

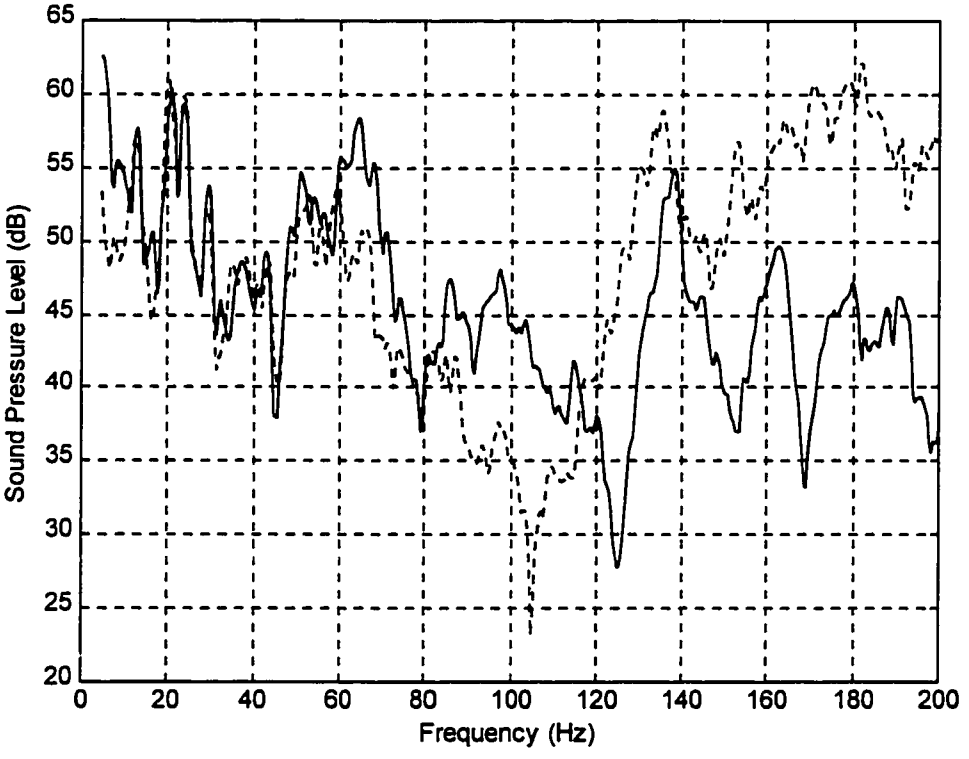

Figure 58. Sound Pressure Levels With (Dashed) and Without (Solid) Control for the Baffled Beam System.

Reproduced with permission of the copyright owner. Further reproduction prohibited without permission.

CHAPTER VI

CONCLUSIONS AND RECOMMENDATIONS

Conclusions

The goal of this research was to develop an active noise control device for the reduction of the noise radiated by a baffled beam. This apparatus was to utilize local volume displacement cancellation techniques to actively control the sound radiated by the beam. The concept behind this technique is not new. It has been widely accepted that minimization of volume displacement results in lower sound radiation. Prior researchers used the concept of the active control of sound radiated from structures by sensing and controlling the total volume displacement of the structure. This control, however, was achieved by altering the structural vibrations using structural actuators.

The methodology presented in this dissertation is different from the work of these authors in that, acoustic actuators were used to control the local volume displacement of the baffled beam. The objective of quieting the beam was broken into four separate problems. First, theoretical analysis of the beam vibrations was performed. This analysis was experimentally verified to ensure a correct laboratory model. Second, volume displacement sensors were developed for the beam and the cancellation loudspeakers. Finally, numerical simulation and experimental noise control was performed.

Reproduced with permission of the copyright owner. Further reproduction prohibited without permission.

The vibration of the beam was studied theoretically and experimentally. A finite element program was developed to calculate the natural frequencies and vibration response of the beam. These predicted values were experimentally verified. A simple modal testing was performed on the beam using an accelerometer. The beam was excited by a shaker and acceleration measurements were taken at 21 points along the x-axis, on the surface of the beam. The natural frequencies and velocity distribution were then extracted from the FRF and found to be in close agreement with the values predicted by the finite element program. This verifies that the laboratory setup closely represents a clamped beam.

The acoustic problem was studied experimentally and theoretically as well. The clamped beam studied in the vibration problem was placed in an enclosure to represent a beam in infinite baffle. For this configuration, the Rayleigh integral was utilized to describe the sound field of the beam above the baffle. A computer program was developed based on the results of the finite element model and the discretized form of the Rayleigh integral to compute the sound pressure radiated by the vibrating baffled beam. These numerical results were compared to the experimental values measured with a microphone. The experimental values were again very close to the predicted values, indicating that the laboratory setup closely represents a clamped beam in an infinite baffle.

The sensing problem was two-fold. First, a sensor to measure the volume displacement of the beam was developed. Second, a feedback sensor was developed

Reproduced with permission of the copyright owner. Further reproduction prohibited without permission.

to measure the volume displacement of the loudspeaker. Theoretical and experimental approaches were adopted in the development of these sensors.

A piezoelectric material (PVDF) was used to design sensors that measure the volume displacement of an arbitrary section of the beam. These PVDF sensors were developed using two approaches: modal expansion and quadratic form. The quadratic form was regarded as a more general case because it generated the sensor shape given by the modal expansion and many other possible sensor shapes. These sensors were numerically and experimentally verified. The experimental verification used measurements made by an accelerometer as a benchmark. Assuming harmonic excitations at each frequency, the measured accelerations were converted into volume displacement and compared to the volume displacement measured by the PVDF. The results showed that the PVDF sensor could accurately measure the local volume displacement of the beam. The numerical simulation was performed for prediction purposes. Knowing the experimental vibration response of the beam, the magnitude and phase of the PVDF sensor output was calculated at each vibration frequency. The PVDF measurements were in good agreement with these calculations, indicating that the PVDF output charge can be accurately predicted.

It is important to note that two PVDF sensors were used in the experiment. Each sensor measured the volume displacement of half of the beam. The first sensor was directly bonded to the surface of the beam. The second sensor was bonded to the top of the first sensor. The measurements from the sensor in direct contact with the beam were found to be more accurate than the second sensor.

Reproduced with permission of the copyright owner. Further reproduction prohibited without permission.

The loudspeaker volume displacement sensor was built using a microphone. A small microphone was mounted inside the loudspeaker enclosure. The pressure variation inside the enclosure was converted into the volume displacement of the loudspeaker. A single cone accelerometer was used to measure the acceleration of the loudspeaker cone which was assumed to have uniform motion. This acceleration was converted into loudspeaker volume displacement and compared to the output of the internal pressure sensor. Both measurements were in agreement. Thus, an internal pressure sensor that measures the volume displacement of a loudspeaker was successfully devised.

The noise control experiments tied together the different pieces of this research. The numerical model and the laboratory model built for the vibration, acoustic and sensor problems were used to experimentally control the volume displacement of the vibrating baffled beam. First, a numerical active noise control simulation was performed. Second, a two-loudspeaker system was utilized to design and experimentally verify the controller used in the beam experiment. Then, two loudspeakers were used to actively control the noise radiated by the beam.

A theoretical demonstration of the concept behind local volume displacement cancellation was presented. Acoustic power radiated was used to show, theoretically and through numerical simulation, that the noise radiated by a baffled beam could be reduced using cancellation loudspeakers. In this numerical experiment, four loudspeakers were utilized to cancel the volume displacement of four sections of the

Reproduced with permission of the copyright owner. Further reproduction prohibited without permission.

beam. The results show that acoustic power radiated by the beam can be reduced using local volume displacement cancellation.

Next, a PD controller was designed for each loudspeaker and tested with a two-loudspeaker system. A loudspeaker was used to cancel the volume displacement of a noise source loudspeaker. The controller for a given loudspeaker was designed by using that loudspeaker as a cancellation device. Thus, two PD controllers were developed. Then, the noise radiated by each loudspeaker was alternatively reduced using the other loudspeaker as cancellation device. The results show a 5 to 30 dB noise reduction.

The controllers were fine-tuned during these tests. These controllers were then used in the noise reduction experiment of the beam. In this experiment, two loudspeakers were used to actively cancel the volume displacement of two sections of the beam. The noise cancellation experiment concluded this work. The results showed a 5 to 15 dB reduction in sound pressure over a 60 to 120 Hz frequency band.

Some sound pressure enhancement occurred above 120 Hz. This could be due to several reasons. The PVDF sensor that was not directly bonded to the beam surface was less accurate. One could solve the sensor problem by using the multiplexed version proposed in Chapter 4. Another source of problems could have come from the loudspeaker. The loudspeaker was less responsive above 120 Hz. One could alleviate this problem by choosing a more responsive loudspeaker. Also a much more sophisticated controller could be designed to compensate the shortcomings of the loudspeaker. Finally, a better test condition must to be created.

Reproduced with permission of the copyright owner. Further reproduction prohibited without permission.

The pressure measurements were done at about 0.5m above the beam. This position corresponds to the near field given the size of the beam and the operating frequencies. A far field measurement could not be performed in the laboratory used for this research because of the high background noise levels. One could make these measurements in an anechoic chamber in order to fairly evaluate the performance of local volume displacement cancellation. However, the Western Michigan University anechoic chamber was found to be too small for the purpose of these experiments.

Recommendations for Future Research

The material presented in this thesis represents the first application of the local volume displacement cancellation concept to a non-uniformly vibrating structure. Thus, it has opened new avenues of research worth investigating. These avenues are sensor development, loudspeaker control and control systems. They need to be further investigated in the context of active local volume displacement cancellation. These new avenues of research will be separately addressed in the following paragraphs.

The sensing issue is critical to any active noise control strategy. A good sensor for active noise control will require no additional signal processing. In other words, the sensor output must be "control- ready". For instance, when the control variable is local volume displacement, the sensor output must be local volume displacement as is the case in the present work. However, the sensor development for sensing the volume displacement of any section of a beam needs to be further

Reproduced with permission of the copyright owner. Further reproduction prohibited without permission.

investigated. As mentioned in Chapter 4, the method of implementation of the PVDF sensors used in this work (surface bonding of each individual sensor) is not particularly well suited for applications where many local sensors are required. The results showed that the second sensor bonded on top of the first sensor is less accurate. One proposed solution was to use "spatial multiplexing". This technique was suggested by Lee and Moon (1990) but was not experimentally verified in the work presented here. Thus, one could perform further research on numerical simulation and experimental verification of the multiplexed version of the sensors developed in this work. Then, the next step would be to extend the design to a two-dimensional structure such as a plate.

Loudspeakers were used as cancellation devices in this thesis. No mention was made of their dynamics. These loudspeakers were simply modeled as baffled pistons. The assumption was that the face of the loudspeaker had uniform motion. This assumption would hold true for relatively small loudspeakers. The problem is that active noise control targets the low frequency range of the noise spectrum. Unfortunately, loudspeakers with good low frequency response have large diameters. Thus, the baffled piston theory may not hold anymore. One could find or use a more accurate model for the loudspeakers and incorporate it into the loudspeaker volume displacement sensor development, but this is not an easy task.

Finally, more research needs to be done on the development of the controller for local volume displacement cancellation application. Note that the goal is to design an active noise control device that is inexpensive. Thus, one should combine the

Reproduced with permission of the copyright owner. Further reproduction prohibited without permission.

above two possible research avenues with the control issue. Upgrading the complexity of the controller should be a last resort.

The next step, after the sensor, loudspeaker and control issues are mastered for the beam, would be to extend the local volume displacement cancellation concept to a two-dimensional vibrating structure. The first candidate for testing would be a rectangular baffled plate. A rectangular plate will exhibit non-uniform vibrations both lengthwise and widthwise. Thus, the one-dimensional sensing, actuating and control strategies developed in this work would be extended to a two-dimensional case. All developments would require the use of specifically developed numerical models and experimental setup.

Following the developments of a baffled beam and a baffled rectangular plate, experiments will be performed on a rectangular box with vibrating sides. As before, all cancellation devices will operate based on the local sensing/cancellation concept. Again, each cancellation device will reduce the sound radiated from the vibrating surface within its proximity. All experimental work will be accompanied by predictions of numerical models based on the solution to the Helmholtz Integral equation.

The most important impact of the research will be that a new, cost-effective means of actively suppressing the noise radiated from vibrating structures will be developed and made ready for the implementation in real-world applications. This technique is distinguished from other techniques by its simplicity, which could result in cost-effective implementation of active sound control in applications where cost is

Reproduced with permission of the copyright owner. Further reproduction prohibited without permission.

very competitive. Once completely developed, this technique will result in dramatic quieting of electrical transformer noise, home appliances, etc.

Reproduced with permission of the copyright owner. Further reproduction prohibited without permission.

REFERENCES

Allemang, R.J. and Brown, D.L. *Handbook on Experimental Modal Analysis.* Prentice-Hall, 1987.

Anthony, D.K., Elliott, S.J. (1991). *A Comparison of Three Methods of Measuring the Volume Velocity of an Acoustic Source.* J. Audio Eng. Soc., Vol. 39, No. 5, 355-3666G.

Balas, M. J. (1978). *Feedback Control of Flexible Systems.* IEEE Trans. Auto. Contr., 23, 673-679.

Berry, A., Charette, F. and Guigou, C. (1995*). Volume Velocity Sensors for Plates.* Internal Report, Gaus. Dept. of Mech. Eng., Sherbrooke University.

Burdisso, R. A. and Fuller, C. R. (1992). *Dynamic Behavior of Structural-Acoustic System in Feedforward Control of Sound Radiation.* J. Acoust. Soc. Am., 92(1), 277-286.

Chandrupatla, T.R. and Belegundu, A.D. (1991). *Introduction to Finite Elements in Engineering.* Prentice-Hall, New Jersey.

Charette, F., Berry, A., Guigou, C. (1998). *Active Control of Sound Radiation from a Plate using a Polyvinylidene Fluoride Volume Displacement Sensor.* J. Acoust. Soc.Am., 103(3), 1493-1503.

Clark, R. L. and C.R. Fuller. (1992a). *Optimal Placement of Piezoeletric Actuators and Polyvinylidene Fluoride (PVDF) Error Sensors.* J. Acoust. Soc. Am., 92(3), 1521-1532.

Clark, R. L. and C.R. Fuller. (1992b). *Experiments on the Active Control of Structurally Radiated Sound Using Multiple Piezoceramic Actuators.* J. Acoust. Soc. Am., 91, 3313-3320.

Crawley, E. F. and De Luis, J. (1987). *Use of Piezoelectric Actuators as an Element of Intelligent Structures.* AIAA J., 25, 1371-1385.

Deffayet, C. and Nelson, P. A. (1988). *Active Control of Low Frequency Harmonic Sound Radiated by a Finite Plane.* J. Acoust. Soc. Am., 84(6), 2192-2199.

Reproduced with permission of the copyright owner. Further reproduction prohibited without permission.

Dimitriadis, E. K., Fuller, C. R. and Rogers, C. R. (1989). *Piezoelectric Actuators for Distributed Vibration Excitation of Thin Plates.* J. Vib. Acoust., 113, 100- 107.

Elliott, S. J. and Nelson, P. A. (1986). *An Adaptive Algorithm for Multi-channel Active Control.* Proc. Inst. Acoust., 8, 135-147.

Elliott, S. J. and Nelson, P.A. (1993). *Active Noise Control.* IEEE Signal Processing Magazine, October 1993.

Elliott, S. J., Sutton, T. J., Rafachy, B. and Johnson, M. (1995). *Design of Feedback Controllers Using a Feedforward Approach.* Active 95 Newport Beach, CA, USA.

Erikson, L.J. and Allie, M.C. (1987). *A Digital Sound Control System for Use in Turbulent Flows.* Noise-con 87, State College, PA, WSA, June 8-10, 1987. Proceedings: P. 365-370.

Ewins, D.J. (1984). *Modal Testing: Theory and Practice.* RSP Ltd., England, 1984.

Fahnline, J. B. and Koopmann, G. H. (1996). *A Lumped Parameter Model for the Acoustic Power Output From a Vibrating Structure.* J. Acoust. Soc. Am., 100(6), 3539-3547.

Ffowes-Williams, J. E. (1984). *Anti-sound.* Proc. R. Soc. London, Ser. A. 395, 63-88.

Fuller, C. R. (1987). *Apparatus and Methods for Global Noise Reduction.* U. S. Patent No. 4,715,599.

Fuller, C. R. (1991). *Active Control of Sound Transmission/Radiation From Elastic Plates by Vibration Inputs: I. Analysis.* J. Sound. Vib., 136(1), 1-15.

Gonzalez, A, Albiol, A. and Elliott, S. *Minimization of the Maximum Error Signal in Active Control.* IEEE Transactions on Speech and Audio Processing, Vol. 6. No. 3, May 1998

Guigou, C., Charette, F. and Berry, A. (1994). *Active Control of Sound by Minimization of Volume Velocity on Finite Beam.* Proc. of the 3rd International Congress on Air and Structure-Borne Sound and Vibration, Montreal, Canada, pp. 1507-1514.

Harris, C. M. (1995). *Shock and Vibration Handbook.* The McGraw-Hill Companies, Inc.

Reproduced with permission of the copyright owner. Further reproduction prohibited without permission.

Jessel, M. (1966). *Traduction du Principe de Huygns en Acoustique Lineaire.* E.R. Acad. Sci. Paris, 262, 1321-1324.

Johnson, M. E. and Elliott, S. J. (1993). *Volume Velocity Sensors for Active Control.* Proc. Inst. Acoust., 15(3), 411-420.

Johnson, M. E. and Elliott, S. J. (1995). *Active Control of Sound Radiation Using Volume Velocity Cancellation.* J. Acoust. Soc. Am., 98(4).

Junger, M. C. and Feit, D. (1972). *Sound Structures and their Interactions* (MIT Press, Cambridge, Massachusetts).

Kamman, J. W., Naghshineh, K., (1998). *A Comparison of Open-Loop Feedforward and Closed-Loop Methods for Active Noise Control Using Volume Velocity Minimization.* J. of Applied Acoustics, 57, 29-37 .

Kinsler, L. E., Frey, A. R., Coppers, A. B., Sanders, J. V. (1982). *Fundamentals of Acoustics.* John Wiley & Sons, Inc.

Lee, C. K. and Moon, F. C., (1990). *Modal sensors/actuators.* Trans. Of ASME, vol. 57, pp. 434-441.

Lueg, P. (1936). *Process of Silencing Sound Oscillations.* US patent No. 2, 043, 416.

Mason, V. B., and Naghshineh, K., (1995). *Method and apparatus for reducing noise radiated from a complex vibrating surface.* US Patent 5,410,607.

Mason, V. B., Naghshineh, K. and Toth, G. K., (1994). *Broadband, wide-area active control of sound radiated from vibrating structures using local surface-mounted radiation suppression devices.* Proc. of Noise-Con, pp. 467-472.

Morse, P. M. (1986). *Vibration and Sound.* American Institute of Physics, New York, 1986.

Naghshineh, K., Kamman, J. W., Mason, V. B. and Toth, G. K. (1995). *Feedforward Controller for Active Reduction of Radiated Noise From a Uniformly Vibrating Plate.* ASME International Mechanical Engineering Congress and Exposition.

Naghshineh, K. and Koopmann, G. H. (1992). *A Design Method for Achieving Weak Radiator Structures Using Active Vibration Control.* J. Acoust. Soc. Am., 92, 856-870.

Reproduced with permission of the copyright owner. Further reproduction prohibited without permission.

Naghshineh, K., and Mason, V. B. (1996). *Reduction of Sound Radiated From Vibrating Structures via Active Control of Local Volume Velocity.* Applied Acoustics, 47 (1996), 27-46.

Nelson, P. A., Curtis, A. R. D., Elliott, S. J. and Bullmore, A. J. (1987). *The Minimum Power Output of Free Field Point Sources and the Active Control of Sound.* J. Sound Vib., 116(3), 397-414.

Oppenheim, A. V., Weinstein, E., Zangi, K. C., Feder, M. and Ganger, D. (1992). *Single Sensor Active Noise Cancellation Based on EM Algorithm.* Proc. ICASSP, 92(1), 277-280.

Phillips, C. L. and Nagle, H.T. *Digital Control Systems Analysis and Design.* Prentice-Hall, 1995.

Rayleigh, J. W. S. (1945). *The theory of sound.* Reprinted by Dover, New York.

Rex, J., (1991). *The use of Integrated Transducers for the Active Control of Structural Vibration.* M.Sc Thesis University of Southampton.

Ross, C.F., (1981). *A demonstration of Active Control of Broadband Sound.* Journal of the Acoustical Society of America , Vol. 74, No.3,1981, pp. 411-417.

Scott, J. P., Snyder, D., Hansen, C. H. and Fuller, C. R. (1992). *Active Control of Far-field Sound Radiated by a Rectangular Panel – A General Analysis.* J. Acoust. Soc. Am., 91(4), 2056-2066.

Sung, Chia-Chi and Jan C. T. (1997). *Active Control of Structurally Radiated Sound From Plates.* J. Acoust. Soc. Am., 102(1).

Swanson, D.C.,(1989). *Active attenuation of Acoustic Noise : Past, Present and Future.* ASHARE transactions, volume 95, part 2.

Swinbanks, M. A., (1982). *The active control of low frequency sound in gas turbine compressor installation.* Internoise 82, San Francisco, CA, May 17-19, 1982. Proceedings: pp. 423-426.

Temkin, S. (1981). *Elements of acoustics.* John Wiley & sons, Inc.

Wallace, C. E. (1972). *The radiation resistance of a baffled beam.* J. Acoust. Soc. Am., 51(3), 936-945.

Warnaka, E. (1982). *Active Attenuation of Noise-The State of the Art.* Noise Control Eng., 18(3), 100-110.

Reproduced with permission of the copyright owner. Further reproduction prohibited without permission.

Zuroski, M. and Roe, T. (1995*). Multi-channel Active Control of Blade Noise on a Rotary Lawnmower.* Active 95 Newport Beach, CA, USA, 697-706.

Reproduced with permission of the copyright owner. Further reproduction prohibited without permission.